DNA 5065F

CHARACTERIZATION OF STARFISH STRIATIONS FROM ANALYSIS OF PHOTOGRAPHIC RECORDS

Information Science, Inc.

123 West Padre Street

Santa Barbara, California 93105

30 June 1979

Final Report for Period 1 May 1978—31 May 1979

CONTRACT No. DNA 001-77-C-0170

APPROVED FOR PUBLIC RELEASE;
DISTRIBUTION UNLIMITED.

Prepared for

Director

DEFENSE NUCLEAR AGENCY

Washington, D. C. 20305

Destroy this report when it is no longer
needed. Do not return to sender.

REPORT DOCUMENTATION PAGE

READ INSTRUCTIONS BEFORE COMPLETING FORM

1. REPORT NUMBER	2. GOVT ACCESSION NO.	3. RECIPIENT'S CATALOG NUMBER
DNA 5065F	AD-A100 884	

4. TITLE *(and Subtitle)*

CHARACTERIZATION OF STARFISH STRIATIONS FROM ANALYSIS OF PHOTOGRAPHIC RECORDS.

5. TYPE OF REPORT & PERIOD COVERED

Final Report, for Period
1 May 78—31 May 79

6. PERFORMING ORG. REPORT NUMBER

RM79ISI101

7. AUTHOR(s)

Walter F. Dudziak
Pradip V. Lad

8. CONTRACT OR GRANT NUMBER(s)

DNA 001-77-C-0170

9. PERFORMING ORGANIZATION NAME AND ADDRESS

Information Science, Inc.
123 West Padre Street
Santa Barbara, California 93105

10. PROGRAM ELEMENT, PROJECT, TASK AREA & WORK UNIT NUMBERS

Subtask 125AAXYX960-15

11. CONTROLLING OFFICE NAME AND ADDRESS

Director
Defense Nuclear Agency
Washington, D.C. 20305

12. REPORT DATE

30 June 1979

13. NUMBER OF PAGES

102

14. MONITORING AGENCY NAME & ADDRESS *(if different from Controlling Office)*

X960

15. SECURITY CLASS *(of this report)*

UNCLASSIFIED

15a. DECLASSIFICATION/DOWNGRADING SCHEDULE

16. DISTRIBUTION STATEMENT *(of this Report)*

Approved for public release; distribution unlimited.

17. DISTRIBUTION STATEMENT *(of the abstract entered in Block 20, if different from Report)*

18. SUPPLEMENTARY NOTES

This work sponsored by the Defense Nuclear Agency under RDT&E RMSS Code
B322078462 125AAXYX96015 H2590D.

19. KEY WORDS *(Continue on reverse side if necessary and identify by block number)*

Striation Characterization	Volume Emission
STARFISH - Canton Island	Electron Density
Relative Radiance	Radius Probability Distribution
Power Spectra (PSD)	Number of Striations

20. ABSTRACT *(Continue on reverse side if necessary and identify by block number)*

The report summarizes the results of an extensive analysis in the frequency domain of photographic records that recorded, over Canton Island, the late time striations which resulted from the STARFISH nuclear detonation. The basis of this analysis are the frequency domain power spectral densities (PSDs) which were determined from relative optical radiances at various altitudes as a function of time. The analysis indicates how well the time/altitude variance of the power spectra can be represented by a simple analytic expression: (1) a log-log linear (power law) fit; (2) an exponential fit in

DD FORM 1473 EDITION OF 1 NOV 65 IS OBSOLETE
1 JAN 73

20. ABSTRACT (Continued)

the frequency domain. It has been found that both of the single simplified expressions underestimate the power at low frequencies. However, for a single simple expression, the log-log linear fit is a better representation of the data at very low frequencies.

The report also synthesizes a value for the total number of striations, a radius probability distribution and the spatial area/volume contained within the striations from the exponential fit; (in this synthesis, the striations are assumed to have Gaussian electron density profiles). On this basis, a volume emission from the striated region is determined from which an estimate can be made of the on-axis striation electron density.

Accession For		
NTIS GRA&I	X	
DTIC TAB	☐	
Unannounced	☐	
Justification		
By		
Distribution/		
Availability Codes		
Dist	Avail and/or Special	
A		

DTIC
S ELECTE D
JUL 1 1981

D

PREFACE

1

SUMMARY

In this report we have summarized results of derived parameters
of simple analytic representations of spatial frequency spectra that
arose from relative radiance measurements of STARFISH striations as
recorded on film at Canton Island. We have tried to establish a time
and altitude dependence of the power spectra. Study of the presented
data reveals that it is not obvious that such a dependence exists in
the time period and location of our analysis. It could very well be,
that at these late times, the striation region, which is far removed
from the burst location, is substantially the same and regions with-
in this striation volume of different character, which ought to be
described by different PSDs, do not exist. In any event, the data is
presented in sufficient detail to allow review by others, as to the
existence of possible time/altitude effects on the determined PSDs.

The prime purpose of these measurements was to establish the
power spectral density from the striation properties and determine
if these striation properties would restrict the PSD to a relatively
simple analytic form. It is clear from the presented results how
well this can be achieved by a single power law or a single exponential
fit. It is also shown how a better fit to the data is achieved by
a two-term exponential fit. Although time did not allow a review of
the data in terms of a similar two-term power law fit, it is certain
that very good representation of the STARFISH PSDs would be achieved
from such a two-term expression.

2

In any event, an adequate simple power law of the PSD description of the STARFISH Canton Island striation region is allowable. Our endeavor to fit all the data by one single power law expression forces the selection of a large L value (as shown in the presented, tabulated data) for the outer scale size. If one eliminates the steep PSD data at very small k values (k > 0.02 radians/km) as being spurious (since we at present do not understand the cause of this initial PSD shape), a single power law expression yields an outer scale size value of L between 40 and 100 km/rad (see Figure 4.1). The slope of the linear portion of the PSD has a value of about 2.0.

In summary, it appears that a reasonable fit to the stochastic radiance fluctuations observed from Canton after the Starfish test is a simple power law PSD with a slope of 2 and outer scale of about 40 km/rad. The reader should note that the radiance profile is the result of a line integral along the sight path through the fluctuations, and is therefore analagous to the phase shift profile of a propagating electromagnetic wave. The results presented here suggest the if the phase shift PSD had been measured at Canton Island, it would also have had a slope of 2.

The measured optical power is presented as relative radiance since calibration information is not available for the film considered. An estimate of the optical radiance (in $ergs/cm^2/sec./ster.$) can be obtained by multiplying this relative radiance by 5.1×10^{-2}. This normalization value assumes that the peak radiance reported by Overbye[11] at 9 minutes is the same as the peak radiance presented in Figure 3.4. The factor which normalizes the area under the PSD curve to 1 is also presented under each PSD curve. This will allow the user of the estimated radiances use of the PSD information in other possible detailed calculations.

CONTENTS

LIST OF PHOTOGRAPHS

LIST OF FIGURES

LIST OF FIGURES CONTINUED

LIST OF FIGURES CONTINUED

LIST OF TABLES

LIST OF TABLES CONTINUED

SECTION 1

INTRODUCTION

In recent years, the effects of nuclear weapon induced electron density fluctuations on propagating electromagnetic signals have been intensely studied. A fairly comprehensive discussion of a subset of these experimental and theoretical activities, based on the theory of thin phase screen approximation, is presented in Reference 1. In many of these studies the electron fluctuations are usually characterized by a power spectral density (PSD) where the major effort is to associate the spatial frequency properties of the PSD with electromagnetic propagation scintillation effects. It is this search for an adequate simple analytic PSD description that is the motivation for this work.

A typical example of current experimental efforts for simulating nuclear weapon effects in the ionosphere was Operation STRESS (Satellite Transmission Effects Simulation). The principle objective of such experiments is the study of actual satellite communication links propagating through structured barium plasma clouds. In such experiments neutral barium is injected into the ionosphere in sufficient quantity that the photoionized barium atoms constitute the locally dominant positive ion species. The assumption of charge neutrality leads to the conclusion that the local electron density fluctuations are directly proportional to the barium ion density variations. As a result of preferred plasma expansion along the magnetic field line, this localized barium induced plasma leads to formation of highly organized striation structures along the field lines, which in many respects simulate those created by high altitude nuclear detonations.

11

This mainly two dimensional variation of plasma density in such a striated region is of particular interest since such electron irregularities impose a corresponding structure on the phase front of a propagating electromagnetic signal. With sufficient distortion of the front, phase and amplitude fluctuations occur in the received signal. The result is a degradation in performance of communication systems.

As a consequence of this interaction between striations and communication reliability this report adds data to these barium studies by presenting results of PSD studies of the late time striated region produced in the ionosphere following the megaton STARFISH nuclear detonation. The nuclear device (with an approximate yield of 1.45 megatons[2]) was detonated at an altitude of 400 km at a latitude and longitude of ground zero of 16.47° north and 169.63° west. Ongoing experiments yielding structured barium plasma clouds try to simulate many aspects of this nuclear disturbed ionosphere.

In this report the experimental data base are the measured relative optical radiance profiles of striated nuclear ionization as recorded in the optical waveband on film. We assume that at the late times of these measurements in the non burst region the optical radiance of the recorded striations is proportional to the integral $\int N_{\epsilon}^{2}dz$, where the integral is along the line of sight and is limited by the volume of the recorded optical image. Thus the optical irradiance recorded by the film is that of a superposition of striations with "profiles" N_{ϵ}^{2} within the optically observed radiating plasma, where N_{ϵ} is the free electron density.

SECTION 2

SUMMARY OF DATA BASE AND REDUCTION PROCEDURES

2.1   STARFISH STRIATION DATA

In this section pertinent data necessary to the data reduction pro-
cess are presented. For geometric orientation Figure 2.1 presents a map of
the Pacific showing the location of Johnston Island - the approximate loca-
tion of the burst point, Canton Island - location of the camera system, the
magnetic meridian through the burst point, the magnetic equator, and various
other optical data gathering stations.

The data base was synthesized from a series of photographic images
of the event that are presented in Plates 3.1 through 3.8. These images
were acquired by a SRI International camera system from Canton Island[3] at
approximately the magnetic equator. Canton Island is at a longitude of 2.97^u
south and a latitude of 171.5^0 west. At this latitude the field line in the
magnetic meridian through the burst point is located at a longitude of 173.06^0
west and an altitude of 833 km. The camera optics system consisted of two
major elements - - (1) a Praktina 35 mm camera with an f/2, 50 mm focal length
lens system, and (2) an 18 inch diameter hemispherical plastic lens capable
of a 130^0 field of view. The plastic lens was placed approximately two feet
above the Praktina camera. The net result was a fourfold increase in the an-
gular field of view of the Praktina camera in the central image region. This
allowed a field of view of approximately 120^0 to be projected onto the 35mm
film. The optic axis of this composite camera system was pointed vertically
toward the sky, yielding an all-sky type of image.

This camera was run by an automatic clock that took a one minute

13
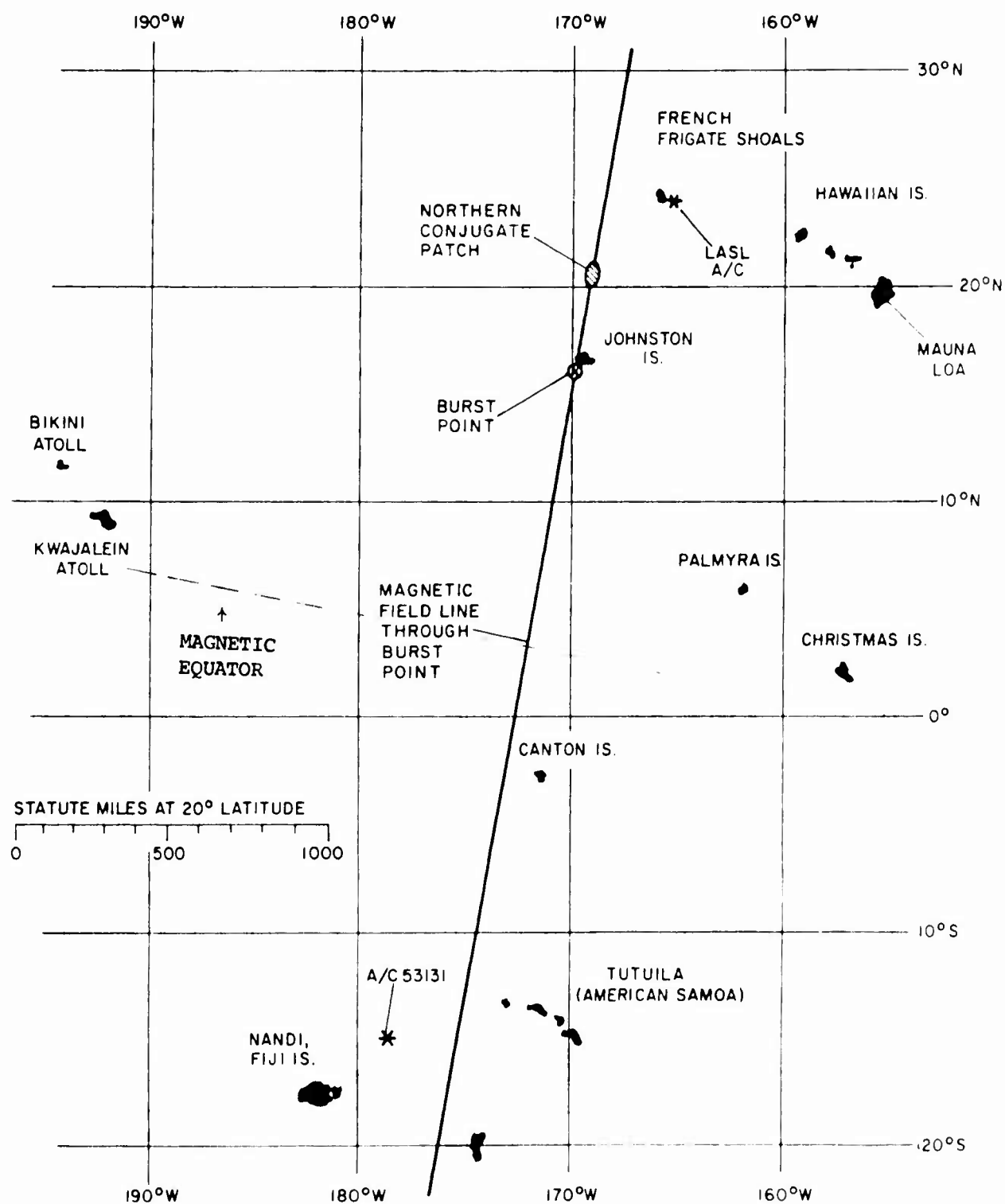
FIGURE 2.1   Location of camera stations during Starfish.

exposure once every minute. Thus the times given in this report are average times of each exposure after burst (i.e., film exposed from 300 to 360 seconds is presented as occurring at 330 seconds).

2.2 SUMMARY OF DATA REDUCTION PROCEDURES

The details of the data processing procedure has been ire   ly described.[4] Only the basic concepts and their variations as they appieu to this film reduction problem will be presented here. The reduced data covers the time period after burst from about 330 to 750 seconds at an estimated altitude of 920 to 1320 kilometers (see below). During this time period, except for the possible 'slow' movement* of the striated region along the magnetic field lines towards the southern conjugate, no other motion is apparent. Thus we assume magnetically aligned striations in which the statistical properties of the striations are azimuthally symmetric about the magnetic field. We likewise assume that the striated cloud is optically thin for which the measured radiance allows the determination of the electron density distribution, N_ε.

To obtain the raw magnetic field aligned data base the selected photographic images, shown in Plates 3.1 to 3.8, repre   q the optical emissions of field ligned spatial distributions of st: ionization, were subjected to a sequence of data reduction cperations. These data

---

* A review of color films during this time period from the LASL aircraft, Maui, Mauna Loa, Johnston Island, Canton and Tonga Islands reveals that the striated region radiates in the yellow and is superimposed on a glowing apparently not structured red sky background. This yellow striated region disappears first in the north, giving the impression to an observer of an apparent southern motion. This apparent motion can also be explained by a decreasing plasma temperature as yielding the earlier decay of the yellow striated region at lower altitudes. In any event, this apparent movement would not introduce a serious across the field line blur factor in the black and white images and is not considered in this data reduction process.

reduction processes[4] can be conceptually separated into four major portions. (1) The first phase of the data reduction process consists of converting the image to digital form. This was accomplished by means of an AFWL (Mann - System) scanning microdensitometer. A selected, approximately magnetic field aligned area (x = 7, y = 13 mm) of each film image (see for example Plate 3.1) was digitized in a raster pattern using an aperture whose dimensions were 10 microns in the horizontal (i.e., across the striations, or x-direction), and 100 microns in the vertical (along the striation, or y-direction).

To form the raster scan pattern, the image density (log of the ratio of light intensity transmitted by the film) was sampled every 5 microns horizontally, and then the aperture was stepped-over vertically by 100 microns (i.e., its own length) between adjacent horizontal scans. Horizontal* strips of data consisting of ten adjacent scan lines were selected from this areal scan and reduced for five different altitude levels for each of the eight photographic images. These selected strips comprised of 10 adjacent horizontal scans are shown as numbered bands on Plates 3.1 to 3.8; each band is 1 mm long on the film or approximately 80 kilometers in real space.

Each of these altitude regions is represented by a single "average power spectrum" which is the average of the 10 individual PSDs contained in the expanded "synthetic aperture" region. This procedure (use of a long 1 mm slit along the striation) in the data reduction process is sufficient to ensure that the data reduction process would be noise-limited by the inherent grain noise; i.e., no striation information (larger than 5 microns on film or approximately 0.? diameter at 1,000 km range) would be lost ("averaged out") due to f₁ ampling parameters.

* Each horizontal (across the striation) scan subregion was initially checked for being perpendicular to the magnetic field (as defined by the striation length) by an automatic pattern search sub-routine. If misalignment was detected (in this case, angles > 0.2^0) a synthetic aperture subroutine would be activated which would compensate for the determined misalignment angle by generating a horizontal scan line of data points from the sea of stored data points from adjacent scan lines that ving a scan line everywhere perpendicular to the magnetic field.

16

As shown below, the data is presented in real-space geometries. To accomplish this a film-plane to real-space transformation at the altitude regions indicated on the plates is required. To establish the spatial locations of these luminous auroral like features various documented results (for example, see references 3 and 6) were reviewed. These studies, and our study, tried to establish the geometric properties of the optically recorded striations by triangulation and also by projecting families of magnetic field lines into the camera field of view. The results of these and our efforts cannot position the location and volume of the radiating auroral structures without ambiguity.

Results of two typical examples taken from prior studies are shown in Figures 2.2.1 and 2.2.2. In Figure 2.2.1 the authors[6] illustrate the projection into the camera system, three magnetic field lines at different altitudes at the burst magnetic meridian plane and also in the 1^0 west meridian plane from this burst meridian. As shown both projections line up well with the observed auroral striations. Similarly in Figure 2.2.2 the authors[3] analyze these photographs (Plates 3.1 - 3.8) with projections of magnetic field lines in the burst magnetic meridian and also with grids of field lines that start at the same altitude (400, 800, and 1200 km) at the burst latitude and are in magnetic meridians displaced in longitude about the burst region. Although in both these, ours and other recorded studies, alignment with the recorded striations is in good agreement with field line projections, the locations of the auroral streaks is ambiguous since projection of magnetic field lines in meridian planes, both east and west, into the camera system have similar shapes.

To partially resolve this geometric ambiguity magnetic field lines were also projected into late time film image records (3 to 13 minutes) taken by cameras on Maui[7] and the LASL aircraft (see for example, Figure 6 in Reference 2). Results of such magnetic field line projections indicate that most of the striation caused (yellow) brightness at these

17
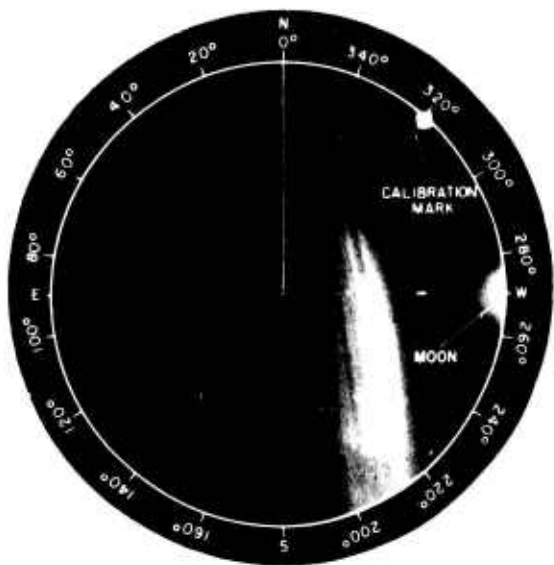
A. Geomagnetically aligned
streaks in the air-zero and
1°-W meridian planes as
photographed from Canton I
at 540 to 600 seconds.

B. With lines superimposed to
identify streaks in the air-
zero meridian plane.

C. With lines superimposed to
identify streaks in the 1°-W
meridian plane.

FIGURE 2.2.1
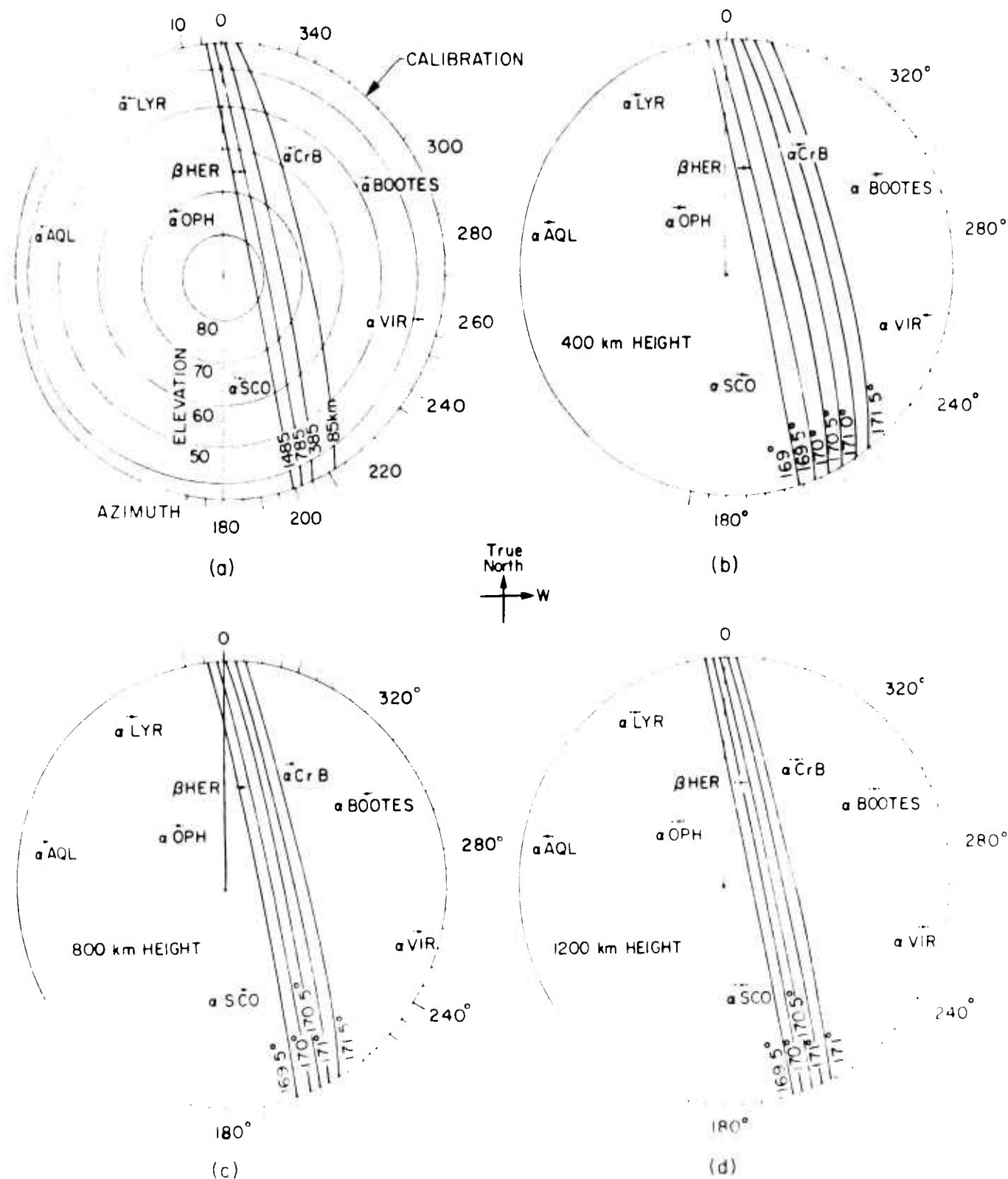
FIGURE 2.2.2 MAGNETIC FIELD PROJECTIONS FOR ALL SKY PHOTOGRAPHS

19

times lies between magnetic field lines in the magnetic meridian that passes through altitudes at the burst point of 300 to 800 kilometers. There are striations which are apparent to the observer that align with magnetic field lines at higher altitudes at the burst location (for example, 1,000 and 1,200 km). However, their brightness is very low and should contribute little if not zero to the recorded radiance values at Canton Island.

Thus, to allow transformation of the film coordinates to real space coordinates and to minimize the effects of perspective on this analysis, and thus simplify the computational problem, it is assumed in this study that the Canton Island striation images (Plates 3.1 to 3.8) are from a radiant energy source that has both vertical and horizontal extent. For computational purposes it has been assumed that the dominant striation radiating region is contained in an area perpendicular to the magnetic field above Canton Island that is approximately $\pm$ 200 km in vertical extent about the mean altitude, and approximately $\pm$ 2.3^0 (or $\pm$ 300 km) in longitudinal extent centered about a meridian plane at the burst region of 170.5^0 west longitude. Because of the geometric ambiguity, a sensitivity of our results to a change of the mean altitude of this striation volume is demonstrated by performing the calculations for mean altitudes of the magnetic field line at burst point of 400, 600 and 800 kilometers.

Figure 2.2.3 illustrates (by using the ONEMAG computer program[8]) the altitude dependence of the field lines on the selected magnetic meridian pertinant to this discussion. Shown also in this figure is the burst point and its relationship to the position of the five windows selected for data analysis.

(2) The computation of the power spectra requires that the scan profiles be converted from film units (image density, film coordinates) to physical units (relati e source brightness, real-space units). This conversion

20

MAGNETIC FIELD LINE PROFILES

FIGURE 2.2.3
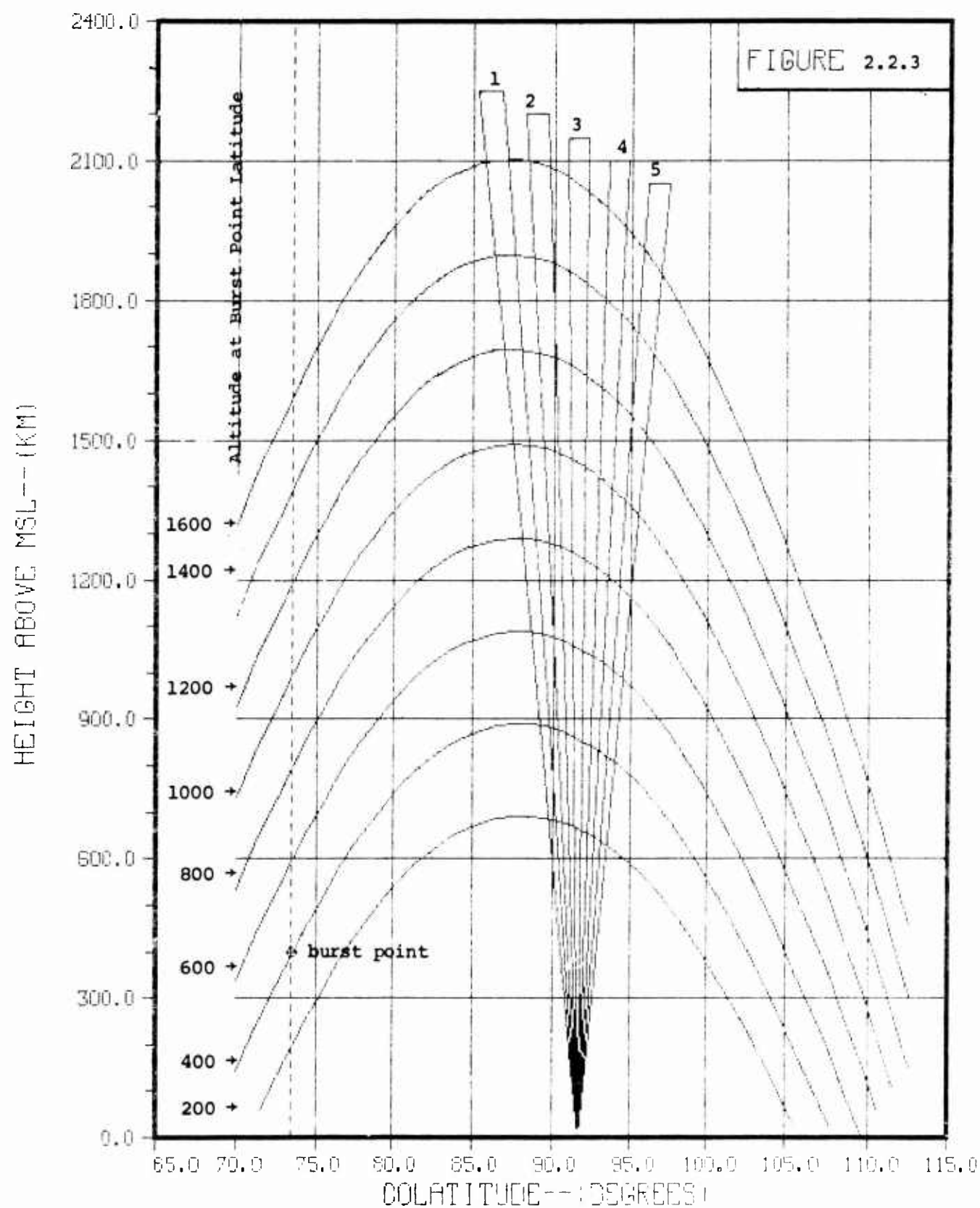
comprises the second phase of the data reduction process. The dimension-
al conversion arises from the 5 micron film sampling increment and the total
scan length. The Fast Fourier Transform algorithm used to create frequency do-
main conversions of the spatial radiance profiles derives its frequency inter-
val from the total scan length. Each digitized horizontal scan resulted in a-
bout 1400 image points. This measured profile was extended artificially to a
scan length of 4096 (2^{12}) points by adding zero radiance values when (after
film background subtraction) both the first and last measured radiance values
were zero. In cases where these two terminal values of the measured radiance
profile were not zero, the radiance value of the 4096 point was set to that of
the first measured radiance value. The artificial points between the last meas-
ured value and this 4096 point were filled by use of a linear slope between
these two values.

The purpose of extending artificially the radiance profile is to mini-
mize possible aliasing which is one of the primary dangers of using finite
Fourier transforms. This smoothing procedure drops the higher frequencies
rather than allow them to be manifested in a confusing manner. The 5 micron
sampling interval thus produces (for 4096 values) an effective scan length of
20.48 mm which determines a frequency interval of 0.04883 cycles/mm on the
film between sample points. The real-space frequency interval (in cycles/km)
is thus $\Delta f = 0.04883/magnification$, where the recording instrument magnifica-
tion factor (km/mm) is determined by dividing the slant range distance from
the camera to the mean striation volume by the effective focal length of 12.5
mm. (The plastic lens has the effect of decreasing the Praktina focal length
by a factor of 4). Thus for a slant range of 1000 km, $\Delta f = 6.104 \times 10^{-4}$ cycles
/km and $\Delta k = 3.835 \times 10^{-3}$ rads/km.

Graphic results presented in this report are scaled in cycles/km and
rads/km in real-space at the altitude level indicated on the plot. The Nyquist
limit (i.e., mamimum possible resolvable spatial frequency under ideal condi-
tions) for the scan data is given by $1/(2\Delta x)$ where Δx is the (0.005 mm) film
sampling interval. Thus this limit for the film is 100 cycles/mm (i.e., 7.8
rads/km in real space for the present data). In this study, signal informat-
ion (as measured by the frequency dependence of the signal/noise (S/N) ratio,
was found to decay into the film grain noise at approximately 10 cycles/mm.

22

The image density information was converted to relative radiance cy using post-facto estimates of the film characteristics. This was necessary since the SRI positive film used for these STARFISH characterizations was not intended to provide quantitative source brightness information and therefore was not calibrated. Thus the standard procedures to convert density to radiance could not be used. The film did posess rectangular steps of constant density of 0.3 d as the variation of each step prior to printing, a relative characteristic curve was established which placed most of the transmittance measurements of the processed film on the linear portion (having a slope, $\gamma = 0.9$) of the diffuse density vs. log (exposure) curve.

(3)   The third phase of the reduction process involves computations which produce a sanitized power spectrum from the average of ten PSD measurements (one for each of the 10 adjacent scan lines in the synthetic aperture)*. Each spatial frequency power spectrum is obtained from the sum of the squares of the A's and B's which arise as the coefficients of the sine and cosine series in the Fourier transformation of the artificially extended radiance profile. In essence, the sanitization process involves the construction of a frequency domain filter[4,5] which compensates for the effects of the modulation transfer function (high frequency suppression) due to motion blur and film/lens frequency response characteristics, and which filters out spurious high frequency power due to film grain noise. In this study the small perspective problem was incorporated as part of a blur correction.[4]

The dominant effect on the frequency domain filter and therefore on the present data is introduced through the signal-to-noise ratio. The

*   Through this computational procedure[4] the oscillations of the PSD are significantly reduced. No other smoothing of the PSD is used since smoothing techniques can seriously effect the data.

23

filter function is close to unity while the S/N ratio is above unity. Once the S/N = 1 frequency has been exceeded the filter function essentially follows the random excursions of the measured (noise) power spectrum.

The noise power model as used in these calculations is given by:

$$\left| N(\nu) \right|^2 = N_0^2 e^{-2\nu/\nu_N} \left| \frac{\sin(\pi w \nu)}{\pi w \nu} \right|^2 + N_a \tag{2.1}$$

$\left| N(\nu) \right|^2$ is the measured noise power at frequency ν; N_a is the frequency independent ambient noise power due to background, instrument, etc., noise. The form for the noise spectrum was chosen as exponential for computational convenience. The $\sin(\pi w \nu)/\pi w \nu$ term indicates the fact that the measured film grain noise is convolved (in the spatial frequency domain) with the slit response of the scan aperture (of slit width w).

(4)   The final phase of the data reduction process involves the actual characterization of the sanitized power spectra in terms of the fitting function and the SRI radius distribution analysis[4,5]. The power law analytic fits were performed over two frequency regions: (1) the larger 'mid frequency' region covered the frequency range $\sim 3.8 \times 10^{-3} \le k \le k_{max}$ radians/km in real space. The lower frequency bound is the first non-zero frequency resolved by the scan parameters; the upper bound is the frequency where the filter function suppresses the "raw" power spectrum by 10db (Table 3.2.3, and Figure 3.3.1). Over the time coverage of this analysis (330 to 750 seconds) this frequency varied between 1.26 and 1.57 radians/km. The 'low frequency' region covered the spatial frequency range from $\sim 3.8 \times 10^{-3} \le k \le 0.24$ radians/km.

For both the 'low' and 'mid' frequency ranges the power law fits were to a form[9]:

$$P(k) = \frac{4\sqrt{\pi} (\Delta n)^2 \Gamma(\nu+1) L^{-2\nu}}{(L^{-2} + k^2)^{\nu+1}} \quad , \text{ where } k = 2\pi f \tag{2.2}$$

24

The fit of Equation 2.2 to the PSD data is obtained by an iteration process. First, an initial estimate of the value ν is obtained by least squares log-log fits to the measured power spectrum; i.e., $\ln[P(k)] = \gamma \ln k + B$. Thus ν is related to the power law slope, γ by: $\nu = -(\gamma/2 + 1)$. Having determined an initial value for ν, an initial value for L in Equation 2.2 is obtained from the relationship $P(k) = \exp(B)/[(L^{-2} + k^2)^{\nu+1}]$ where B is the value obtained from the least squares fit. An improved value for ν is then found (using the initial value of L) by refitting the log-log linear representation of the PSD. This improved value for ν then leads to an improved value for L, etc. Iteration between ν and L continues until their values converge. With L and ν determined, the value of $(\Delta n)^2$ can be determined. This parameter is related to the variance from the mean of the index of refraction (hence, electron density) in the striated region.

<u>Exponential fits</u> $[P(f) = P_0 e^{-f/f_0}]$ were also performed over the frequency interval $0.016 < k < 0.24$ rads/km. As will be shown later in expanded frequency scale plots, this frequency range represents somewhat of a compromise, in that below a frequency of 0.03 rads/km, significant departure from a single exponential of the data is observed. Because of this, a second exponential is also fitted for the very low frequency $k \leq 0.03$ rads/km region, and is also presented in the graphic presentation of the data. The addition of this second exponential fit allows the low frequencies to be included. Otherwise, the low frequency power that exists in the striation structure could be considerably underestimated.

Following a procedure developed at SRI[5], the exponential fit parameters were also used to estimate the striation characterization in terms of the total number of striations. The details of these calculations are also presented in Reference 4. In this procedure:

$$N_T = \frac{3P_{DC}}{P_0} \tag{2.3}$$

25

and defines the total number of striations in terms of the measured zero frequency DC power (P_{DC}) and the zero-frequency intercept of the exponential fit P_O.

The striation radius probability distribution is assumed to be:

$$N(r) = \frac{8N_T(2\pi f_O)}{3\sqrt{\pi}(2\pi f_O r)^6} \exp [-1/(2\pi f_O r)^2] \qquad (2.4)$$

where $N(r)$ is the relative number of striations with Gaussian radius r; f_O is the e-folding frequency from the exponential fit. The most probable radius (r_p) defined by the above expression is given by:

$$r_p = 1/2\pi\sqrt{3}f_O \qquad (2.5)$$

As detailed by Reference 5, Equation 2.4 depends on several assumptions about the physical nature of the striations. Such assumptions include: (1) the observed cloud is an assemblage of individual striations; (2) the striations are rendomly positioned throughout the cloud; (3) the observed radiance is due to recombination only -- thus, it is proportional to the square of the electron density; (4) the cloud is optically thin to its own radiation; (5) the striations are radially symmetric about the magnetic field lines; (6) the electron density profile is Gaussian about each striation axis; (7) the peak (on-axis) electron density is independent of striation size.

26

SECTION 3

DATA PRESENTATION

This section summarizes the time/altitude characteristics of possible index of refraction variations in the ionosphere in the time period over which the STARFISH striations were measured. These characterizations arise from relative radiance measurements from a specific SRI Canton Island film and are presented by power spectrum plots and tabulated parameters describing simple analytic functions fit to these PSDs which approximately describe the empirical data. The PSDs cover a spatial frequency range which contains essentially 100 percent of the measured power.

Only a limited number of spectral power plots are presented to illustrate the time/altitude ionospheric variations. The time evolution of ionospheric striations was explored by selecting eight frames which covered a time span of 330 to 750 seconds after burst. The altitude variation (see Figure 2.2.3 and Plate 3.1) at each time, was obtained by selecting experimental data from five non adjacent windows from the scanned area of each frame. For a mean altitude of the magnetic field of the striation volume at the burst point of 800 km, the altitude of the five selected windows varied from 1000 to 1120 kilometers. At a burst point altitude of 400 km, the analyzed altitude range is between 810 and 920 kilometers, while if the altitude at burst latitude is taken as 800 km, then the altitude variation of the selected windows is between 1190 and 1320 kilometers.

Figures 3.1 to 3.8 graphically illustrate at each altitude irregularities in the relative radiance above film threshold as measured perpendicular to the earth's magnetic field defined by the elongated striation direction. These graphic illustrations are for the 600 km
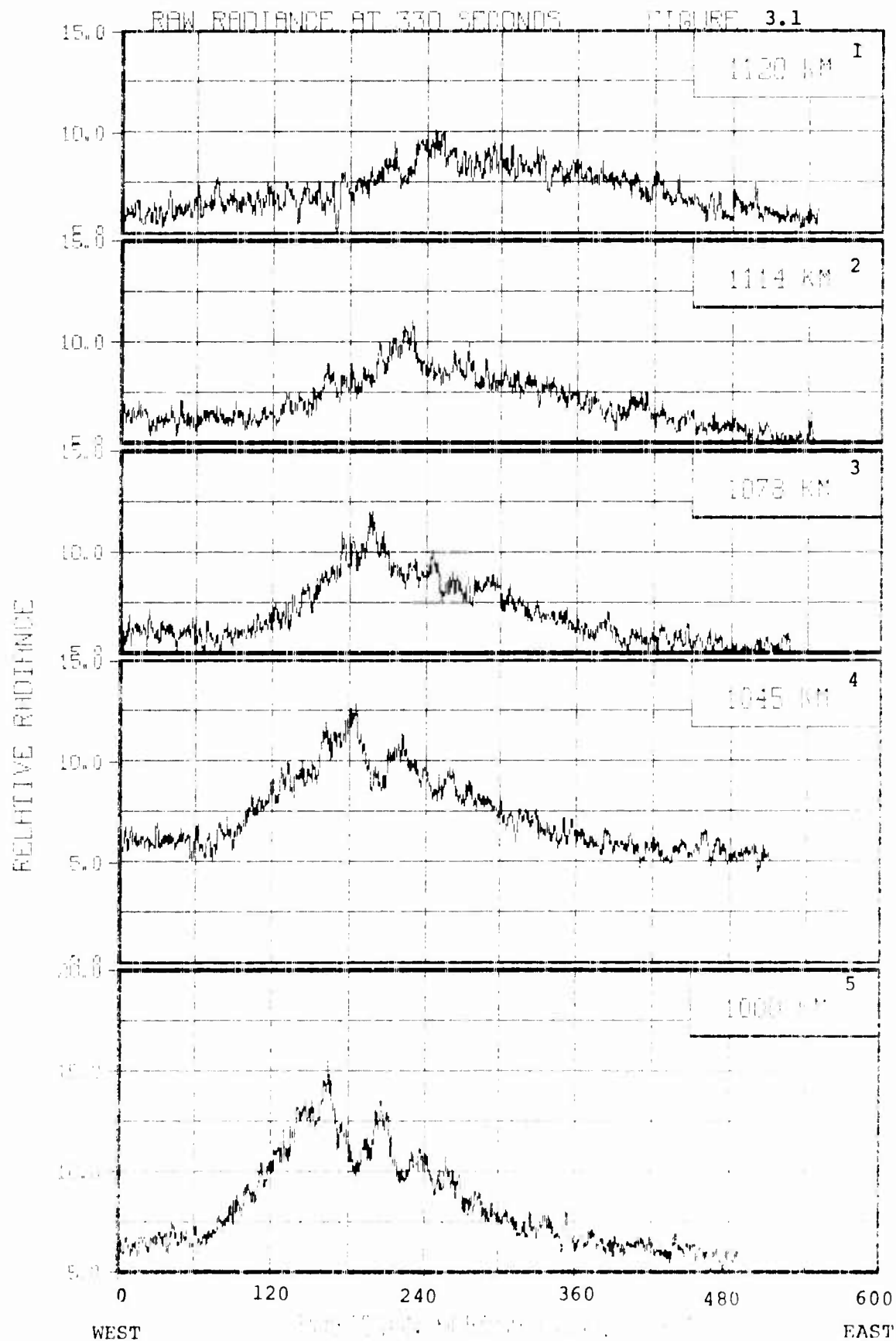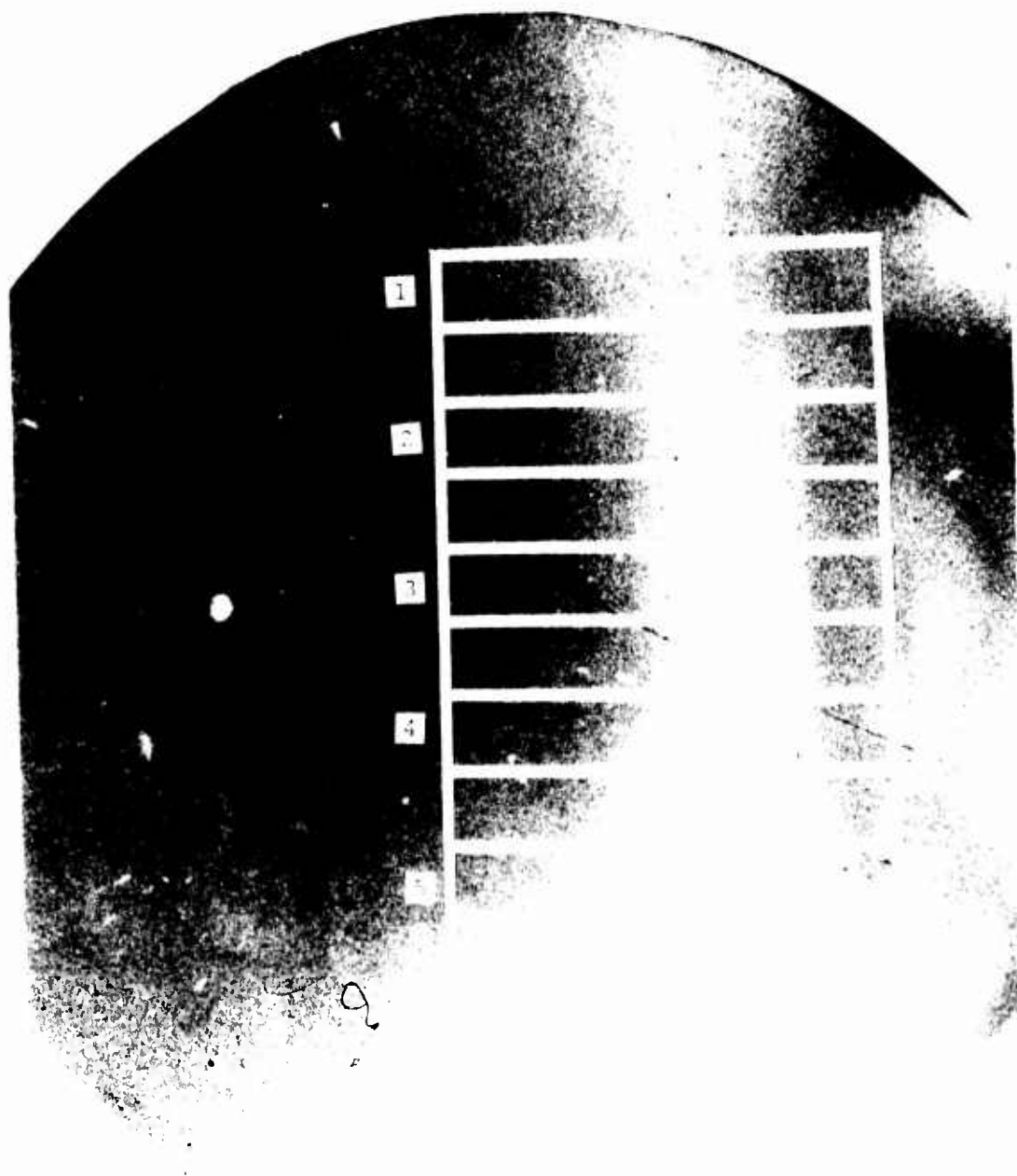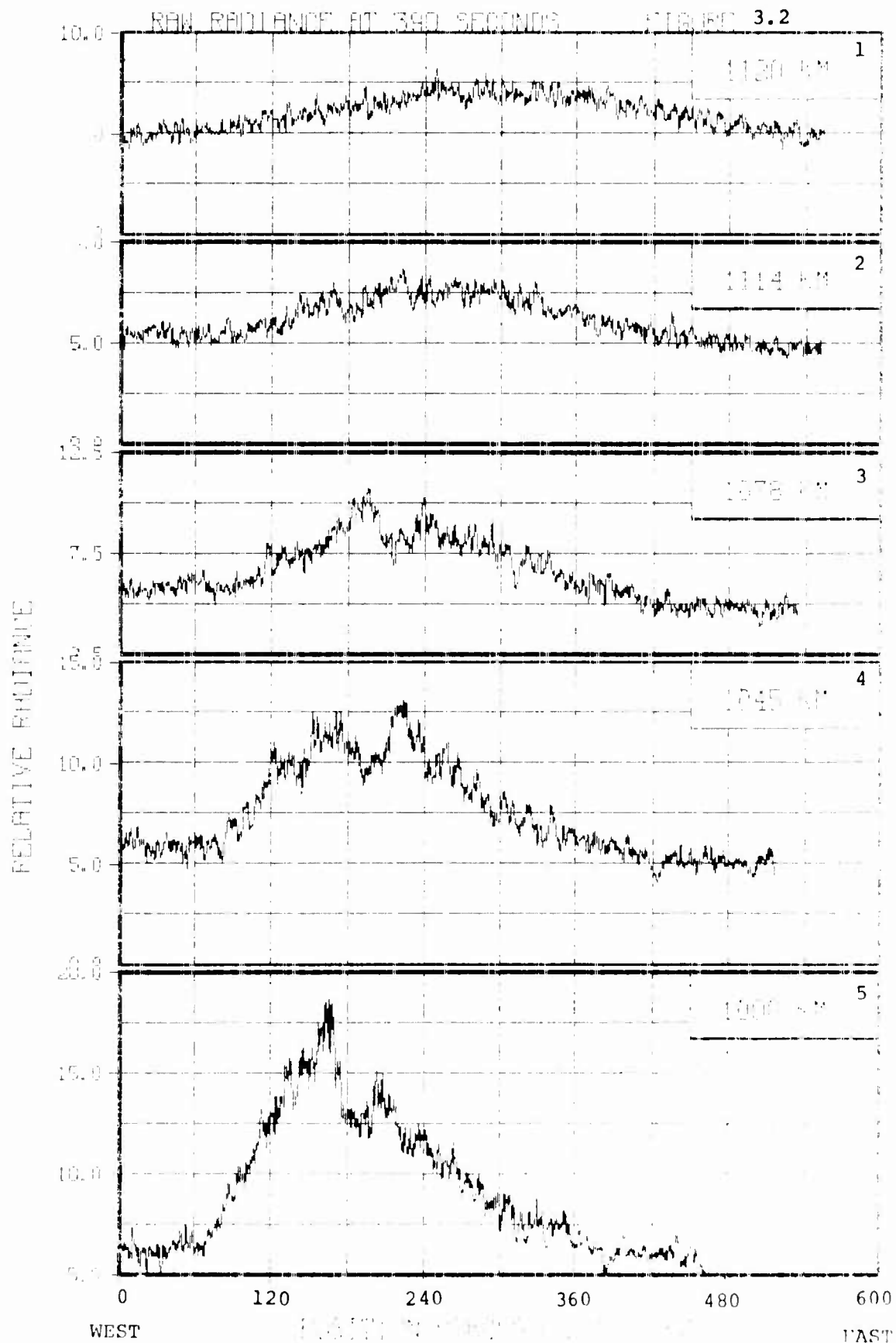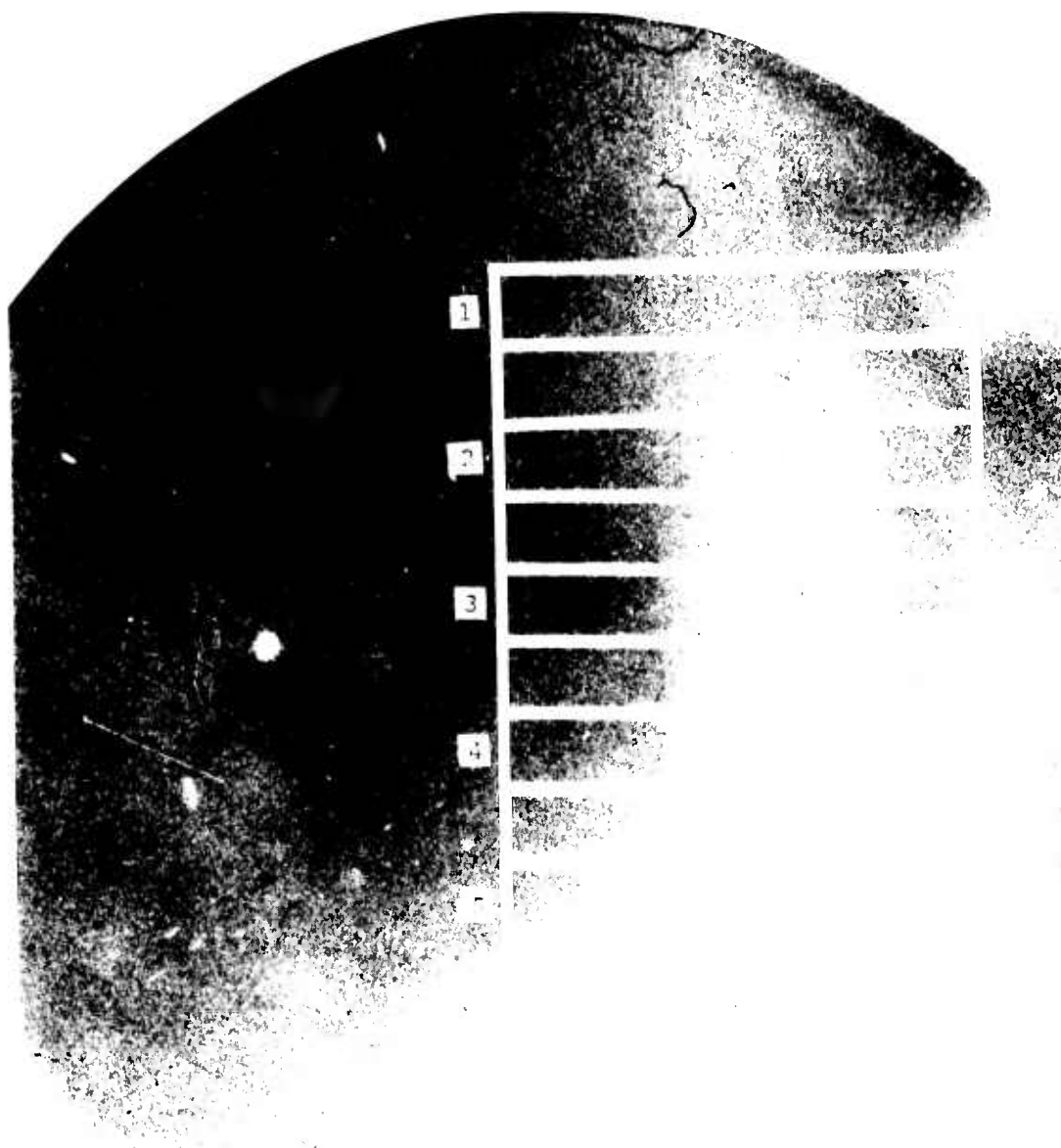
27

NORTH

EAST

WEST

1

2

3

4

5

SOUTH

PLATE 3.1   28   TIME 300 - 360 seconds

RAW RADIANCE AT 330 SECONDS   FIGURE 3.1

NORTH

SOUTH

PLATE 3.2   30   TIME   45 - 420 seconds

RAW RADIANCE AT 390 SECONDS   FLIGHT 3.2

RELATIVE RADIANCE

0   120   240   360   480   600

WEST   EAST

31

NORTH

EAST

WEST

1

2

3

4

SOUTH

PLATE 4.3   32   TIME 420 - 480 seconds

Figure 3.3

NORTH

EAST

WEST

SOUTH

PLATE 3.4 34 TIME 480 - 540 seconds

3.4

1

2

3

4

5

RELATIVE BRIGHTNESS

0   120   240   360   480   600

WEST   EAST

35

NORTH

EAST

WEST

SOUTH

PLATE 3.5   36   TIME 540 - 600 seconds

RAW RADIANCE AT 570 SECONDS   FIGURE **3.5**
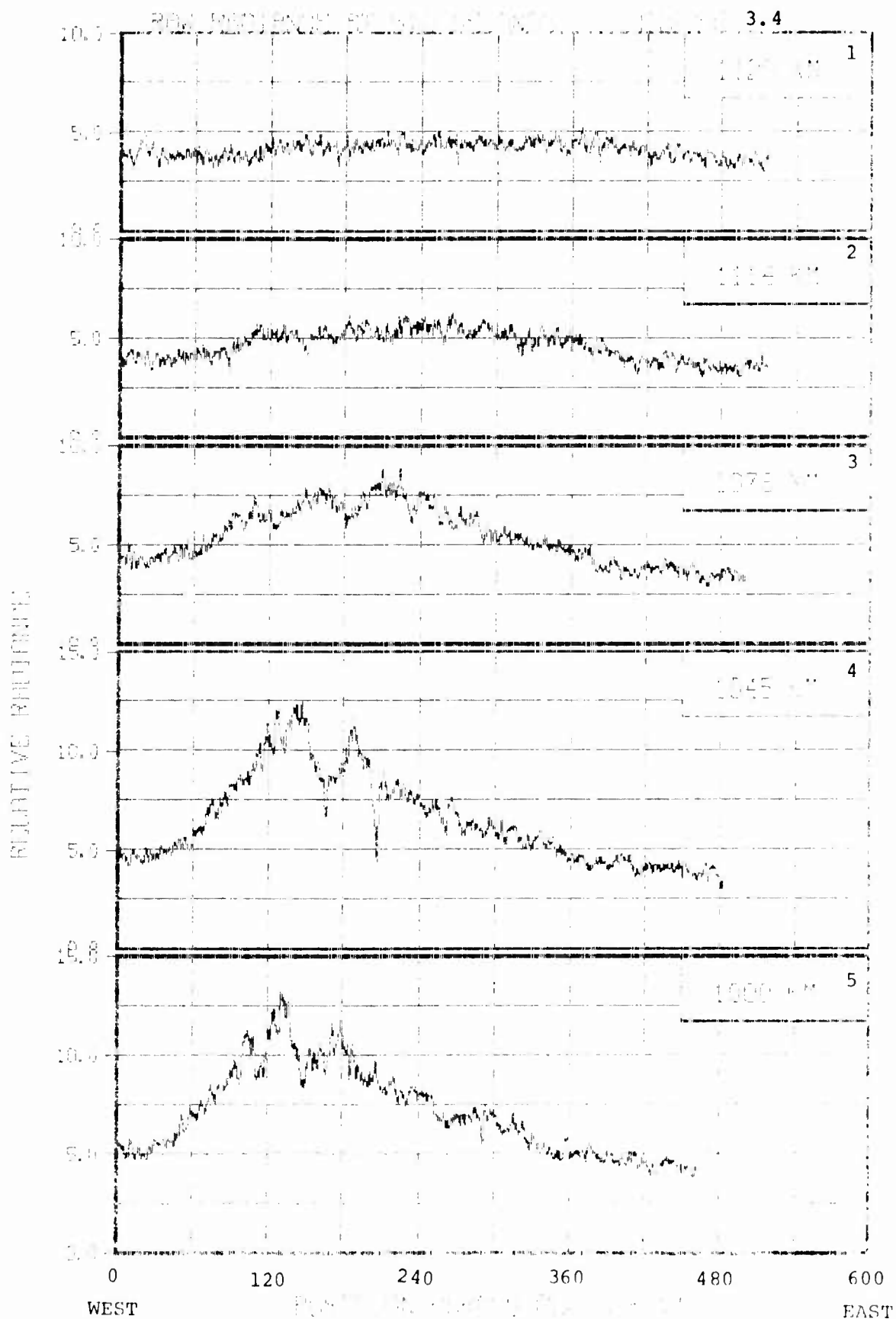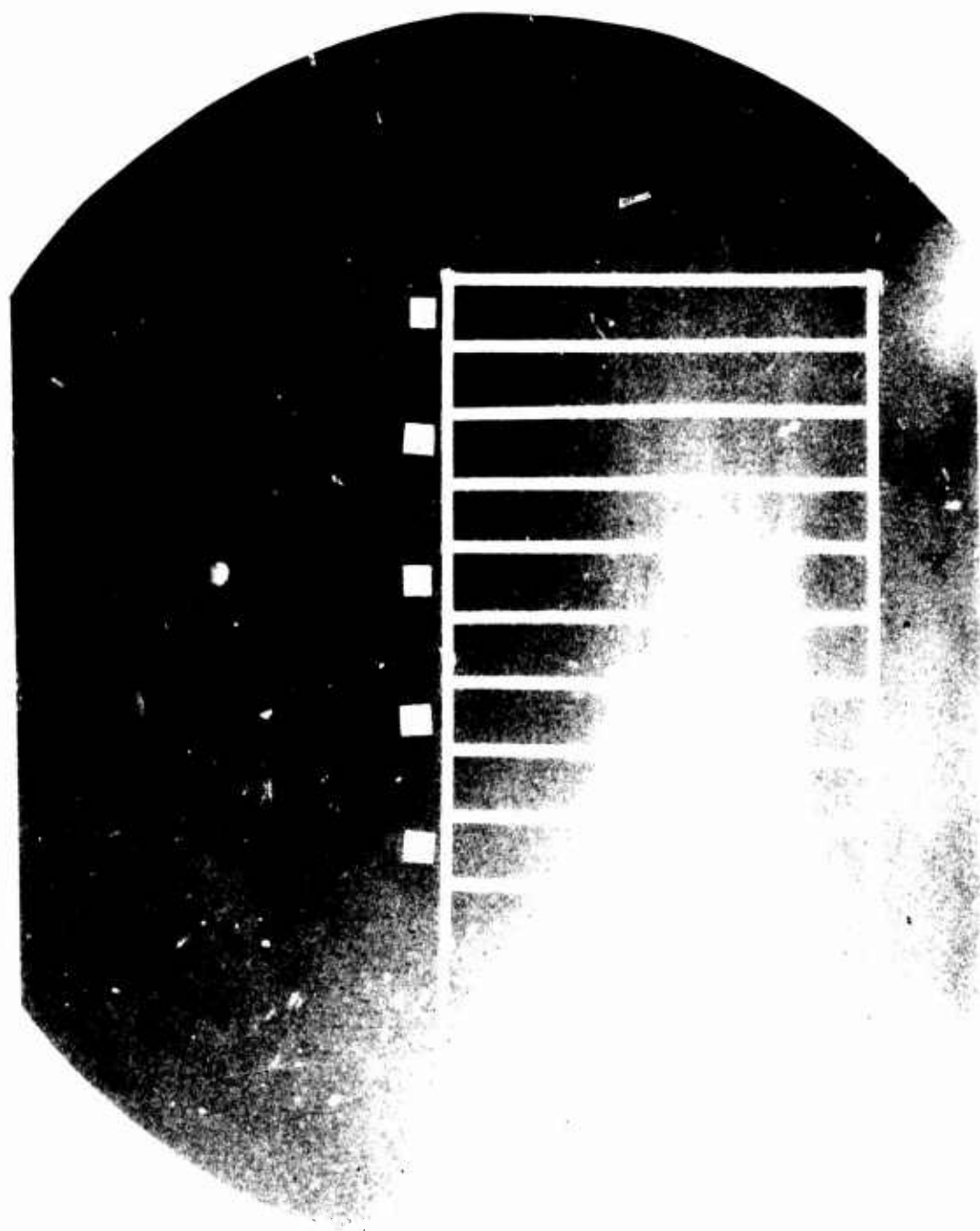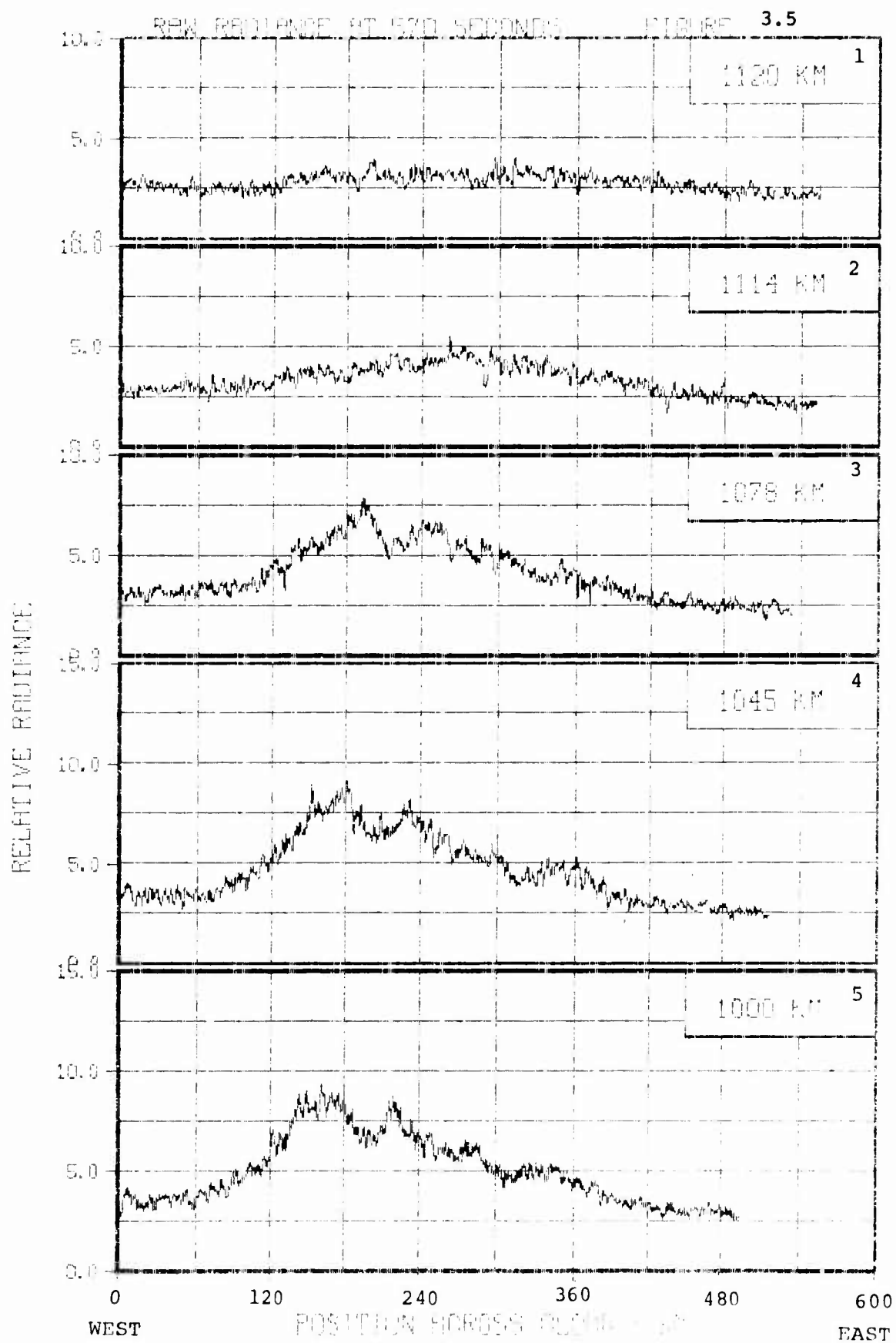
NORTH

EAST

WEST

SOUTH

PLATE 3.6   38   TIME 600 - 660 seconds

ROW RADIANCE AT 630 SECONDS   FIGURE 3.6

RELATIVE RADIANCE

POSITION (POINT)

WEST   EAST

39
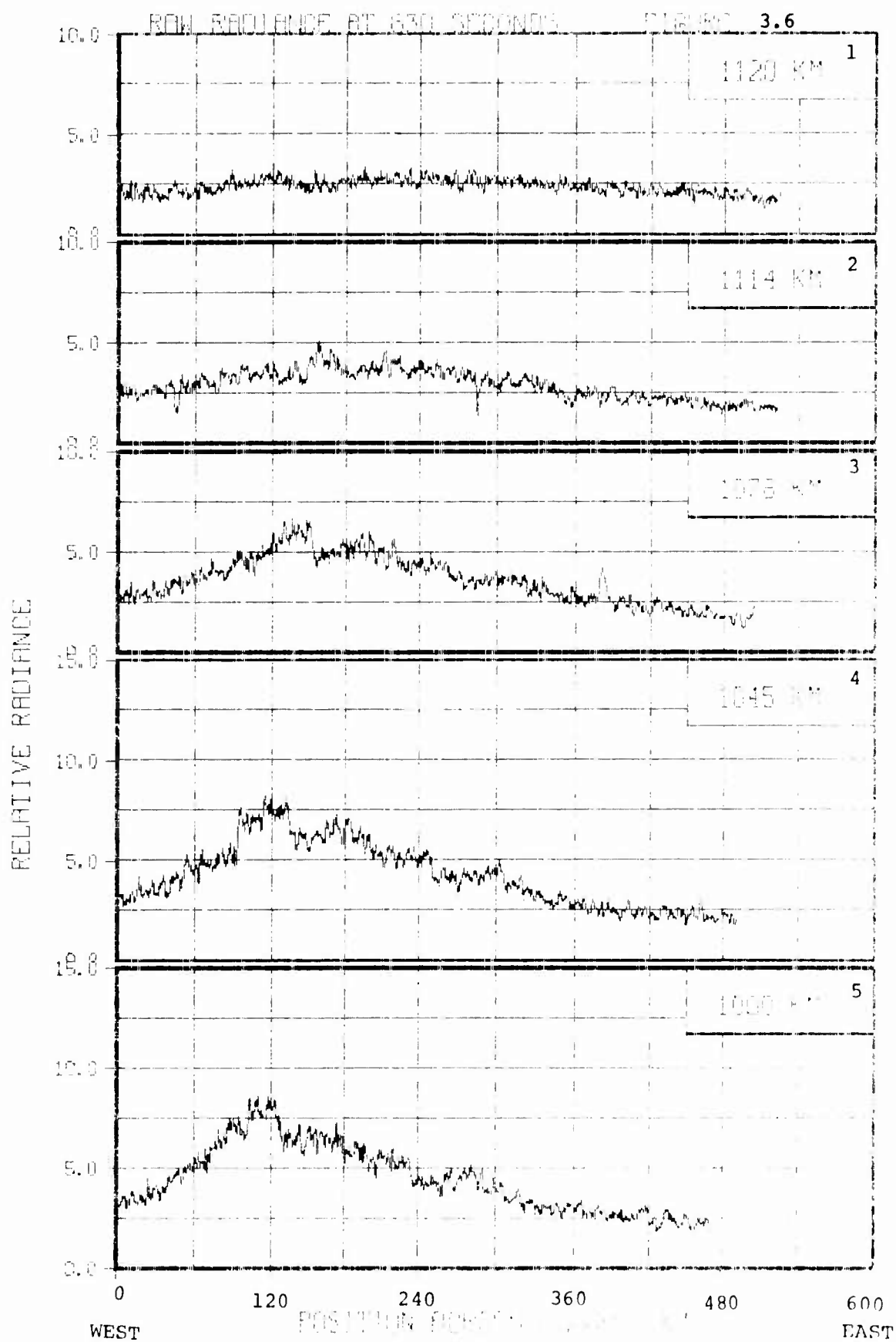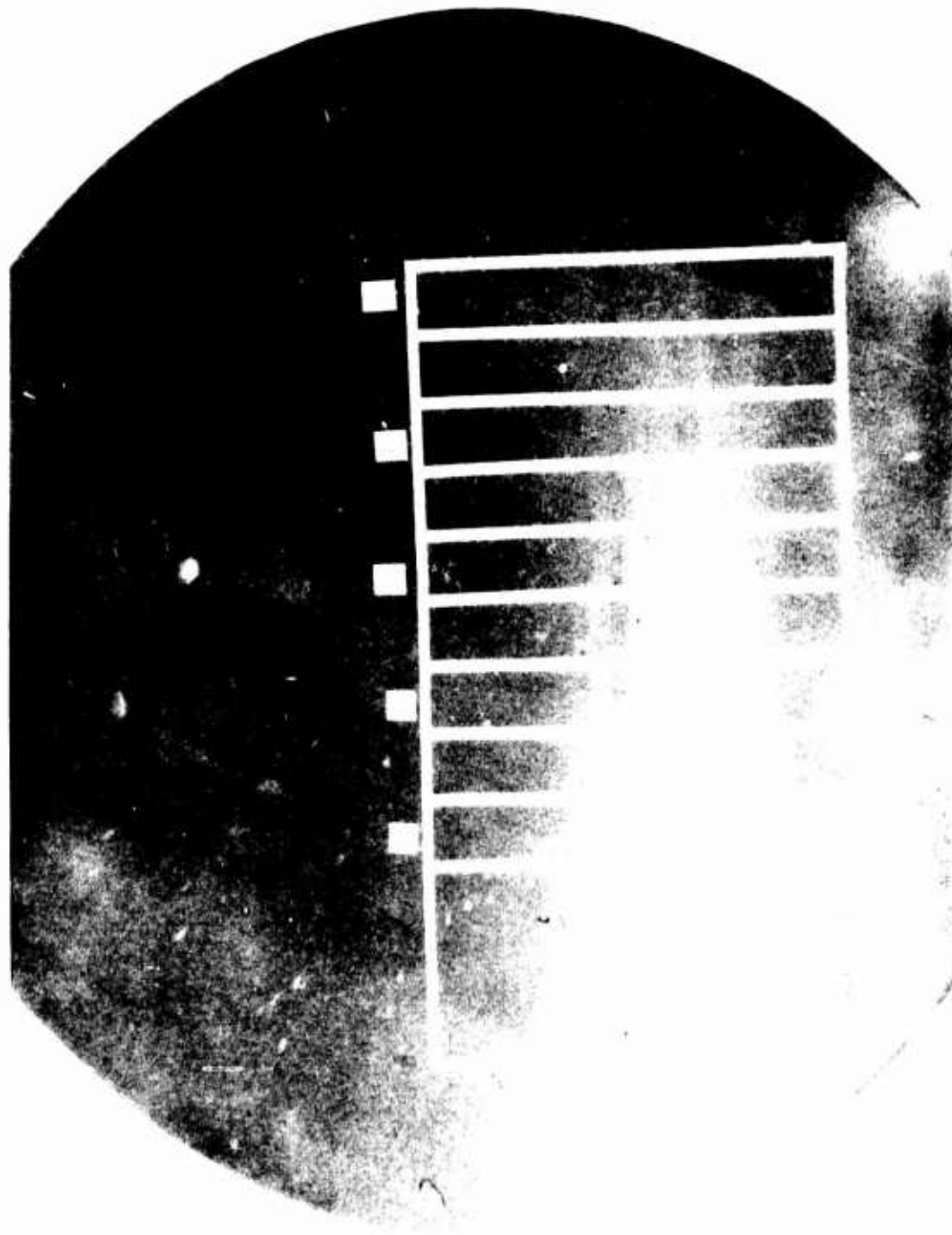
NORTH

WEST

EAST

SOUTH

PLATE 40 TIME 660 - 720 seconds

RAW RADIANCE AT 600 SECONDS   FIGURE 3.7

NORTH

EAST

WEST

SOUTH

PLATE 2.8 42 TIME 7.0 – 750 seconds

3.8
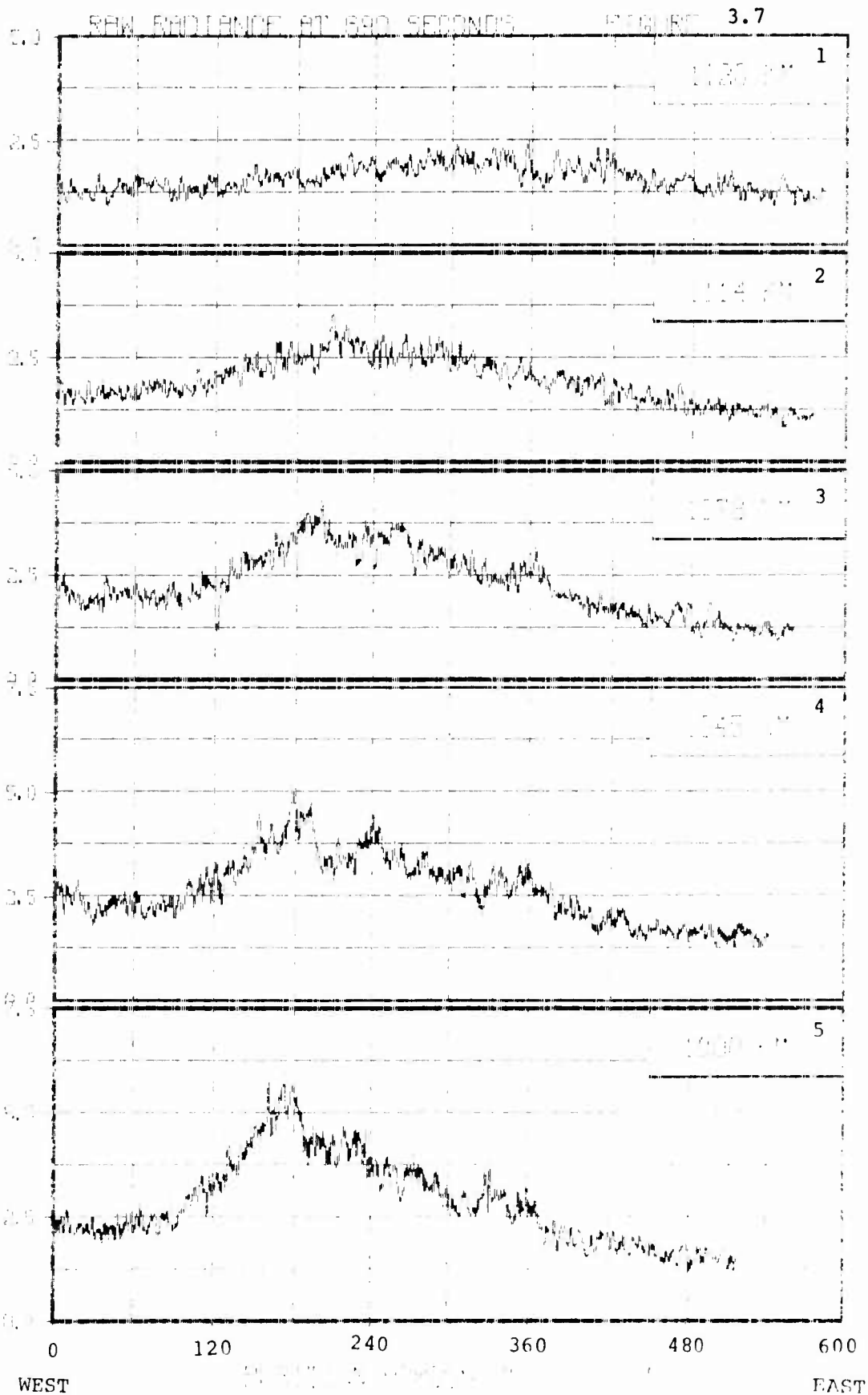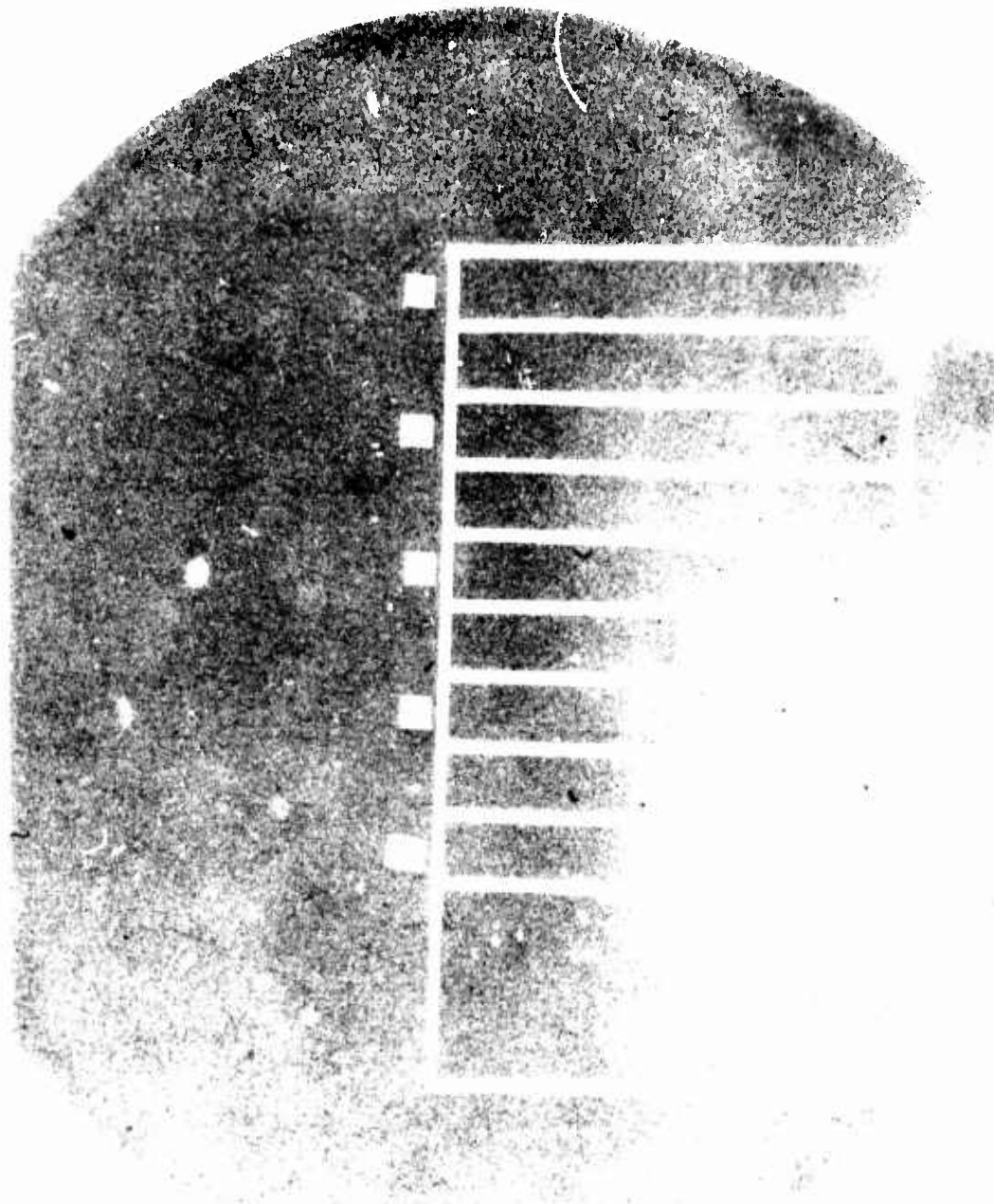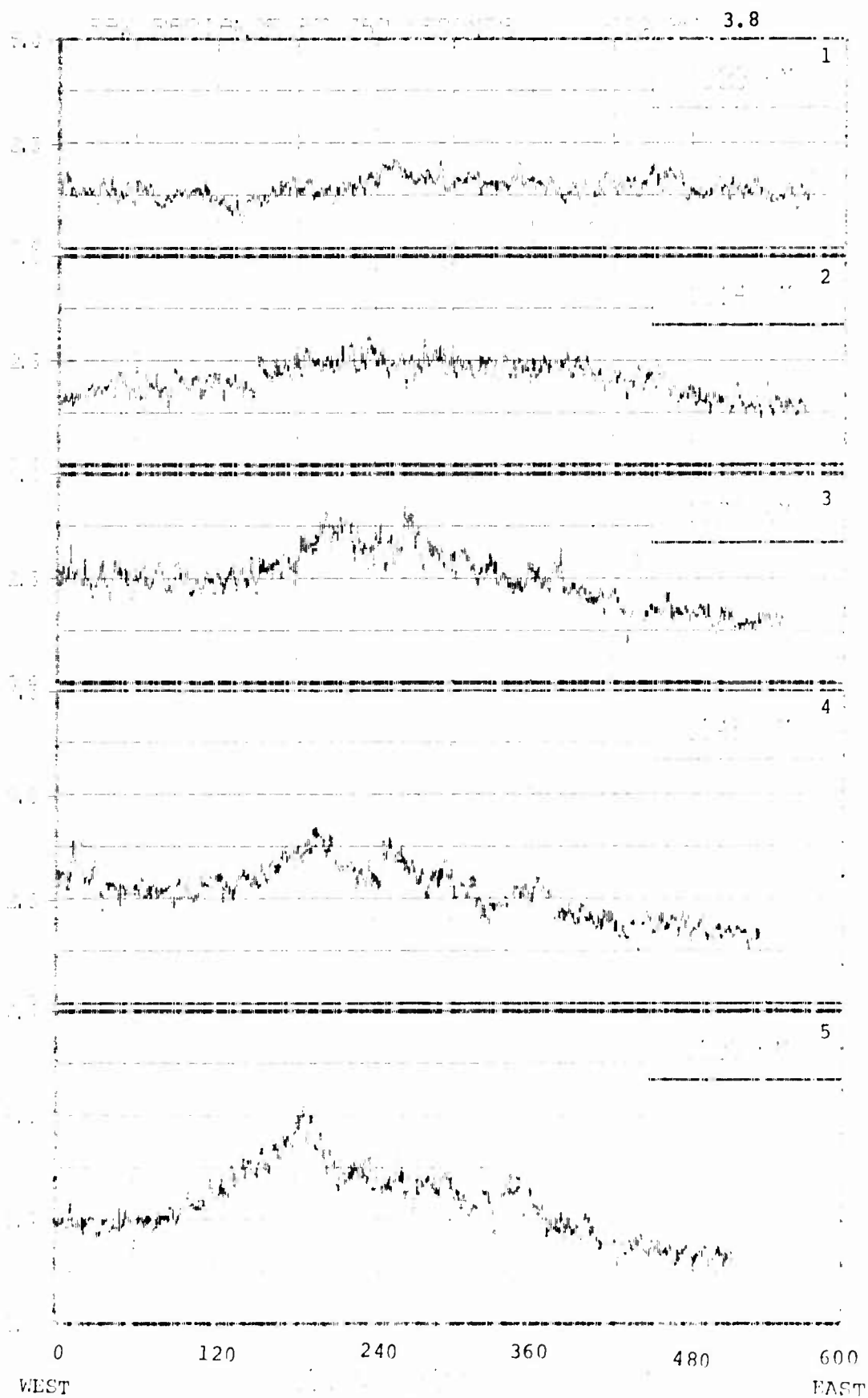
mean burst altitude of the striation volume. For example Figure 3.1 presents the spatial variation of the relative radiance of the first of the two scan lines analyzed in each of the five windows which were used to create the sanitized PSD at 330 seconds after the burst. At this time the film recorded image is presented in Plate 3.1. As quickly observed by a review of Figure 2.4 and 3.1 and also Plate 3.1, the relative radiance values for the analyzed window 1, are shown at the top. As one goes down the field line towards the southern conjugate, the radiance values are shown lower and lower in the graphic illustration. Thus window 5 data is at the bottom.

As also quickly observed the plotted radiance is for a right-to-left (i.e. West to East) scan line of the photographic image illustration. Similar information for the analyzed five windows at different times are presented in Figures 3.2 through 3.8 and Plates 3.2 through 3.8.

3.1 PSD, POWER LAW DATA PARAMETERS

Figure 3.1.1 to 3.1.10 present, as a function of time at a given altitude and also as a function of altitude at a given time, the behavior of the normalized power spectrum at the spatial frequencies within which essentially all the measured power resides. Although such representations of the data were produced for all three burst altitudes considered only those for the magnetic field line representing the luminous striation volume which passes through 600 km altitude at the burst point latitude are illustrated by these graphical presentations. The power spectrum was normalized so that the area under the curve is equal to one. The magnitude and its variation with time of this normalization factor ($\sim 10^8$) is illustrated in Figures 3.1.1 and 3.1.2.

In order to observe how the power behaves at the lowest frequencies

44

the power spectra were plotted against the log of spatial frequency ($k=2\pi f$).
The expansion of the region at the low frequencies shows that in a log-log
representation, the data indicates that at near zero frequency, the power
spectrum possesses a small plateau followed by a steep, approximately two
decade drop in the spectral power. This PSD behavior was not observed in
similar analysis of CHECKMATE striations[4]. The PSD also reveals that as the
spatial frequency increases, a frequency interval exists where the log (pow-
er) vs log (frequency) behavior approaches linearity.

Overlaying the measured data on these plots is the power law fit
expression given by Equation 2.2 as determined by analytic fits in the 'low'
($k \leq 0.24$) frequency interval. Similar overlays were also produced for the
'mid' frequency ($k \leq 1.4$) interval. The low frequency fit interval analytic
overlays were selected since these gave more frequently a better fit to the
measured data.

It is important to note that the power spectrum does not yield
a unique solution to Equation 2.2. The solution depends on the selected
frequency interval of the power spectrum fitting range that is used to ar-
rive at the desired parameters given in Equation 2.2.

The low frequency interval is defined as the interval that in-
cludes all frequencies up to a maximum frequency of 0.24 rads/km. Thus
the selected cut-off frequency is independent of the measured PSD and there-
fore does not vary with time and altitude.

Tables 3.1.1 through 3.1.8 summarize all the least square fit
values for the parameters which allow Equation 2.2 to best fit the data
for each of the measured PSDs in this study. Included in these tables
are the results from all three burst altitudes (400, 600, and 800 km) con-
sidered, thus allowing a comparison of the variation of these parameters,
which result from the altitude ambiguity of the striation region.

45

Tables 3.1.1, 3.1.3, 3.1.5 and 3.1.7 present values that define the analytic fits as obtained from use of the 'low frequency interval', while Tables 3.1.2, 3.1.4, 3.1.6 and 3.1.8 present values that define the analytic fits as obtained from use of the 'mid frequency interval'. Because the selected cut-off frequency, k_{max} , for the 'mid frequency interval' is defined as the frequency where the filter function decays by -10 db, it is dependent on the measured PSD and therefore does vary with time and altitude. Its time/altitude behavior is presented in Table 3.2.3 which lists all the k_{max} values that were used to arrive at the 'mid frequency interval' values.

Time and altitude variation of the power exponent, ν, shown in Equation 2.2, are presented in Tables 3.1.1 and 3.1.2 while Tables 3.1.3 and 3.1.4 present the outer scale size, L. Table 3.1.5 presents the variation of the slope associated with the linear portion of the log(power) vs. log (frequency) plot, while Table 3.1.7 and 3.1.8 give the value of the scaling factor, A, which represents the numerator of Equation 2.2. Also shown in these tables are the average values of these parameters where the values were averaged over altitude and time.

To give some insight into the time dependence of the power law parameters, the values which were averaged over altitude at each time are presented in plotted form. Thus Figure 3.1.11 presents the time behavior of the average value of the exponent, ν, and the outer scale size, L; Figure 3.1.12 illustrates the time behavior of the slope and of the altitude averaged value of the scale factor, A, in Equation 2.2. These sets of graphic illustrations are shown for the three different considered altitude locations of the striation volume, as well as, the arrived at results from the two different frequency intervals used in computing the analytic fits for overlaying the measured data. Other plotted representations of these parameters are possible from the presented tabulations. These are left as an exercise for the interested reader. The data is detailed enough to arrive at an understanding of the sensitivity of the data to the ambiguity in our knowledge of the altitude of the striated region.

46

1.295E09

9.713E08

7.168E08   ABCISSA x $\frac{\pi}{7}$ = k (radians/kilometer)   4.194E08

3.1.2
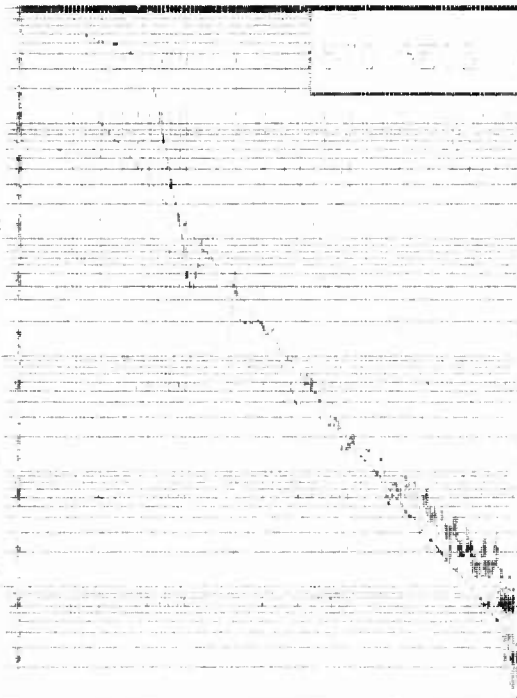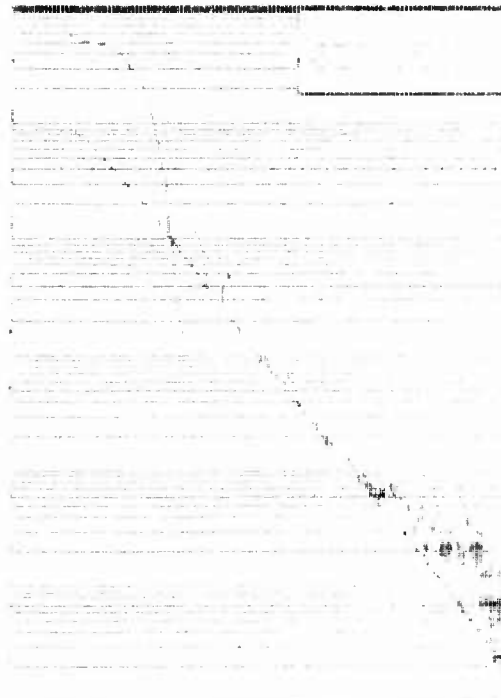
2.155E08   1.534E08

7.918E08   ABCISSA x $\frac{\pi}{2}$ = k (radians/kilometer)   6.865E07

48

1.237E09

1.030E09

8.108E08   ABCISSA x $\frac{\eta}{2}$ = k (radians/kilometer)   5.457E08

3.268E08

2.414E08
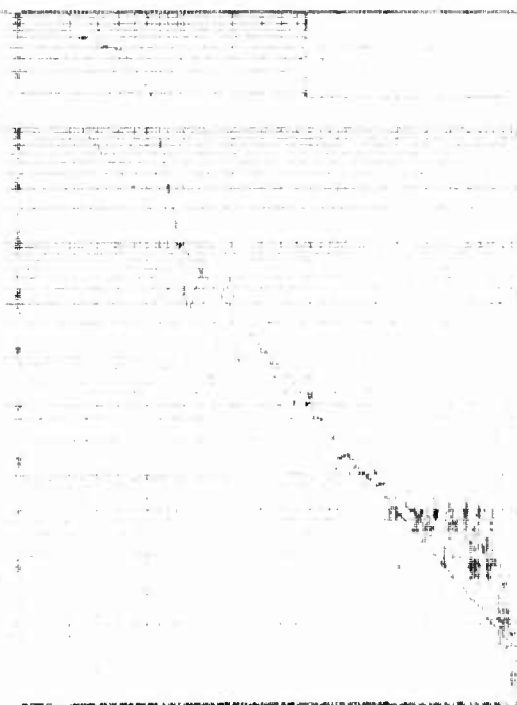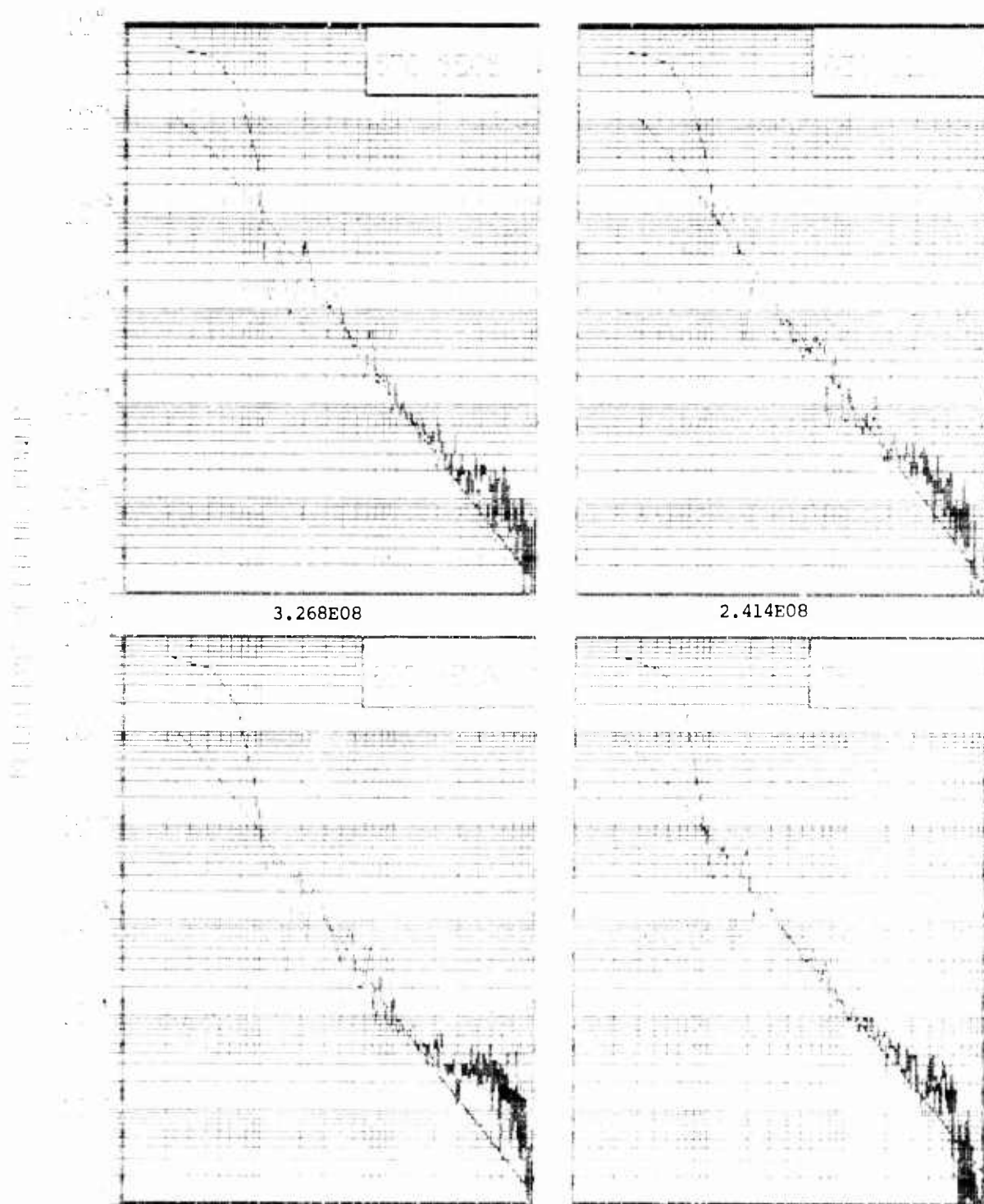
1.197E08

1.286E08

$$\text{ABCISSA} \times \frac{\pi}{2} = k \text{ (radians/kilometer)}$$
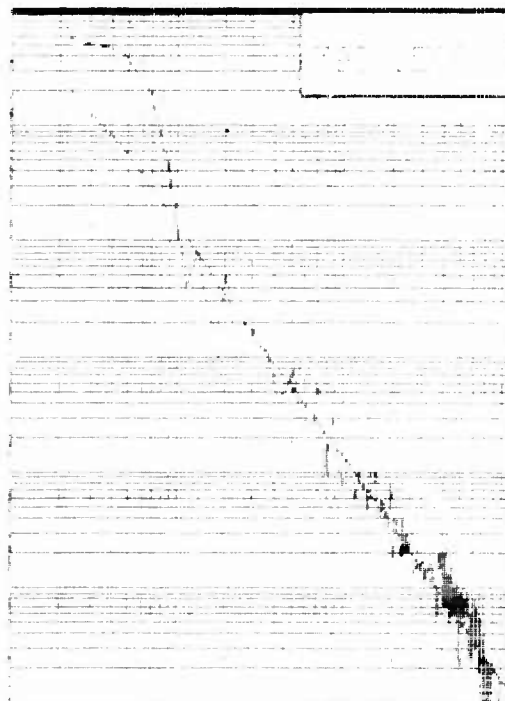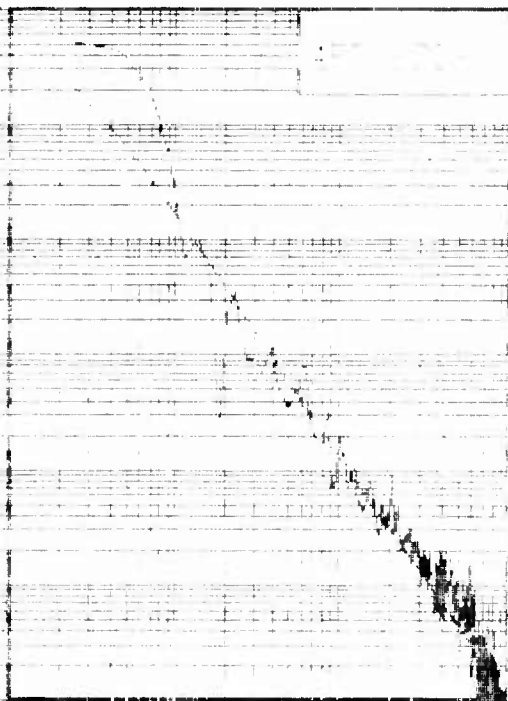
50

3.1.5

1.238E09   1.191E09

1.099E09   ABCISSA $\times \frac{\pi}{2}$ = k (radians/kilometer)   7.796E08

51

FIGURE 3.1.6

5.052E08   3.712E08
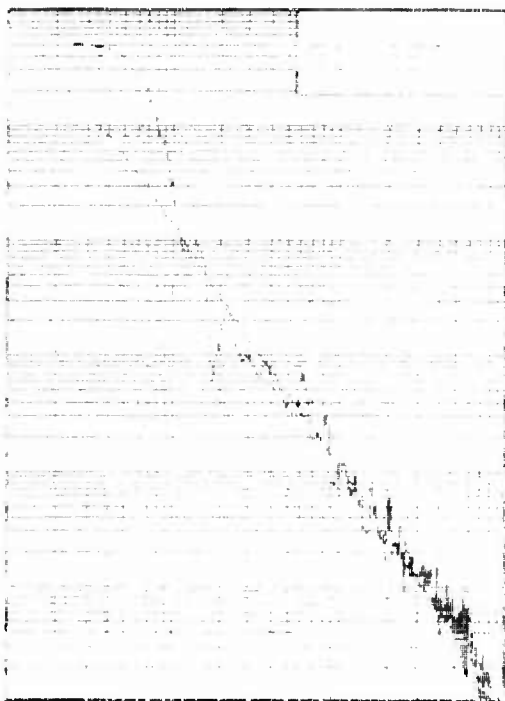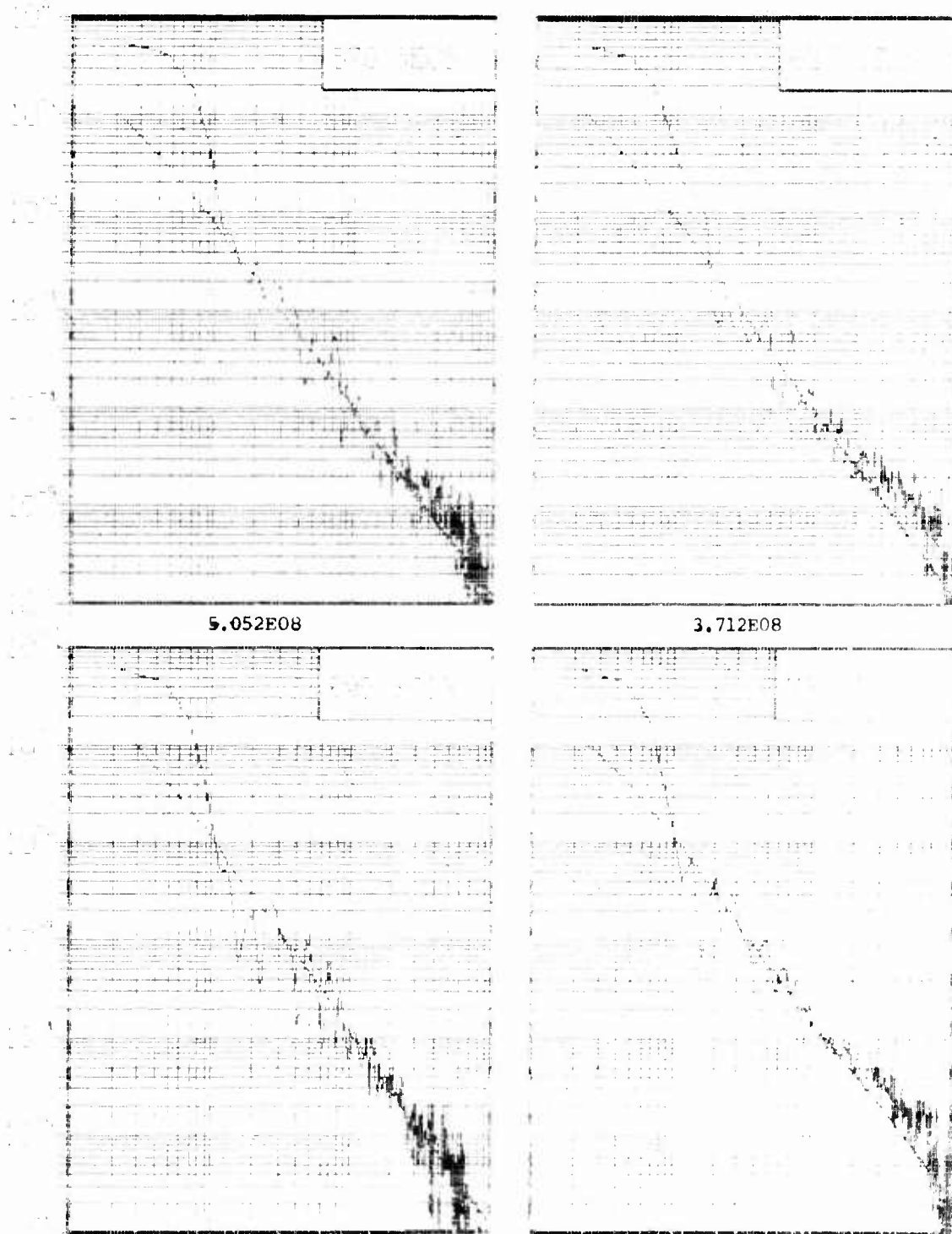
1.597E08   ABCISSA x $\frac{\pi}{2}$ = k (radians/kilometer)   1.733E08

52

NORMALIZED POWER SPECTRUM
AT 105 KILOMETERS   FIGURE   **3.1.7**

1.508E09   1.746E09

1.770E09   ABCISSA x $\frac{\pi}{2}$ = k (radians/kilometer)   1.164E09

53
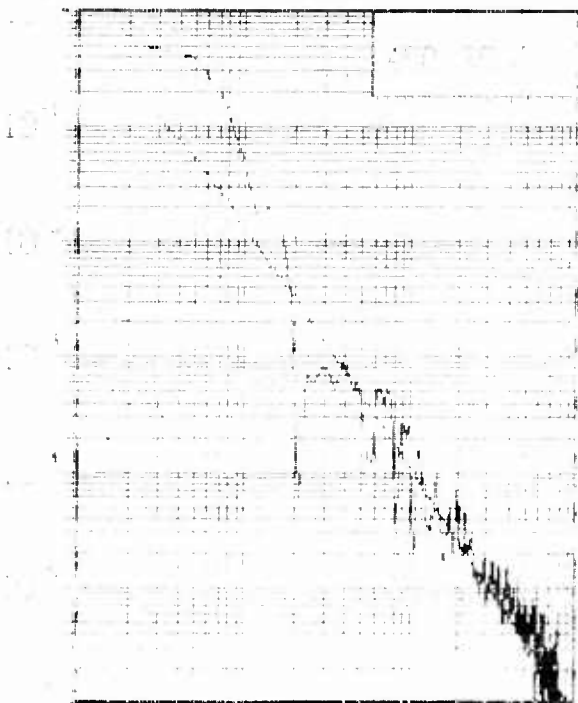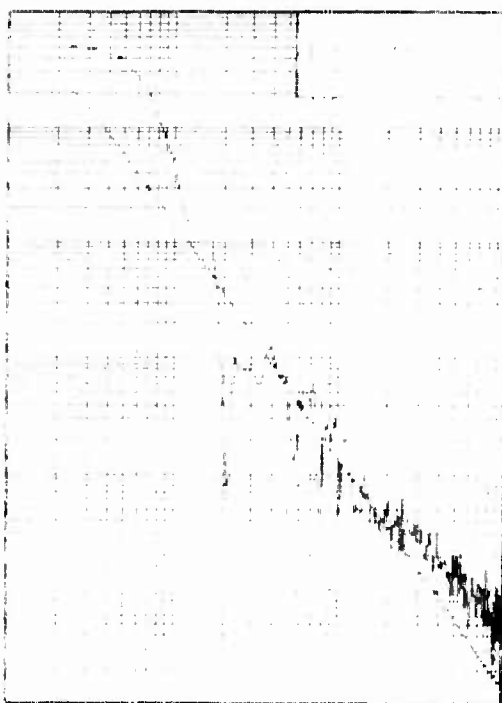
SANITIZED POWER SPECTRA
AT 1045 KILOMETERS   FIGURE 3.1.8

6.481E08   5.180E08

FIGURE 3.1.9

2.034E09

2.539E09
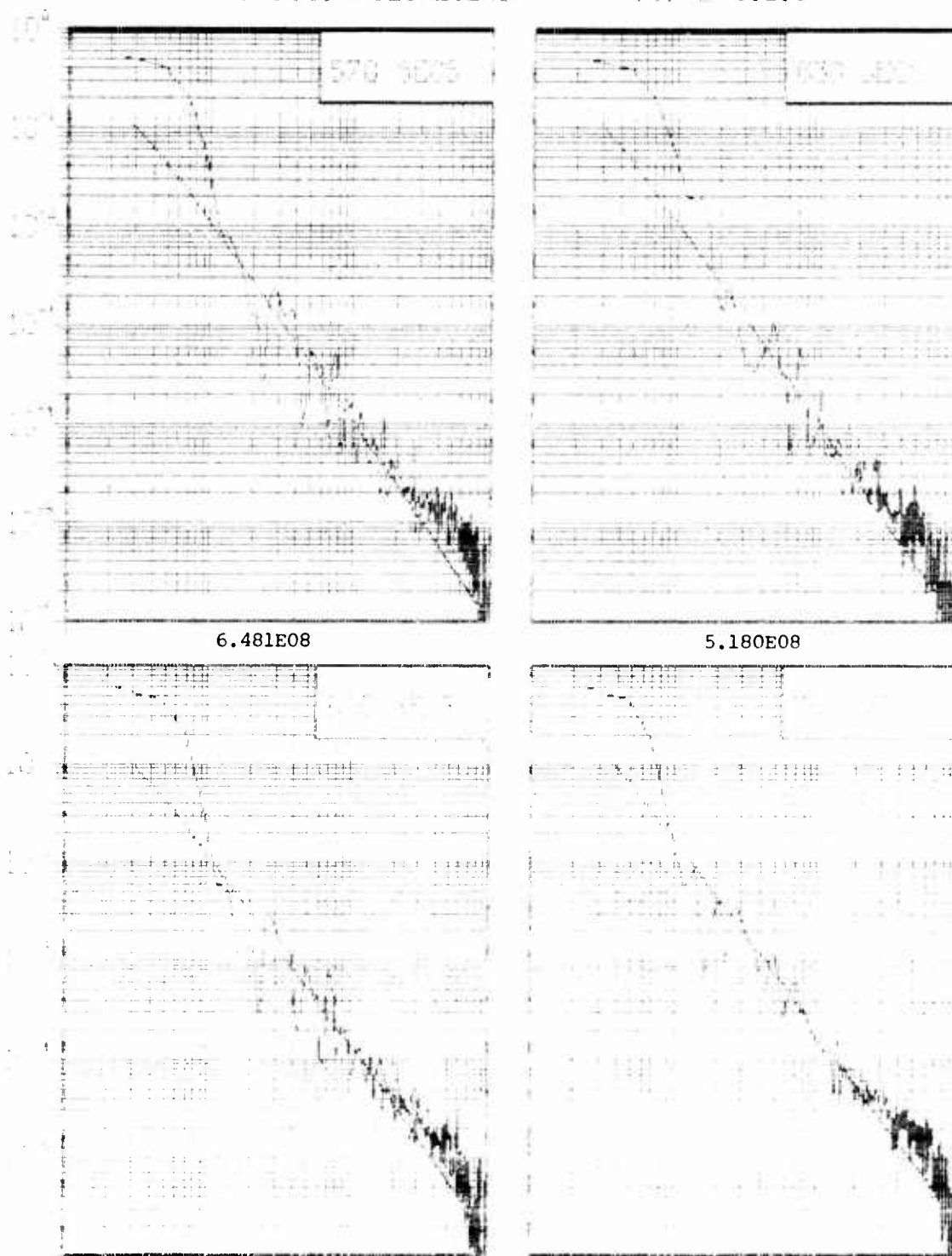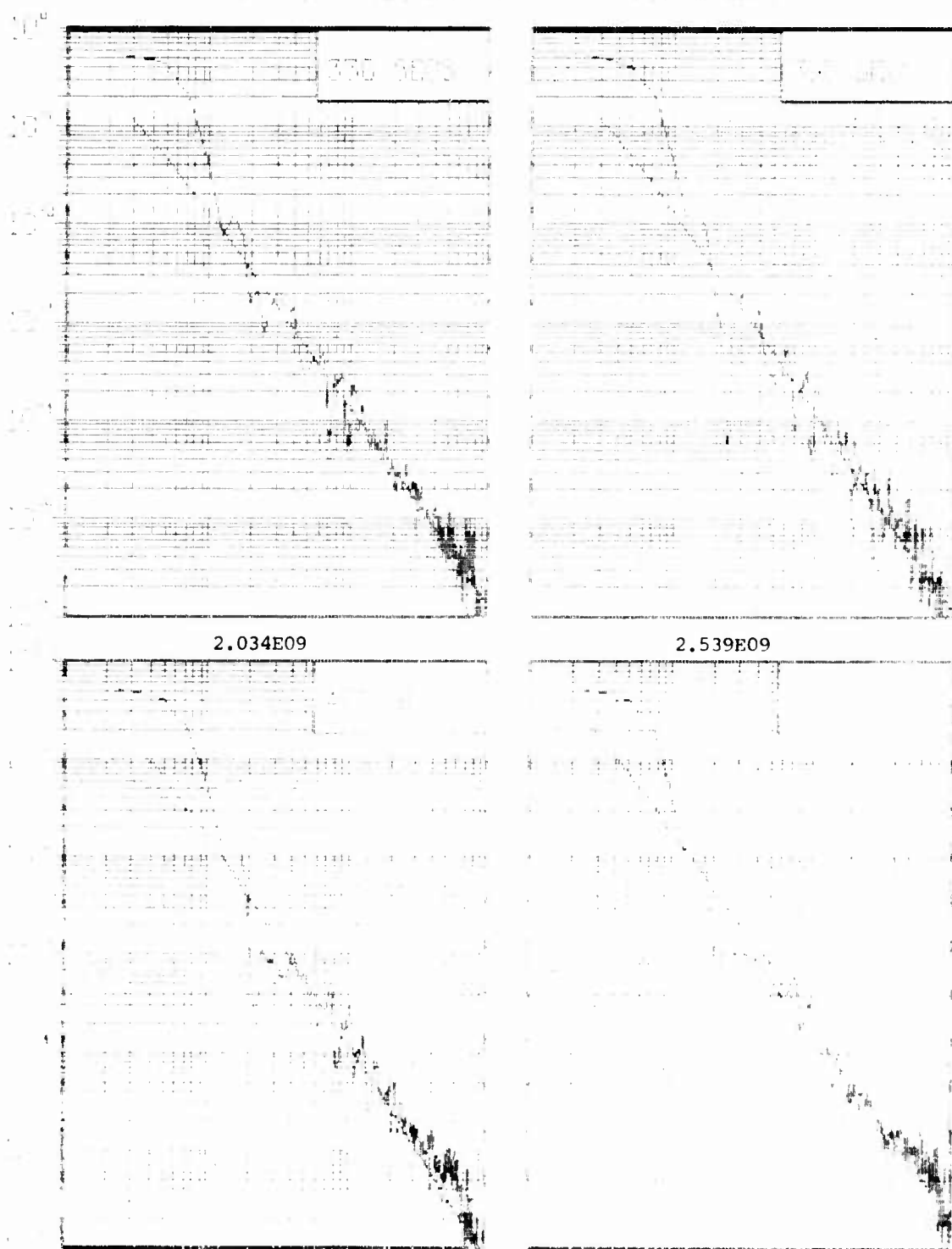
2.201E09

$ABCISSA \times \frac{\pi}{2} = k$ (radians/kilometer)

1.362E09

55

SANITIZED POWER SPECTRA

AT 1000 KILOMETERS   FIGURE 3.1.10
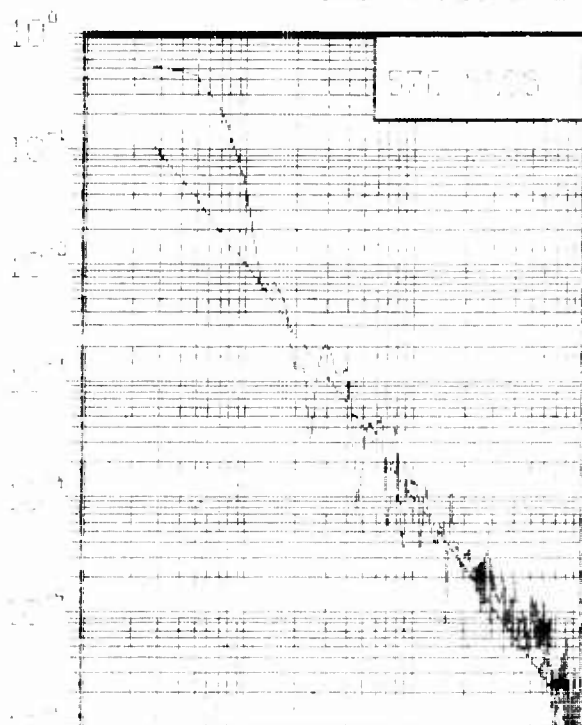
7.52E08   5.592E08

2.400E08   ABCISSA x $\frac{\pi}{2}$ = k (radians/kilometer)   2.383E08

56
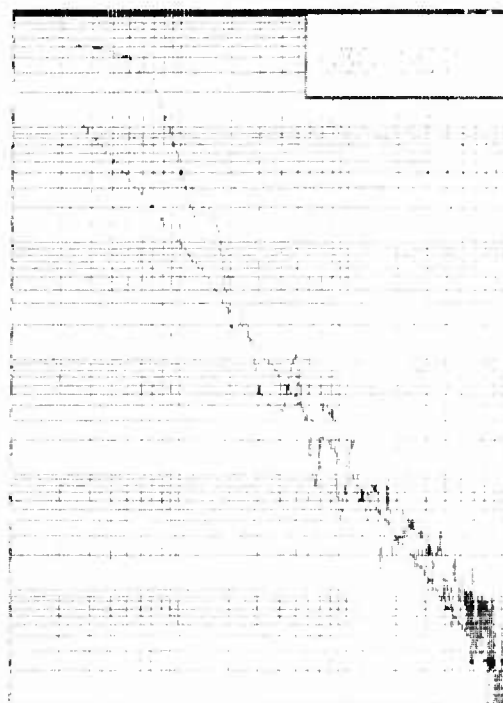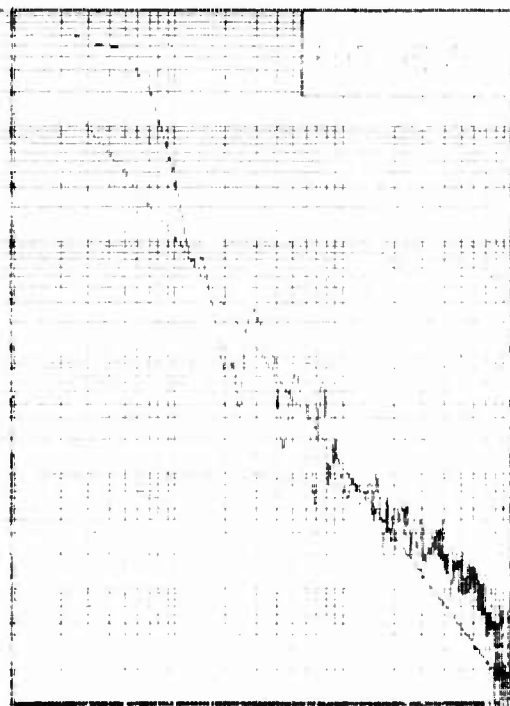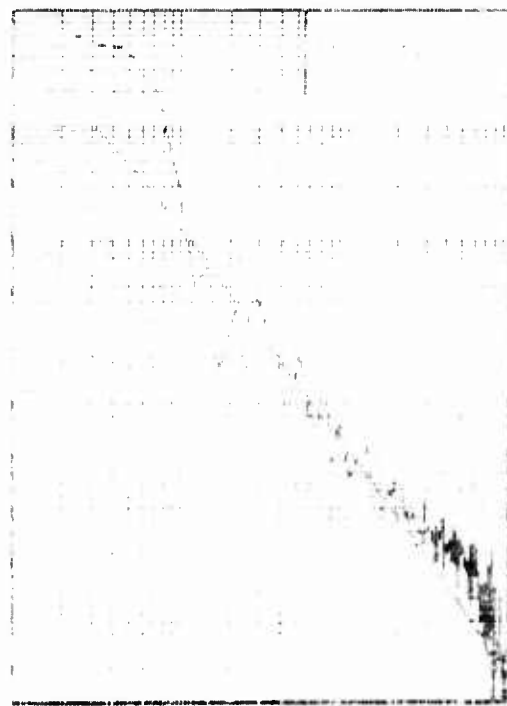
TABLE 3.1.1

MID FREQUENCY POWER LAW FIT EXPONENT NU (EQ. 2.2) 400 KM AT BURST POINT

TIME (SEC)	ALTITUDE (KM) 420.	915.	890.	851.	810.	AVG OVER ALTITUDE
330.	-4.95F-02	-1.25F-02	3.05F-02	-1.89F-02	-2.12E-02	-1.43E-02
390.	-5.33E-02	-6.26F-02	6.77F-02	6.42F-02	6.04E-02	1.55E-02
450.	-8.42E-02	5.84E-03	4.74E-02	7.12F-02	7.53F-02	2.27E-02
510.	-9.33F-02	5.36F-02	8.66F-02	4.3 F-03	2.00E-02	1.42E-02
570.	-8.01F-02	-4.88E-02	-3.7F-02	-5.26F-02	-5.85F-02	-5.56E-02
630.	-6.57E-02	-5.72F-02	-3.84E-02	-1.71F-02	-2.15E-02	-4.00E-02
690.	-9.55F-02	-6.64E-02	-4.46F-03	1.82E-02	6.64E-03	-2.83E-02
750.	-6.03E-02	-5.40F-02	-4.29F-03	-3.47F-02	-2.77E-03	-3.14E-02
TIME AVG	-7.27F-02	-3.03F-02	1.79E-02	4.95F-03	7.05F-03	

MID FREQUENCY POWER LAW FIT EXPONENT NU (EQ. 2.2) 600 KM AT BURST POINT

TIME (SEC)	ALTITUDE (KM) 1120.	1114.	1074.	1045.	1000.	AVG OVER ALTITUDE
330.	-4.55E-02	6.31F-02	6.46E-02	3.44E-03	-1.45F-02	1.22E-02
390.	-4.61F-02	-3.94F-02	5.67F-02	4.78F-02	1.79F-02	5.36F-03
450.	-8.43F-02	-3.91F-03	2.46E-02	1.77F-03	2.91E-02	-6.56E-03
510.	-5.74E-02	1.16E-02	2.55F-02	-2.06F-03	2.06E-02	3.09E-04
570.	-5.28E-02	-6.27F-02	-2.87F-02	-7.66F-02	-3.51E-03	-4.56E-02
630.	-1.44F-01	-1.31F-02	-1.15F-02	3.25F-03	-5.53F-02	-4.34E-02
690.	-1.77F-01	-4.25F-03	1.15F-02	-5.46F-02	-4.40E-02	-5.56E-02
750.	-1.48F-01	-1.44F-01	-5.52F-02	-1.05F-02	-3.89E-04	-7.07E-02
TIME AVG	-9.35E-02	-2.53F-02	1.05F-02	-1.04F-02	-7.06F-03	

MID FREQUENCY POWER LAW FIT EXPONENT NU (EQ. 2.2) 800 KM AT BURST POINT

TIME (SEC)	ALTITUDE (KM) 1320.	1315.	1265.	1234.	1140.	AVG OVER ALTITUDE
330.	7.06F-02	4.05F-02	7.59F-02	3.34F-02	3.60F-02	4.51F-02
390.	-5.01F-02	-3.81F-02	6.60F-02	7.65F-02	3.04E-02	2.34E-02
450.	-9.44F-02	1.77F-02	8.04F-02	3.49F-02	3.86F-02	3.82E-02
510.	-5.47F-02	4.52F-02	8.7F-02	-5.44F-02	3.74E-02	3.15F-03
570.	-1.46F-01	-4.64F-02	-2.24F-02	-5.31F-02	1.25E-02	-6.28E-02
630.	-1.52F-01	-1.73F-01	-1.65F-01	3.73F-03	-4.69F-02	-1.03E-01
690.	-1.39F-01	-2.47F-01	-5.39F-02	-2.74F-02	6.62E-02	-7.58E-02
750.	-1.44F-01	-1.24F-01	-1.14F-01	-1.34F-01	1.40F-02	-1.07E-01
TIME AVG	-9.73F-02	-7.90F-02	-6.44F-03	-4.14F-03	3.74F-02	

57

TABLE 3.1.2

LOW FREQUENCY POWER LAW FIT EXPONENT NU (EQ. 2.2) 400 KM AT BURST POINT

TIME (SEC)	ALTITUDE (KM)					AVG OVER ALTITUDE
	920.	915.	890.	861.	810.	
330.	4.53E-12	-4.06E-02	3.67E-02	-1.70E-02	-1.66E-02	1.56E-03
390.	-2.26E-02	-1.69E-02	6.66E-02	1.10E-01	8.11E-02	4.36E-02
450.	-6.14E-02	1.01E-02	4.74E-02	4.66E-02	5.63E-02	2.01E-02
510.	-9.33E-02	2.25E-02	3.65E-02	-3.46E-02	4.46E-02	-4.89E-03
570.	-7.13E-02	8.55E-03	1.85E-02	1.93E-02	-7.15E-03	9.58E-03
630.	-5.64E-02	-8.36E-02	1.89E-02	1.31E-01	4.12E-03	2.43E-03
690.	-1.26E-01	-1.45E-01	-3.52E-02	3.0E-02	-3.18E-03	-5.57E-02
750.	-2.33E-02	3.18E-02	-4.86E-02	-7.17E-02	7.76E-02	-6.86E-03
TIME AVG	-5.14E-02	-2.65E-02	2.76E-02	2.67E-02	2.98E-02	

LOW FREQUENCY POWER LAW FIT EXPONENT NU (EQ. 2.2) 600 KM AT BURST POINT

TIME (SEC)	ALTITUDE (KM)					AVG OVER ALTITUDE
	1120.	1114.	1078.	1045.	1000.	
330.	-3.52E-02	1.53E-02	-1.93E-02	1.19E-02	-1.89E-03	-5.82E-03
390.	-2.93E-02	-9.25E-02	1.29E-02	4.49E-02	2.11E-02	-8.42E-03
450.	-4.21E-02	-4.95E-02	5.06E-02	4.7E-02	8.07E-02	1.74E-02
510.	-2.90E-02	-1.46E-02	4.41E-02	1.26E-02	-2.44E-03	2.1E-03
570.	-8.96E-02	-3.29E-02	-4.74E-02	1.79E-02	-1.36E-03	-3.05E-02
630.	-7.91E-02	-1.11E-02	-3.04E-02	1.44E-02	-2.64E-02	-2.53E-02
690.	-1.21E-01	-4.32E-02	-9.65E-03	-2.56E-02	-1.19E-02	-4.23E-02
750.	-1.44E-01	-1.02E-01	-7.26E-02	-3.28E-02	-2.84E-02	-7.58E-02
TIME AVG	-7.10E-02	-4.13E-02	-8.92E-03	1.19E-02	3.91E-03	

LOW FREQUENCY POWER LAW FIT EXPONENT NU (EQ. 2.2) 800 KM AT BURST POINT

TIME (SEC)	ALTITUDE (KM)					AVG OVER ALTITUDE
	1320.	1315.	1285.	1239.	1190.	
330.	-6.45E-02	2.66E-02	1.66E-02	-3.28E-02	-9.94E-03	-1.24E-02
390.	-5.01E-02	-1.03E-01	-6.57E-02	7.62E-02	1.42E-01	-1.10E-04
450.	-6.07E-02	-5.30E-02	5.56E-02	1.73E-02	1.17E-01	1.53E-02
510.	-8.29E-02	-3.76E-02	3.95E-02	-5.77E-02	3.79E-02	-1.62E-02
570.	-5.27E-02	-2.96E-02	1.53E-02	3.45E-02	-7.89E-02	-2.26E-02
630.	-1.18E-01	-1.27E-01	-7.07E-02	-2.65E-02	7.74E-02	-5.37E-02
690.	-7.50E-02	-1.74E-01	5.53E-04	5.74E-03	3.80E-02	-4.00E-02
750.	-6.30E-02	-6.94E-02	-1.20E-01	-7.66E-02	1.25E-01	-3.54E-02
TIME AVG	-7.09E-02	-7.13E-02	-1.64E-02	-4.26E-03	5.67E-02	

58

TABLE 3.1.3

MID FREQUENCY POWER LAW FIT OUTER SCALE L (EQ. 2.2 - KM/RADIAN) AT 400 KM

TIME	ALTITUDE (KM)					AVG OVER
(SEC)	920.	915.	890.	851.	810.	ALTITUDE
330.	2.08E+02	3.49E+02	3.71E+02	4.35E+02	5.06E+02	3.74E+02
390.	2.87E+02	3.29E+02	3.61E+02	3.91E+02	4.98E+02	3.73E+02
450.	3.40E+02	3.96E+02	4.25E+02	4.04E+02	4.47E+02	4.02E+02
510.	3.59E+02	3.98E+02	4.10E+02	4.42E+02	3.83E+02	3.98E+02
570.	4.81E+02	3.86E+02	4.43E+02	4.78E+02	3.98E+02	4.37E+02
630.	3.82E+02	4.12E+02	4.20E+02	4.46E+02	4.63E+02	4.24E+02
690.	3.62E+02	4.22E+02	4.94E+02	4.21E+02	3.96E+02	4.19E+02
750.	3.75E+02	5.46E+02	3.94E+02	4.56E+02	3.91E+02	4.32E+02
TIME						
AVG	3.49E+02	4.05E+02	4.15E+02	4.34E+02	4.35E+02	

MID FREQUENCY POWER LAW FIT OUTER SCALE L (EQ. 2.2 - KM/RADIAN) AT 600 KM

TIME	ALTITUDE (KM)					AVG OVER
(SEC)	1120.	1114.	1078.	1045.	1000.	ALTITUDE
330.	2.49E+02	2.47E+02	2.83E+02	3.61E+02	4.00E+02	3.08E+02
390.	2.33E+02	2.45E+02	2.79E+02	3.82E+02	3.94E+02	3.06E+02
450.	2.19E+02	3.05E+02	3.22E+02	3.61E+02	4.56E+02	3.33E+02
510.	2.81E+02	3.12E+02	3.47E+02	3.99E+02	3.61E+02	3.40E+02
570.	2.42E+02	3.66E+02	3.70E+02	5.04E+02	3.69E+02	3.70F+02
630.	4.08E+02	4.77E+02	5.08E+02	3.25E+02	3.72E+02	4.18E+02
690.	3.04E+02	3.43E+02	4.40E+02	4.08E+02	3.73E+02	3.74E+02
750.	3.34E+02	3.64E+02	4.20E+02	4.80E+02	3.66E+02	3.93E+02
TIME						
AVG	2.84E+02	3.32E+02	3.71E+02	4.02E+02	3.86E+02	

MID FREQUENCY POWER LAW FIT OUTER SCALE L (EQ. 2.2 - KM/RADIAN) AT 800 KM

TIME	ALTITUDE (KM)					AVG OVER
(SEC)	1320.	1315.	1265.	1239.	1190.	ALTITUDE
330.	2.78E+02	3.08E+02	2.97E+02	3.48E+02	4.00E+02	3.26E+02
390.	4.00E+02	4.80E+02	3.52E+02	4.77E+02	4.70E+02	4.35E+02
450.	5.15E+02	3.92E+02	3.60E+02	6.51E+02	3.91E+02	4.62E+02
510.	3.62E+02	3.51E+02	4.40E+02	6.44E+02	3.85E+02	4.38E+02
570.	3.74E+02	3.82E+02	4.40E+02	3.99E+02	3.20E+02	3.83E+02
630.	4.40E+02	5.12E+02	5.38E+02	2.43E+02	3.01E+02	4.07E+02
690.	4.40E+02	3.96E+02	4.35E+02	3.68E+02	2.55E+02	3.79E+02
750.	4.80E+02	3.94E+02	4.36E+02	4.60E+02	2.65E+02	4.07E+02
TIME						
AVG	4.11E+02	4.03E+02	4.13E+02	4.49E+02	3.48E+02	

TABLE 3.1.4

LOW FREQUENCY POWER LAW FIT OUTER SCALE L (EQ. 2.2 - KM/RADIAN) AT 400 KM

TIME			ALTITUDE (KM)			AVG OVER
(SEC)	920.	915.	890.	851.	810.	ALTITUDE
330.	3.73E+02	3.51E+02	2.89E+02	3.19E+02	5.59E+02	3.80E+02
390.	4.57E+02	4.12E+02	3.80E+02	3.69E+02	5.09E+02	4.25E+02
450.	3.72E+02	4.45E+02	3.99E+02	3.80E+02	4.45E+02	4.08E+02
510.	4.00E+02	4.89E+02	3.32E+02	3.63E+02	4.01E+02	3.97E+02
570.	3.61E+02	4.04E+02	4.37E+02	4.53E+02	4.23E+02	4.16E+02
630.	3.95E+02	3.11E+02	5.45E+02	4.01E+02	4.78E+02	4.26E+02
690.	2.95E+02	3.30E+02	4.55E+02	4.46E+02	4.72E+02	4.00E+02
750.	3.70E+02	3.83E+02	4.10E+02	3.84E+02	3.85E+02	3.86E+02
TIME AVG	3.78E+02	3.92E+02	4.06E+02	3.89E+02	4.59E+02	

LOW FREQUENCY POWER LAW FIT OUTER SCALE L (EQ. 2.2 - KM/RADIAN) AT 600 KM

TIME			ALTITUDE (KM)			AVG OVER
(SEC)	1120.	1114.	1078.	1045.	1000.	ALTITUDE
330.	3.90E+02	4.40E+02	3.77E+02	3.33E+02	4.09E+02	3.90E+02
390.	3.79E+02	4.40E+02	4.21E+02	4.24E+02	4.28E+02	4.19E+02
450.	3.98E+02	4.68E+02	3.67E+02	3.68E+02	3.24E+02	3.85E+02
510.	4.45E+02	3.18E+02	3.99E+02	4.72E+02	4.27E+02	4.12E+02
570.	4.94E+02	3.72E+02	4.16E+02	4.29E+02	4.32E+02	4.29E+02
630.	3.95E+02	4.64E+02	4.39E+02	4.89E+02	4.77E+02	4.53E+02
690.	7.02E+02	4.46E+02	4.60E+02	4.30E+02	4.86E+02	5.05E+02
750.	4.54E+02	4.08E+02	3.98E+02	4.28E+02	3.71E+02	4.12E+02
TIME AVG	4.57E+02	4.19E+02	4.10E+02	4.22E+02	4.19E+02	

LOW FREQUENCY POWER LAW FIT OUTER SCALE L (EQ. 2.2 - KM/RADIAN) AT 800 KM

TIME			ALTITUDE (KM)			AVG OVER
(SEC)	1320.	1315.	1265.	1239.	1190.	ALTITUDE
330.	4.11E+02	4.00E+02	3.88E+02	3.90E+02	4.38E+02	4.05E+02
390.	4.43E+02	5.41E+02	4.02E+02	3.48E+02	3.67E+02	4.20E+02
450.	3.83E+02	3.89E+02	4.33E+02	4.77E+02	4.06E+02	4.18E+02
510.	4.00E+02	3.66E+02	4.27E+02	3.98E+02	4.24E+02	4.03E+02
570.	4.00E+02	3.71E+02	3.48E+02	3.83E+02	5.07E+02	4.02E+02
630.	4.81E+02	4.28E+02	4.68E+02	4.05E+02	3.71E+02	4.31E+02
690.	3.60E+02	4.58E+02	3.39E+02	4.19F+02	4.30E+02	4.01E+02
750.	3.70E+02	3.30E+02	3.75E+02	4.54E+02	4.07E+02	3.87E+02
TIME AVG	4.06E+02	4.10E+02	3.97E+02	4.09E+02	4.19E+02	
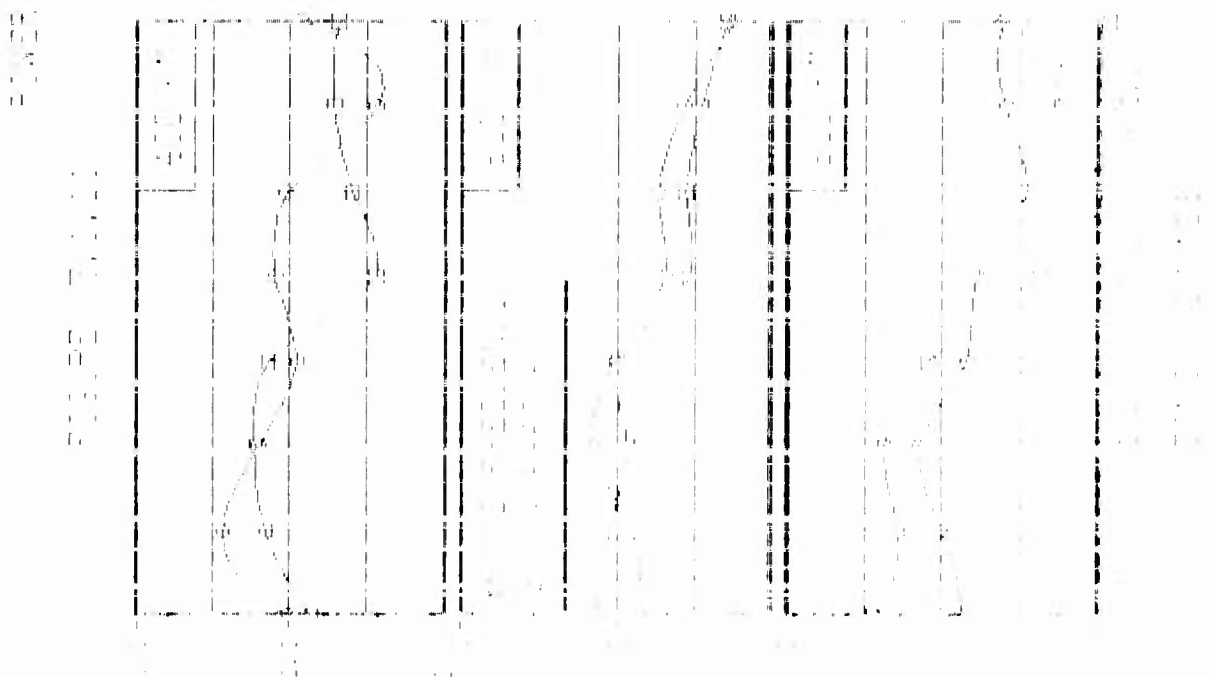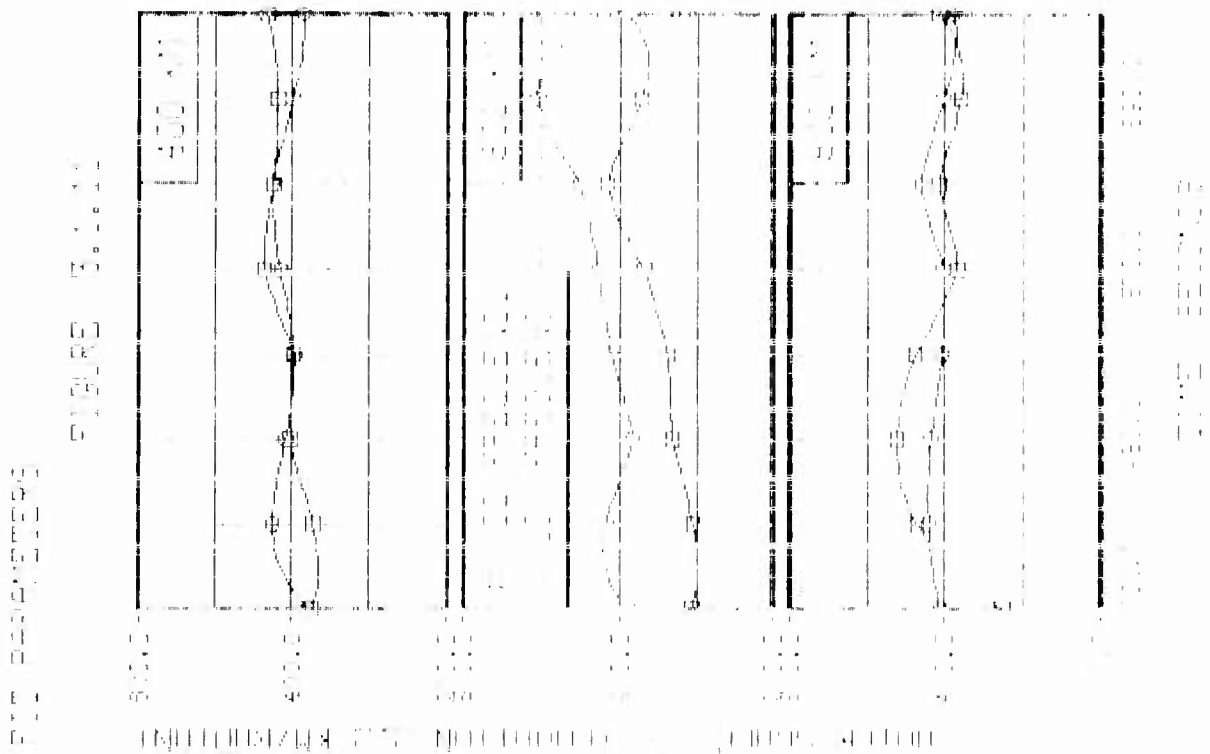
60

TABLE 3.1.5

MIC FREQUENCY POWER LAW SLOPE 400 KM AT BURST POINT

TIME (SEC)	920.	915.	890.	851.	810.	AVG OVER ALTITUDE
330.	-1.90E+00	-1.98F+00	-2.06F+00	-1.96F+00	-1.96E+00	-1.97E+00
390.	-1.89E+00	-1.88E+00	-2.13F+00	-2.14E+00	-2.12E+00	-2.09 F+00
450.	-1.83F+00	-2.01F+00	-2.10F+00	-2.14E+00	-2.15E+00	-2.05E+00
510.	-1.91F+00	-2.11E+00	-2.17E+00	-2.01F+00	-2.04E+00	-2.03E+00
570.	-1.84E+00	-1.90F+00	-1.92F+00	-2.08E+00	-2.17E+00	-1.98E+00
630.	-1.87F+00	-1.89F+00	-1.92E+00	-1.97E+00	-1.96E+00	-1.92E+00
690.	-1.81E+00	-1.86E+00	-1.99F+00	-2.04F+00	-2.01E+00	-1.94E+00
750.	-1.88F+00	-1.89F+00	-1.91F+00	-1.93E+00	-1.95E+00	-1.91E+00
TIME AVG	-1.85E+00	-1.94F+00	-2.03F+00	-2.03F+00	-2.04E+00	

MIC FREQUENCY POWER LAW SLOPE 600 KM AT BURST POINT

TIME (SEC)	1120.	1114.	1078.	1045.	1000.	AVG OVER ALTITUDE
330.	-1.91E+00	-2.11F+00	-2.13F+00	-2.01F+00	-1.97E+00	-2.02E+00
390.	-1.91E+00	-1.92F+00	-2.09E+00	-2.17F+00	-2.04E+00	-2.01E+00
450.	-1.83F+00	-1.99F+00	-2.05E+00	-2.00E+00	-2.06E+00	-1.99E+00
510.	-1.89F+00	-2.02E+00	-2.05F+00	-1.95F+00	-2.04E+00	-1.99E+00
570.	-1.90F+00	-1.86F+00	-1.94E+00	-1.86F+00	-1.98E+00	-1.91E+00
630.	-1.71E+00	-1.97E+00	-1.94F+00	-2.02E+00	-1.89E+00	-1.91E+00
690.	-1.65F+00	-1.44F+00	-2.02F+00	-1.89E+00	-1.91E+00	-1.78E+00
750.	-1.70F+00	-1.71F+00	-1.90F+00	-1.98F+00	-2.00E+00	-1.86F+00
TIME AVG	-1.81F+00	-1.88E+00	-2.02E+00	-1.97F+00	-1.99E+00	

MIC FREQUENCY POWER LAW SLOPE 800 KM AT BURST POINT

TIME (SEC)	1320.	1315.	1278.	1234.	1190.	AVG OVER ALTITUDE
330.	-2.00F+00	-2.09F+00	-2.15F+00	-2.07F+00	-2.08E+00	-2.09E+00
390.	-1.90E+00	-1.92F+00	-2.13F+00	-2.15F+00	-2.19E+00	-2.06E+00
450.	-1.91F+00	-2.04E+00	-2.16E+00	-2.14E+00	-2.20E+00	-2.08E+00
510.	-1.96E+00	-2.09F+00	-2.14F+00	-1.89F+00	-2.08F+00	-2.02E+00
570.	-1.71F+00	-1.82E+00	-1.95E+00	-1.84F+00	-2.03E+00	-1.87E+00
630.	-1.70F+00	-1.65F+00	-1.68F+00	-2.03E+00	-1.91F+00	-1.79E+00
690.	-1.74E+00	-1.61E+00	-1.90E+00	-1.95F+00	-2.11E+00	-1.85E+00
750.	-1.61F+00	-1.76F+00	-1.78F+00	-1.78F+00	-2.03F+00	-1.74E+00
TIME AVG	-1.90F+00	-1.85F+00	-1.99F+00	-1.99F+00	-2.08E+00	

MID FREQUENCY = k ≤ 1.4 radians/km

62

TABLE 3.1.6

LOW FREQUENCY POWER LAW SLOPE 400 KM AT BURST POINT

TIME	ALTITUDE (KM)					AVG OVER
(SEC)	920.	915.	890.	851.	810.	ALTITUDE
330.	-2.09E+00	-1.92E+00	-2.07E+00	-1.97E+00	-1.97E+00	-2.00E+00
390.	-1.95E+00	-1.97E+00	-2.15E+00	-2.22E+00	-2.16E+00	-2.09E+00
450.	-1.08E+00	-2.02E+00	-2.10E+00	-2.09E+00	-2.12E+00	-2.04E+00
510.	-1.81E+00	-2.05E+00	-2.07E+00	-1.93E+00	-2.09E+00	-1.99E+00
570.	-1.86E+00	-2.02E+00	-2.20E+00	-2.04E+00	-1.99E+00	-2.02E+00
630.	-1.68E+00	-1.83E+00	-2.04E+00	-2.26E+00	-2.01E+00	-2.06E+00
690.	-1.75E+00	-1.71E+00	-1.93E+00	-2.07E+00	-1.99E+00	-1.89E+00
750.	-1.95E+00	-2.06E+00	-1.90E+00	-1.86E+00	-2.16E+00	-1.99E+00
TIME AVG	-1.90E+00	-1.95E+00	-2.06E+00	-2.05E+00	-2.06E+00	

LOW FREQUENCY POWER LAW SLOPE 600 KM AT BURST POINT

TIME	ALTITUDE (KM)					AVG OVER
(SEC)	1120.	1114.	1078.	1045.	1000.	ALTITUDE
330.	-1.93E+00	-2.03E+00	-1.96E+00	-2.02E+00	-2.00E+00	-1.99E+00
390.	-1.94E+00	-1.82E+00	-2.03E+00	-2.04E+00	-2.04E+00	-1.96E+00
450.	-1.92E+00	-1.95E+00	-2.10E+00	-2.09E+00	-2.16E+00	-2.05E+00
510.	-1.94E+00	-1.97E+00	-2.09E+00	-2.03E+00	-2.00E+00	-2.00E+00
570.	-1.82E+00	-1.93E+00	-1.91E+00	-2.04E+00	-2.00E+00	-1.94E+00
630.	-1.84E+00	-1.98E+00	-1.94E+00	-2.04E+00	-1.95E+00	-1.95E+00
690.	-1.76E+00	-1.91E+00	-1.96E+00	-1.95E+00	-1.98E+00	-1.92E+00
750.	-1.71E+00	-1.80E+00	-1.86E+00	-1.93E+00	-1.94E+00	-1.85E+00
TIME AVG	-1.86E+00	-1.92E+00	-1.96E+00	-2.02E+00	-2.01E+00	

LOW FREQUENCY POWER LAW SLOPE 800 KM AT BURST POINT

TIME	ALTITUDE (KM)					AVG OVER
(SEC)	1320.	1315.	1265.	1239.	1190.	ALTITUDE
330.	-1.87E+00	-2.05E+00	-2.03E+00	-1.93E+00	-1.95E+00	-1.97E+00
390.	-1.90E+00	-1.79E+00	-1.87E+00	-2.15E+00	-2.28E+00	-2.00E+00
450.	-1.68E+00	-1.89E+00	-2.11E+00	-2.04E+00	-2.23E+00	-2.03E+00
510.	-1.63E+00	-1.93E+00	-2.08E+00	-1.95E+00	-2.06E+00	-1.97E+00
570.	-1.90E+00	-1.94E+00	-2.03E+00	-2.07E+00	-1.84E+00	-1.95E+00
630.	-1.77E+00	-1.75E+00	-1.86E+00	-1.95E+00	-2.15E+00	-1.89E+00
690.	-1.85E+00	-1.65E+00	-2.03E+00	-2.02E+00	-2.06E+00	-1.92E+00
750.	-1.87E+00	-1.86E+00	-1.76E+00	-1.95E+00	-2.27E+00	-1.92E+00
TIME AVG	-1.36E+00	-1.86E+00	-1.97E+00	-1.99E+00	-2.13E+00	

Low Frequency = $k \leq 0.24$ radians/km

63

TABLE 3.1.7

MID FREQUENCY POWER LAW FIT NUMERATOR (EQ. 2.2) 400 KM AT BURST POINT					
TIME			ALTITUDE (KM)		AVG OVER
(SEC)	920.	915.	890.	851.	810.	ALTITUDE
330.	5.52E-06	5.86E-06	5.51E-06	5.10E-06	4.84E-06	5.57E-06
390.	5.46E-06	6.56E-06	4.99E-06	4.86E-06	4.73E-06	5.32E-06
450.	7.56E-06	5.56E-06	4.93E-06	4.29E-06	5.15E-06	5.50E-06
510.	6.01E-06	5.62E-06	4.10E-06	7.88E-06	7.44E-06	6.21E-06
570.	8.81E-06	5.34E-06	4.14E-06	4.70E-06	4.36E-06	5.47E-06
630.	7.69E-06	5.14E-06	4.57E-06	4.50E-06	5.09E-06	5.40E-06
690.	6.25E-06	6.73E-06	4.07E-06	4.28E-06	4.18E-06	5.10E-06
750.	8.29E-06	8.28E-06	8.57E-06	8.78E-06	8.97E-06	8.58E-06
TIME AVG	6.95E-06	6.14E-06	5.11E-06	5.67E-06	5.60E-06	

MID FREQUENCY POWER LAW FIT NUMERATOR (EQ. 2.2) 600 KM AT BURST POINT					
TIME			ALTITUDE (KM)		AVG OVER
(SEC)	1120.	1114.	1078.	1045.	1000.	ALTITUDE
330.	3.83E-06	3.96E-06	3.50E-06	4.27E-06	3.21E-06	3.75E-06
390.	3.82E-06	4.69E-06	3.23E-06	3.02E-06	2.73E-06	3.50E-06
450.	5.32E-06	3.66E-06	3.11E-06	2.43E-06	2.92E-06	3.49E-06
510.	4.49E-06	3.57E-06	2.92E-06	4.80E-06	4.79E-06	4.12E-06
570.	8.12E-06	4.25E-06	3.06E-06	3.52E-06	3.21E-06	4.43E-06
630.	5.34E-06	3.31E-06	3.31E-06	3.49E-06	3.76E-06	4.04F-06
690.	6.04E-06	2.80E-06	2.88E-06	4.75E-06	4.85E-06	4.26E-06
750.	7.82E-06	4.80E-06	5.56E-06	5.90E-06	5.88E-06	5.99E-06
TIME AVG	5.72E-05	3.88E-05	3.45E-06	4.02E-06	3.92E-06	

MID FREQUENCY POWER LAW FIT NUMERATOR (EQ. 2.2) 800 KM AT BURST POINT					
TIME			ALTITUDE (KM)		AVG OVER
(SEC)	1320.	1315.	1265.	1239.	1190.	ALTITUDE
330.	3.29E-06	2.77E-06	2.55E-06	3.24E-06	2.50E-06	2.87E-06
390.	2.77E-06	3.44E-06	2.42E-06	2.20E-06	2.17E-06	2.60E-06
450.	3.85E-06	2.75E-06	2.49E-06	1.98E-06	2.33E-06	2.68E-06
510.	3.27E-06	2.59E-06	1.92E-06	3.22E-06	3.48E-06	2.90E-06
570.	4.81E-06	2.92E-06	2.27E-06	2.68E-06	2.37E-06	3.01E-06
630.	4.78E-06	2.90E-06	2.60E-06	2.56E-06	2.75E-06	3.12E-06
690.	5.38E-06	3.69E-06	1.92E-06	2.70E-06	3.64E-06	3.47E-06
750.	5.41E-06	3.77E-06	4.61E-06	4.70E-06	4.61E-06	4.62E-06
TIME AVG	4.19E-06	3.10E-06	2.60E-06	2.91E-06	2.98E-06	

64

TABLE 3.1.8

LOW FREQUENCY POWER LAW FIT NUMERATOR (EQ. 2.2) 400 KM AT BURST POINT					
TIME			ALTITUDE (KM)		AVG OVER
(SEC)	920.	915.	890.	851.	810.	ALTITUDE
330.	4.38E-06	4.71E-06	4.75E-06	4.64E-06	4.68E-06	4.63E-06
390.	4.00E-06	5.30E-06	3.92E-06	4.10E-06	4.21E-06	4.31E-06
450.	4.92E-06	4.21E-06	4.42E-06	3.81E-06	4.61E-06	4.40E-06
510.	4.81E-06	4.30E-06	3.87E-06	5.33E-06	7.53E-06	5.17E-06
570.	3.84E-06	3.79E-06	3.25E-06	3.49E-06	3.70E-06	3.62E-06
630.	3.79E-06	3.51E-06	3.23E-06	3.00E-06	3.81E-06	3.49E-06
690.	3.63E-06	3.44E-06	3.66E-06	3.59E-06	3.70E-06	3.60E-06
750.	6.03E-06	4.57E-06	5.36E-06	6.41E-06	4.92E-06	5.46E-06
TIME AVG	4.43E-06	4.24E-06	4.06E-06	4.30E-06	4.65E-06	

LOW FREQUENCY POWER LAW FIT NUMERATOR (EQ. 2.2) 600 KM AT BURST POINT					
TIME			ALTITUDE (KM)		AVG OVER
(SEC)	1120.	1114.	1078.	1045.	1000.	ALTITUDE
330.	3.18E-06	3.58E-06	3.73E-06	3.17E-06	3.28E-06	3.39E-06
390.	2.87E-06	4.43E-06	3.36E-06	3.66E-06	2.90E-06	3.44E-06
450.	3.61E-06	3.36E-06	3.12E-06	2.55E-06	2.73E-06	3.08E-06
510.	3.46E-06	3.03E-06	2.65E-06	3.42E-06	4.99E-06	3.51E-06
570.	5.34E-06	2.79E-06	2.52E-06	2.49E-06	2.48E-06	3.12E-06
630.	3.53E-06	2.87E-06	2.47E-06	2.43E-06	2.91E-06	2.84E-06
690.	4.34E-06	2.68E-06	2.91E-06	3.49E-06	2.85E-06	3.25E-06
750.	5.04E-06	3.73E-06	4.27E-06	5.20E-06	3.95E-06	4.44E-06
TIME AVG	3.92E-06	3.31E-06	3.13E-06	3.30E-06	3.26E-06	

LOW FREQUENCY POWER LAW FIT NUMERATOR (EQ. 2.2) 800 KM AT BURST POINT					
TIME			ALTITUDE (KM)		AVG OVER
(SEC)	1320.	1315.	1265.	1239.	1190.	ALTITUDE
330.	2.32E-06	2.24E-06	2.60E-06	2.30E-06	2.43E-06	2.38E-06
390.	2.20E-06	3.43E-06	2.44E-06	2.24E-06	1.95E-06	2.45E-06
450.	2.50E-06	2.36E-06	2.13E-06	1.57E-06	1.85E-06	2.08E-06
510.	2.45E-06	2.30E-06	1.79E-06	2.24E-06	2.77E-06	2.31E-06
570.	4.01E-06	2.11E-06	1.68E-06	1.67E-06	1.85E-06	2.26E-06
630.	2.74E-06	2.21E-06	1.99E-06	1.72E-06	1.75E-06	2.08E-06
690.	3.52E-06	2.01E-06	1.92E-06	2.36E-06	2.00E-06	2.36E-06
750.	4.08E-06	2.95E-06	3.21E-06	3.16E-06	2.64E-06	3.21E-06
TIME AVG	2.98E-06	2.45E-06	2.22E-06	2.16E-06	2.15E-06	

66

3.2   PSD, EXPONENTIAL FIT DATA PARAMETERS
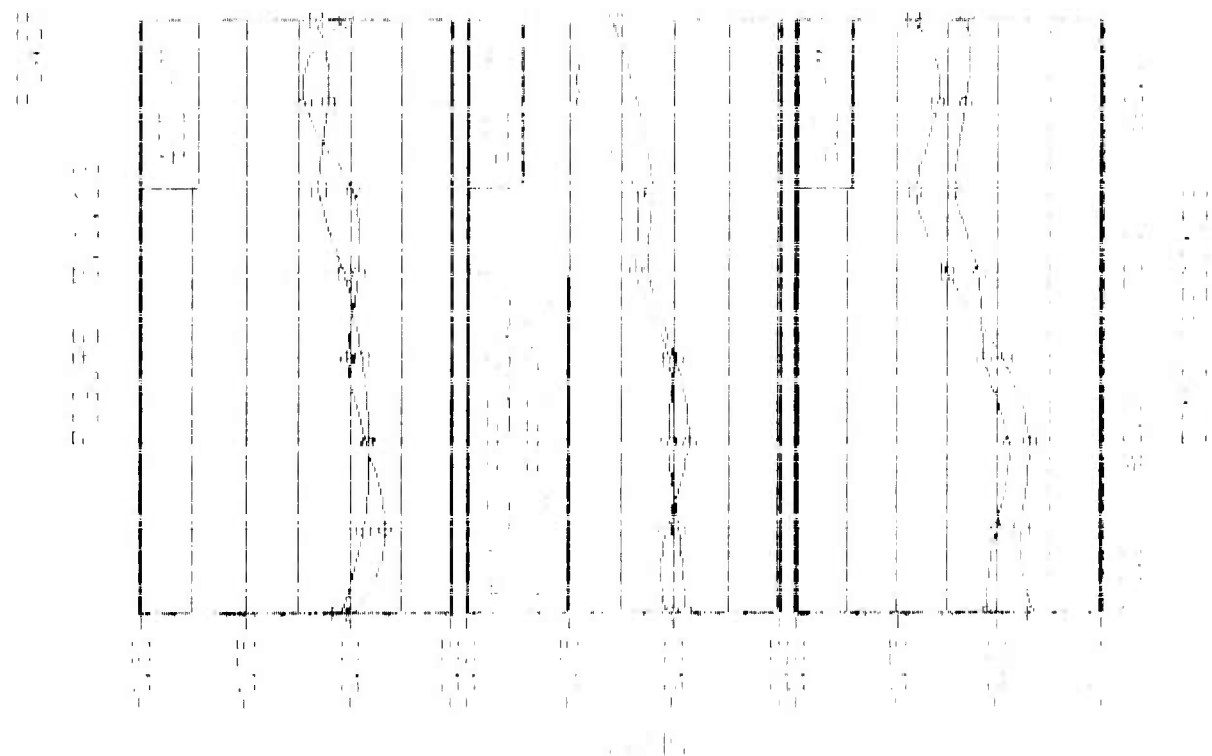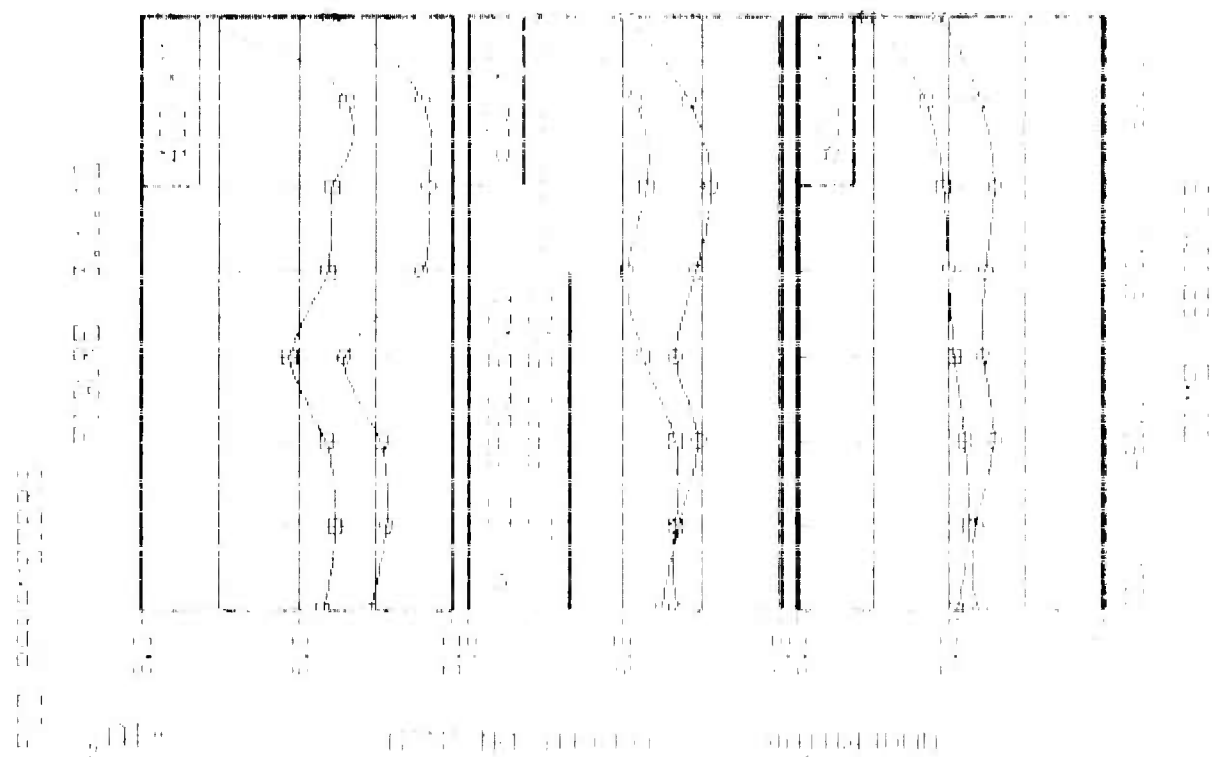
In this section we overlay the measured data b a two term exponential fit. A similar PSD representation for the STARFISH northern conjugate beta patch striations is presented in Reference 10. Figures 3.2.1 through 3.2.10 present part of our PSD overlayed data as a function of time, at constant altitudes. In a review of these plots it is evident that a departure occurs from the data (at $k \leq 0.04$ radians/km) when fit by a single exponential $P(f) = I_1 \exp(-k/k_0)$ over the range $0.016 \leq k \leq 0.236$ radians/km. Thus to prevent the underestimation of the very low frequency power ($k \leq 0.04$ radians/km) a second semi-log linear curve I_2 is added to represent this low frequency region.

Tables 3.2.1 through 3.2.3 summarize the least square fit values for the semi-log linear analytic fit parameters. Tables 3.2.1 and 3.2.2 present the intercept, I_1, and slope $(1/k_{01})$ for the frequency fit interval $(0.016 \leq k \leq 0.236$ radians/km) for the three different locations of the striated region. Table 3.2.3 presents the intercept I_2, $(1/k_{02})$ for the very low frequency range $(0 < k \leq 0.04$ radians/km) at only one altitude. Because of the steepness of the data in this frequency range, these parameters do not vary significantly with altitude and therefore tabulated values of the parameters are omitted for the other two altitudes of the luminous striation volume. The tables also present the values of these parameters averaged over time and over altitude. The time variation of these parameters (of the slope, the intercepts I_1 and I_2) are presented in Figure 3.2.11.

SANITIZED POWER SPECTRUM
AT 1120 KILOMETERS   FIGURE 3.2.1

ABCISSA $x \ \dfrac{\pi}{2} = k$ (radians/kilometer)

68
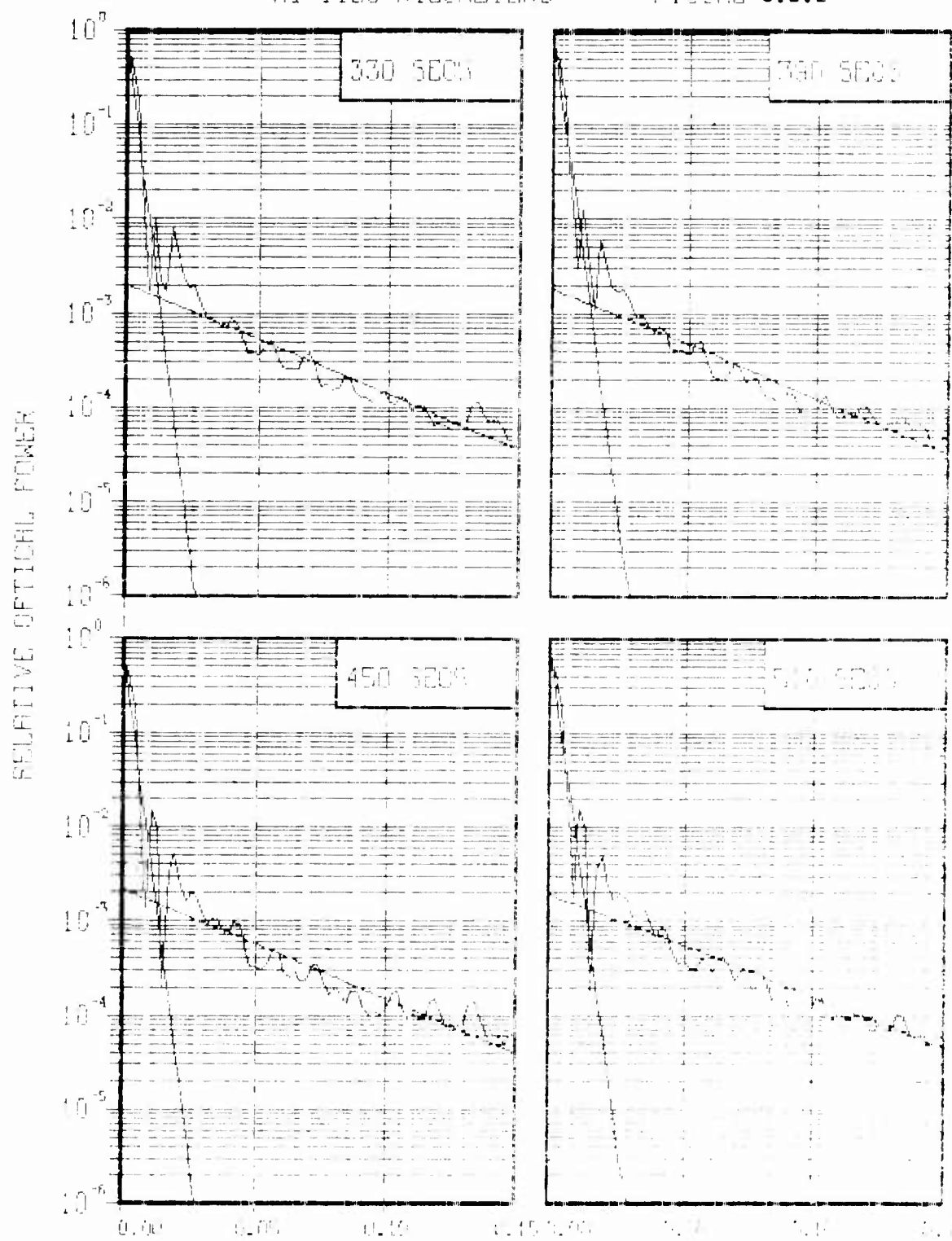
SANITIZED POWER SPECTRUM
AT 1120 KILOMETERS   FIGURE **3.2.2**

ABCISSA x $\frac{\pi}{2}$ = k (radians/kilometer)

69
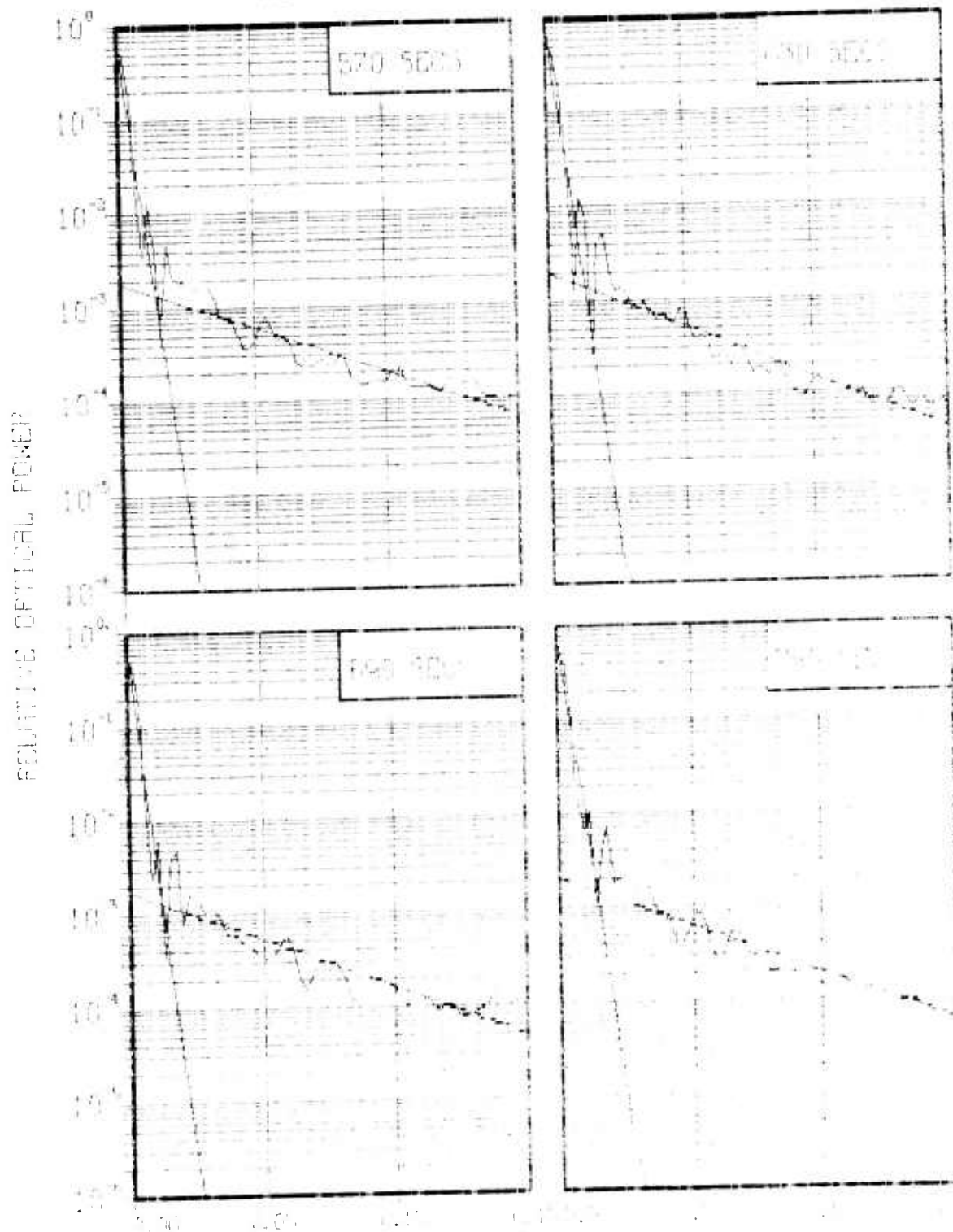
SANITIZED POWER SPECTRUM

AT 1114 KILOMETERS   FIGURE **3.2.3**

$$\text{ABCISSA} \times \frac{\pi}{2} = k \text{ (radians/kilometer)}$$

70
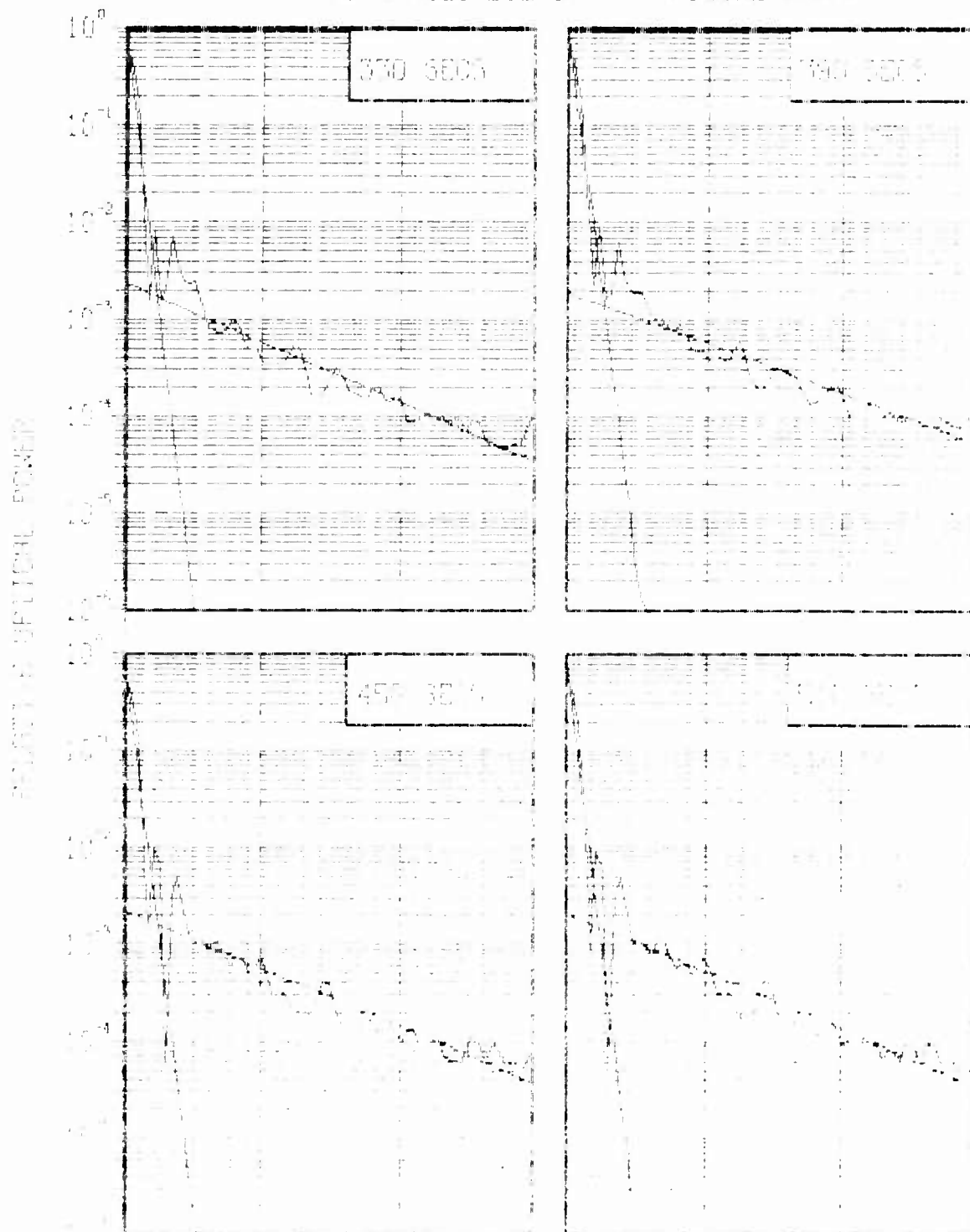
SANITIZED POWER SPECTRUM

AT 1114 KILOMETERS   FIGURE 3.2.4

$$\text{ABCISSA} \ x \ \frac{\pi}{2} = k \ \text{(radians/kilometer)}$$

71
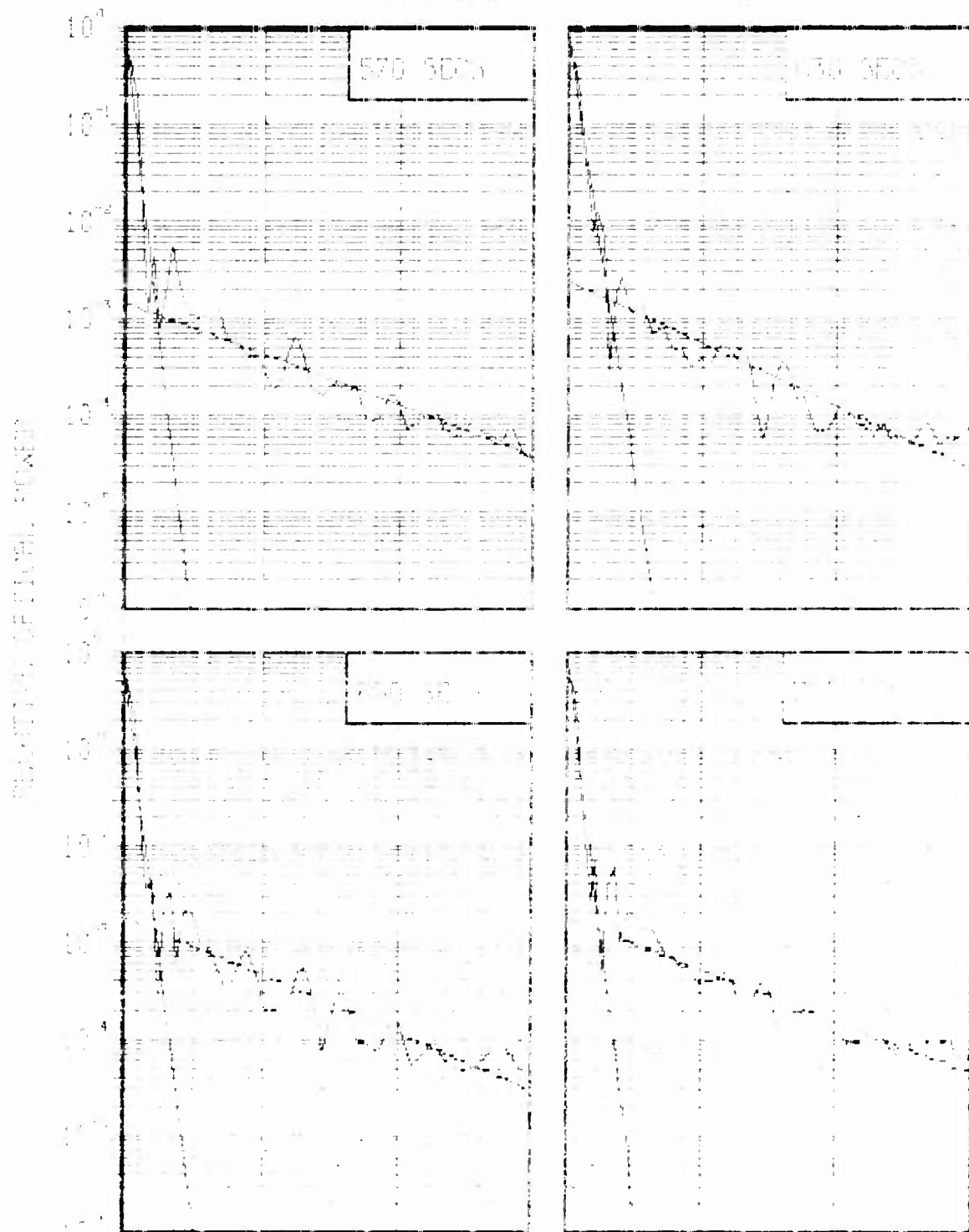
SANITIZED POWER SPECTRUM
AT 1078 KILOMETERS   FIGURE 3.2.5

ABCISSA x $\frac{\pi}{2}$ = k (radians/kilometer)

72

ABCISSA $\times \dfrac{\pi}{2} = k$ (radians/kilometer)

73
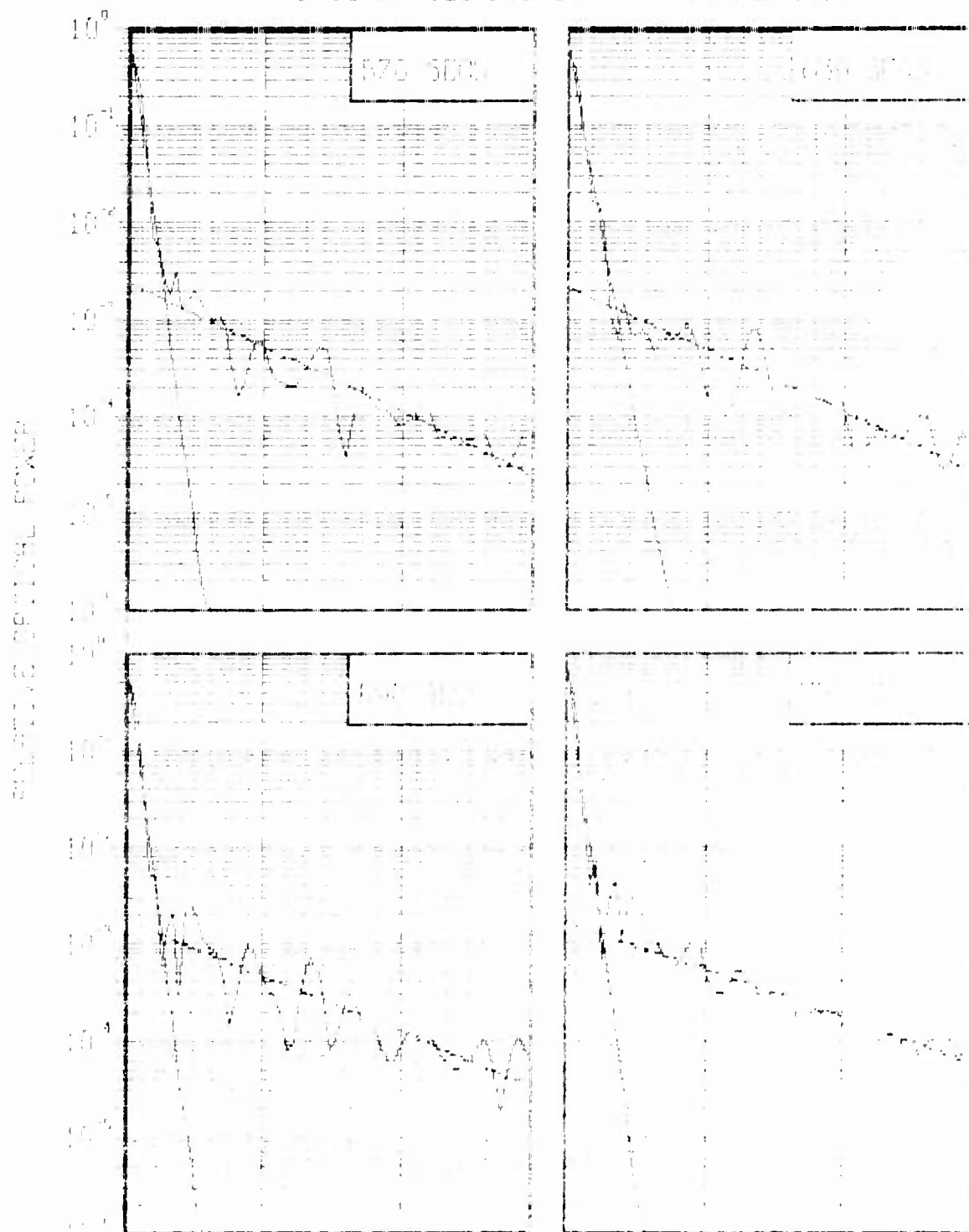
ABCISSA $x \frac{\pi}{2} = k$ (radians/kilometer)
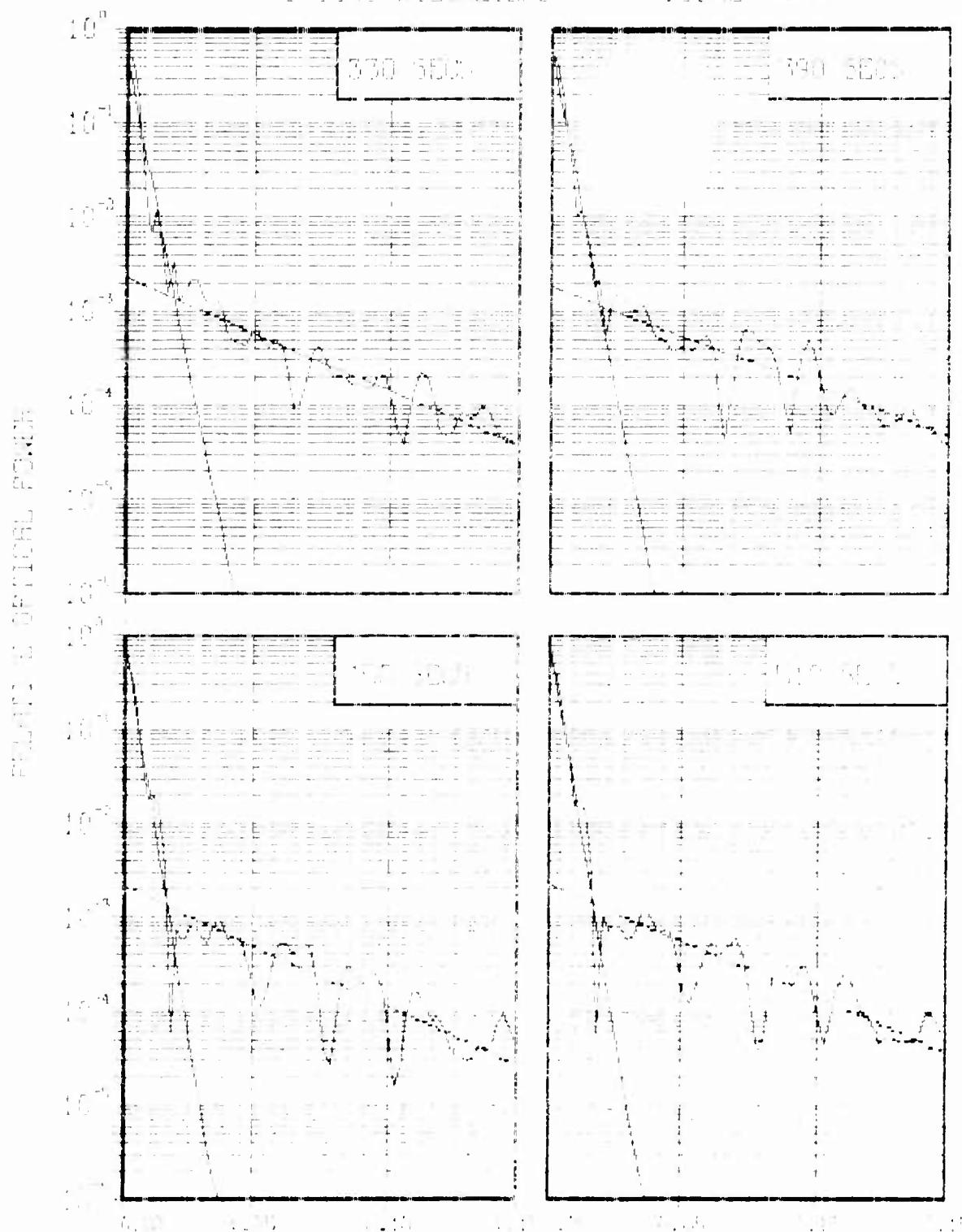
SANITIZED POWER SPECTRUM
AT SOME KILOMETERS   FIGURE 3.2.8
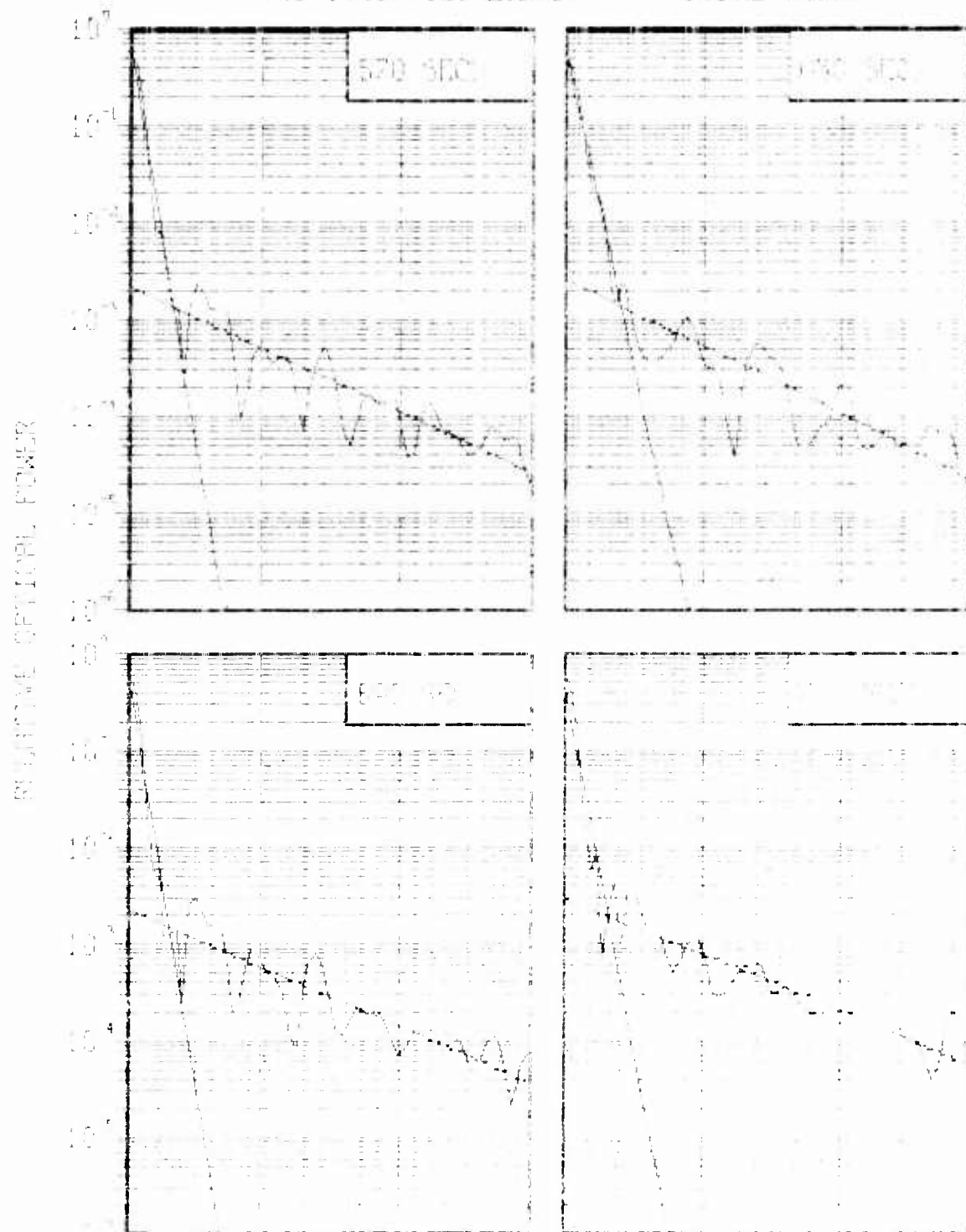
$$\text{ABCISSA} \times \frac{\pi}{2} = k \text{ (radians/kilometer)}$$

75

SANITIZED POWER SPECTRUM
AT 1000 KILOMETERS   FIGURE **3.2.9**

ABCISSA x $\frac{\pi}{2}$ = k (radians/kilometer)

76

SANITIZED POWER SPECTRUM
AT 1000 KILOMETERS   FIGURE 3.2.10

ABCISSA x $\frac{\pi}{2}$ = k (radians/kilometer)

77
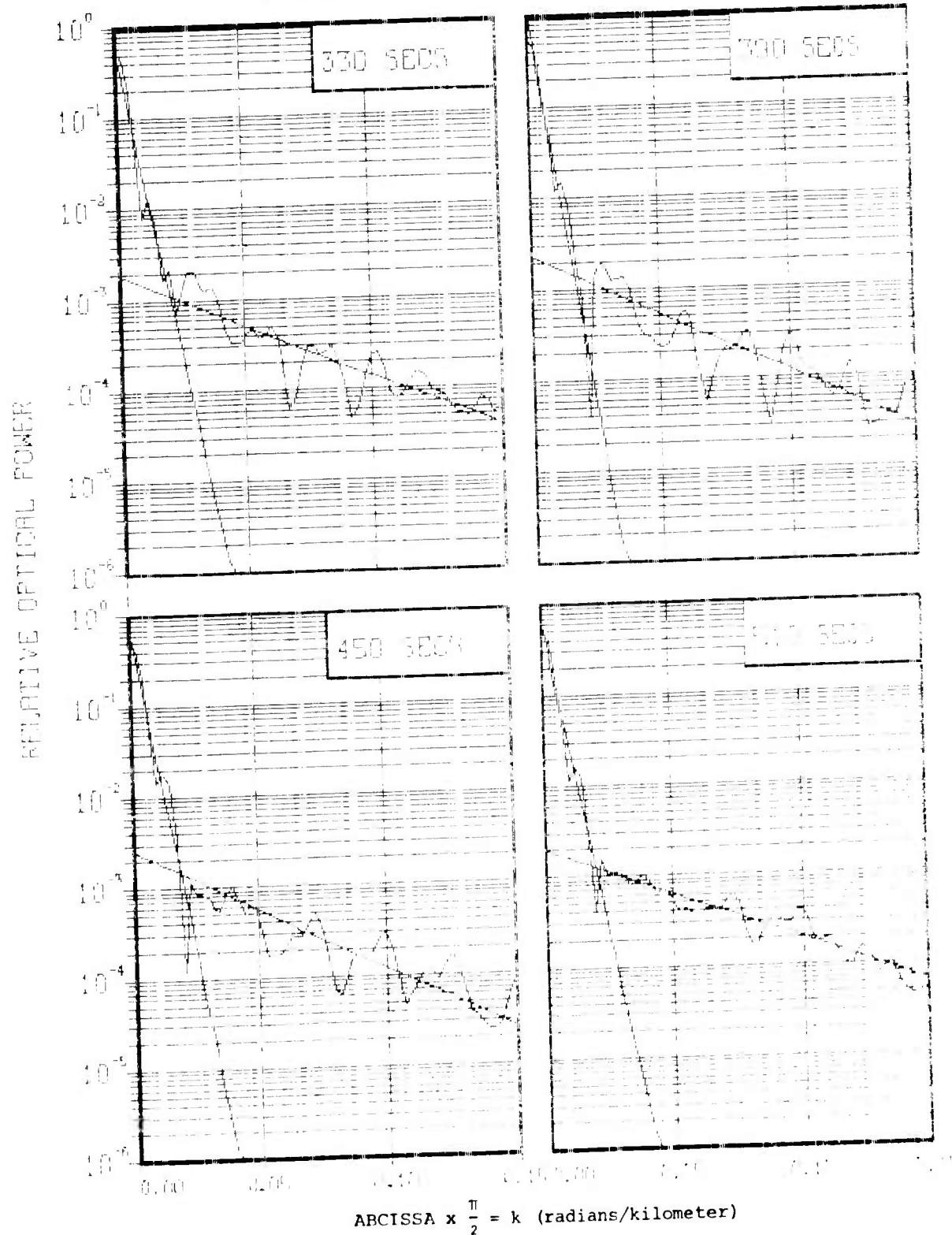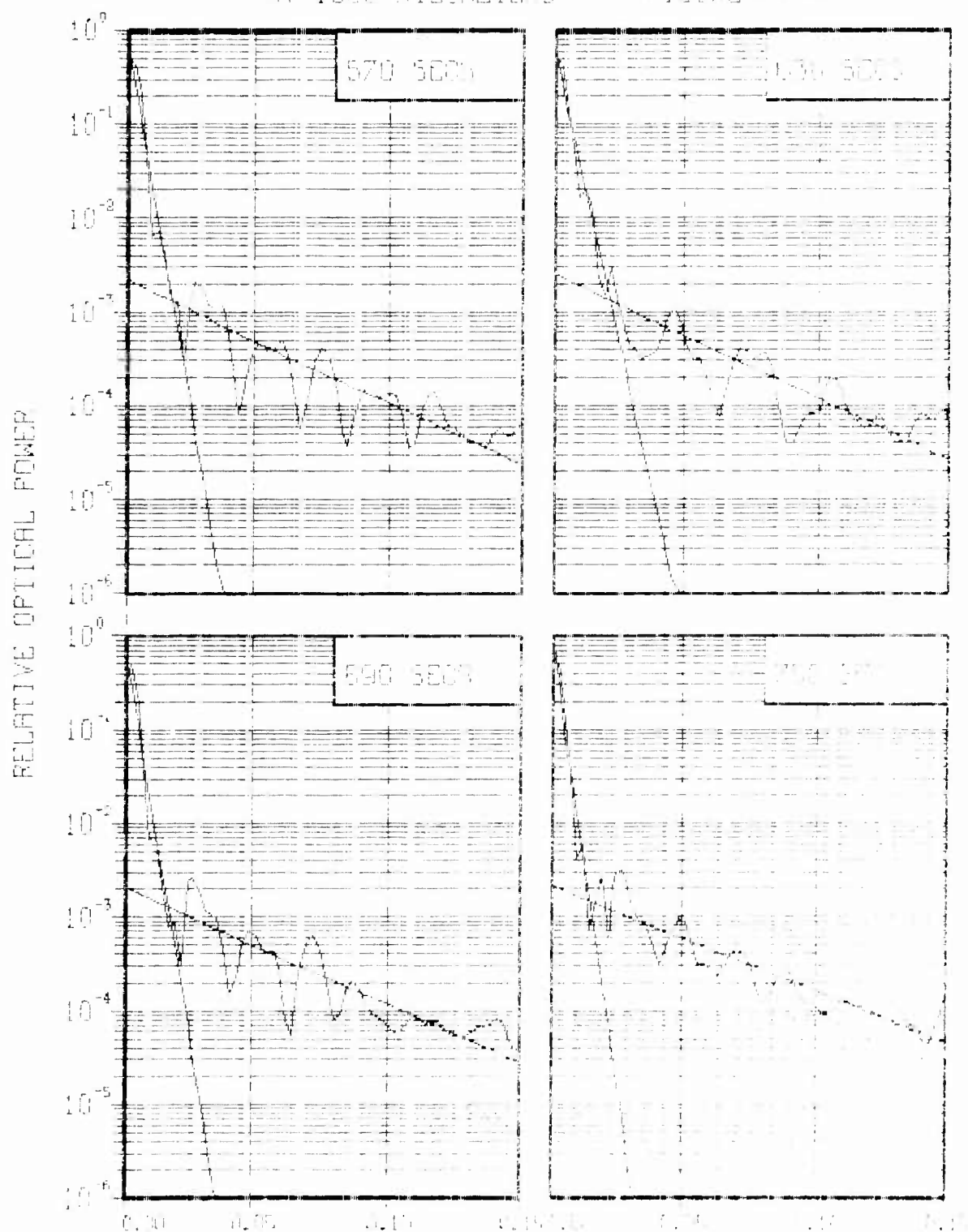
TABLE 3.2.1

MID FREQUENCY EXPONENTIAL FIT INTERCEPT I1 400 KM AT BURST POINT

TIME (SEC)	ALTITUDE (KM)					AVG OVER ALTITUDE
	920.	916.	890.	851.	810.	
330.	3.18E-03	3.18E-03	3.30E-03	3.27E-03	2.88E-03	3.16E-03
390.	2.71E-03	2.93E-03	2.93E-03	2.28E-03	3.73E-03	2.91E-03
450.	2.55E-03	3.57E-03	2.03E-03	3.65E-03	4.10E-03	3.17E-03
510.	2.61E-03	2.10E-03	2.23E-03	3.41E-03	1.83E-03	2.44E-03
570.	2.60E-03	1.93E-03	4.11E-03	3.84E-03	3.86E-03	3.27E-03
630.	2.41E-03	4.10E-03	3.97E-03	4.93E-03	4.99E-03	4.08E-03
690.	2.93E-03	3.07E-03	3.02E-03	3.43E-03	3.87E-03	3.25E-03
750.	3.39E-03	3.05E-03	2.46E-03	3.62E-03	2.68E-03	3.1-E-03
TIME AVG	2.79E-03	2.99E-03	3.06E-03	3.55E-03	3.49E-03	

MID FREQUENCY EXPONENTIAL FIT INTERCEPT I1 600 KM AT BURST POINT

TIME (SEC)	ALTITUDE (KM)					AVG OVER ALTITUDE
	1120.	1114.	1078.	1045.	1000.	
330.	2.03E-03	2.37E-03	2.68E-03	2.32E-03	1.88E-03	2.26E-03
390.	1.91E-03	1.87E-03	1.56E-03	1.81E-03	2.33E-03	1.88E-03
450.	2.10E-03	2.24E-03	2.16E-03	2.20E-03	2.61E-03	2.26E-03
510.	1.93E-03	2.08E-03	2.25E-03	2.27E-03	2.02E-03	2.11E-03
570.	1.84E-03	1.46E-03	2.47E-03	2.22E-03	2.21E-03	2.04E-03
630.	1.93E-03	2.41E-03	2.16E-03	2.61E-03	2.57E-03	2.34E-03
690.	1.77E-03	1.85E-03	1.81E-03	2.34E-03	2.12E-03	1.98E-03
750.	2.01E-03	1.79E-03	1.68E-03	2.95E-03	2.16E-03	2.12E-03
TIME AVG	1.94E-03	2.01E-03	2.10E-03	2.34E-03	2.24E-03	

MID FREQUENCY EXPONENTIAL FIT INTERCEPT I1 800 KM AT BURST POINT

TIME (SEC)	ALTITUDE (KM)					AVG OVER ALTITUDE
	1320.	1315.	1265.	1230.	1190.	
330.	1.50E-03	1.73E-03	1.67E-03	1.54E-03	1.38E-03	1.56E-03
390.	1.55E-03	1.44E-03	1.47E-03	1.54E-03	1.80E-03	1.51E-03
450.	1.62E-03	1.48E-03	1.45E-03	1.60E-03	2.06E-03	1.64E-03
510.	1.24E-03	1.53E-03	1.44E-03	1.64E-03	1.94E-03	1.56E-03
570.	1.48E-03	1.65E-03	1.76E-03	1.58E-03	1.69E-03	1.63E-03
630.	1.73E-03	1.55E-03	1.37E-03	1.61E-03	1.06E-03	1.39E-03
690.	1.32E-03	1.36E-03	1.39E-03	1.69E-03	1.85E-03	1.52E-03
750.	1.53E-03	1.41E-03	1.71E-03	2.18E-03	1.61E-03	1.68E-03
TIME AVG	1.41E-03	1.53E-03	1.55E-03	1.67E-03	1.67E-03	

MID FREQUENCY = $(0.016 < k \leq 0.236$ radians/km)

TABLE 3.2.2

MID FREQUENCY EXPONENTIAL FIT SLOPE (KM/RADIAN) AT 400 KM BURST LATITUDE

TIME	ALTITUDE (KM)					AVG OVER
(SEC)	920.	915.	890.	851.	810.	ALTITUDE
330.	-1.73E+01	-1.59E+01	-1.70E+01	-1.68E+01	-1.64E+01	-1.69E+01
390.	-1.71E+01	-1.58E+01	-1.70E+01	-1.39E+01	-1.87E+01	-1.65E+01
450.	-1.55E+01	-1.80E+01	-1.47E+01	-1.88E+01	-1.92E+01	-1.73E+01
510.	-1.55E+01	-1.48E+01	-1.59E+01	-1.71E+01	-1.07E+01	-1.48E+01
570.	-1.45E+01	-1.52E+01	-2.03E+01	-1.97E+01	-1.99E+01	-1.79E+01
630.	-1.55E+01	-1.98E+01	-2.06E+01	-2.17E+01	-2.12E+01	-1.97E+01
690.	-1.67E+01	-1.85E+01	-1.81E+01	-1.72E+01	-1.97E+01	-1.80E+01
750.	-1.61E+01	-1.67E+01	-1.54E+01	-1.56E+01	-1.53E+01	-1.58E+01
TIME AVG	-1.60E+01	-1.70E+01	-1.74E+01	-1.76E+01	-1.76E+01	

MID FREQUENCY EXPONENTIAL FIT SLOPE (KM/RADIAN) AT 600 KM BURST LATITUDE

TIME	ALTITUDE (KM)					AVG OVER
(SEC)	1120.	1114.	1078.	1045.	1000.	ALTITUDE
330.	-1.71E+01	-1.80E+01	-1.78E+01	-1.76E+01	-1.65E+01	-1.74E+01
390.	-1.69E+01	-1.50E+01	-1.55E+01	-1.56E+01	-1.87E+01	-1.63E+01
450.	-1.69E+01	-1.74E+01	-1.74E+01	-1.87E+01	-1.95E+01	-1.80E+01
510.	-1.58E+01	-1.73E+01	-1.87E+01	-1.76E+01	-1.46E+01	-1.69E+01
570.	-1.40E+01	-1.55E+01	-1.97E+01	-1.89E+01	-1.92E+01	-1.75E+01
630.	-1.63E+01	-1.89E+01	-1.89E+01	-2.02E+01	-1.95E+01	-1.88E+01
690.	-1.52E+01	-1.75E+01	-1.71E+01	-1.77E+01	-1.83E+01	-1.72E+01
750.	-1.49E+01	-1.56E+01	-1.44E+01	-1.68E+01	-1.64E+01	-1.56E+01
TIME AVG	-1.59E+01	-1.69E+01	-1.74E+01	-1.79E+01	-1.78E+01	

MID FREQUENCY EXPONENTIAL FIT SLOPE (KM/RADIAN) AT 800 KM BURST LATITUDE

TIME	ALTITUDE (KM)					AVG OVER
(SEC)	1320.	1315.	1265.	1239.	1190.	ALTITUDE
330.	-1.68E+01	-1.76E+01	-1.67E+01	-1.70E+01	-1.62E+01	-1.69E+01
390.	-1.63E+01	-1.49E+01	-1.66E+01	-1.70E+01	-1.84E+01	-1.65E+01
450.	-1.58E+01	-1.66E+01	-1.59E+01	-1.94E+01	-1.95E+01	-1.78E+01
510.	-1.53E+01	-1.69E+01	-1.77E+01	-1.78E+01	-1.69E+01	-1.69E+01
570.	-1.40E+01	-1.81E+01	-1.96E+01	-1.90E+01	-1.90E+01	-1.79E+01
630.	-1.53E+01	-1.75E+01	-1.76E+01	-1.92E+01	-1.59E+01	-1.71E+01
690.	-1.46E+01	-1.73E+01	-1.74E+01	-1.74E+01	-1.86E+01	-1.71E+01
750.	-1.41E+01	-1.54E+01	-1.60E+01	-1.71E+01	-1.62E+01	-1.58E+01
TIME AVG	-1.54E+01	-1.68E+01	-1.73E+01	-1.80E+01	-1.76E+01	

TABLE 3.2.3

LOW FREQUENCY EXPONENTIAL FIT INTERCEPT I2 600 KM AT BURST POINT

TIME (SEC)	ALTITUDE (KM) 1120.	1114.	1078.	1045.	1000.	AVG OVER ALTITUDE
330.	8.50E-01	8.94E-01	8.43E-01	4.63E-01	5.47E-01	7.19E-01
390.	7.80E-01	8.55E-01	8.65E-01	5.92E-01	9.94E-01	8.17E-01
450.	7.83E-01	8.75E-01	8.20E-01	8.90E-01	7.53E-01	8.24E-01
510.	7.65E-01	9.10E-01	8.11E-01	8.34E-01	6.17E-01	7.88E-01
570.	7.58E-01	1.04E+00	9.22E-01	7.04E-01	6.37E-01	8.12E-01
630.	8.21E-01	7.71E-01	7.11E-01	5.67E-01	5.38E-01	6.81E-01
690.	9.02E-01	9.80E-01	9.43E-01	5.87E-01	6.38E-01	8.10E-01
750.	7.35E-01	8.85E-01	8.66E-01	4.40E-01	7.64E-01	7.38E-01
TIME AVG	7.99E-01	9.01E-01	8.48E-01	6.35E-01	6.86E-01	

LOW FREQUENCY EXPONENTIAL FIT SLOPE (KM/RADIAN) AT 600 KM BURST LATITUDE

TIME (SEC)	ALTITUDE (KM) 1120.	1114.	1078.	1045.	1000.	AVG OVER ALTITUDE
330.	-3.28E+02	-3.34E+02	-2.98E+02	-1.95E+02	-1.98E+02	-2.71E+02
390.	-3.04E+02	-3.23E+02	-3.32E+02	-2.13E+02	-2.49E+02	-2.84E+02
450.	-3.10E+02	-3.24E+02	-2.71E+02	-2.40E+02	-2.16E+02	-2.72E+02
510.	-3.02E+02	-3.37E+02	-2.65E+02	-2.38E+02	-1.99E+02	-2.68E+02
570.	-2.99E+02	-3.64E+02	-2.93E+02	-2.39E+02	-2.23E+02	-2.84E+02
630.	-3.19E+02	-2.67E+02	-2.28E+02	-1.89E+02	-1.77E+02	-2.36E+02
690.	-3.40E+02	-3.38E+02	-3.09E+02	-2.41E+02	-2.33E+02	-2.92E+02
750.	-2.93E+02	-3.32E+02	-3.05E+02	-2.13E+02	-2.67E+02	-2.82E+02
TIME AVG	-3.12E+02	-3.28E+02	-2.88E+02	-2.21E+02	-2.20E+02	

FREQUENCY WHERE FILTER FUNCTION CROSSES -10BD RADIANS/KM AT 600 KM

TIME (SEC)	ALTITUDE (KM) 1120.	1114.	1078.	1045.	1000.	AVG OVER ALTITUDE
330.	1.56E+00	1.51E+00	1.51E+00	1.51E+00	1.30E+00	1.48E+00
390.	1.60E+00	1.35E+00	1.27E+00	1.15E+00	1.35E+00	1.35E+00
450.	1.68E+00	1.38E+00	1.46E+00	1.23E+00	1.49E+00	1.45E+00
510.	1.47E+00	1.38E+00	1.16E+00	1.81E+00	1.70E+00	1.50E+00
570.	1.63E+00	1.47E+00	1.39E+00	1.65E+00	1.33E+00	1.49E+00
630.	1.45E+00	1.22E+00	1.44E+00	1.49E+00	1.46E+00	1.41E+00
690.	1.60E+00	1.59E+00	1.06E+00	1.46E+00	1.65E+00	1.47E+00
750.	1.45E+00	1.19E+00	1.38E+00	1.51E+00	1.62E+00	1.43E+00
TIME AVG	1.55E+00	1.39E+00	1.33E+00	1.47E+00	1.49E+00	
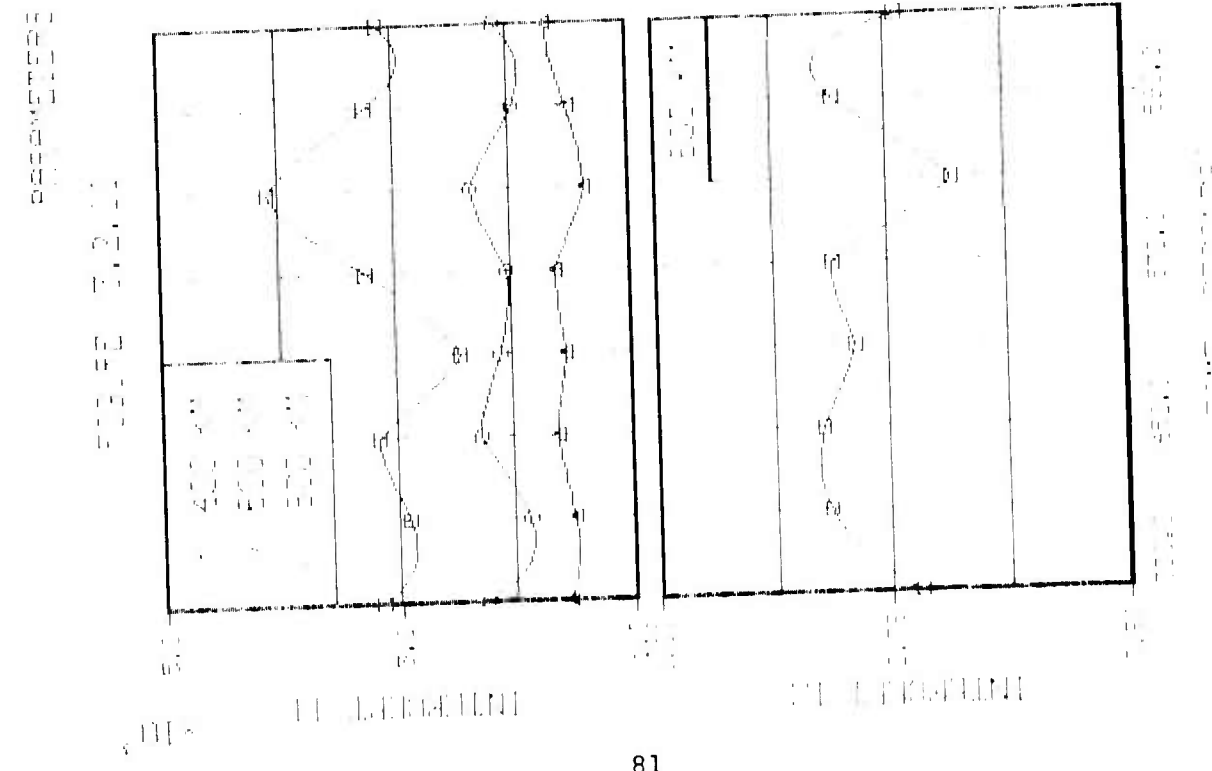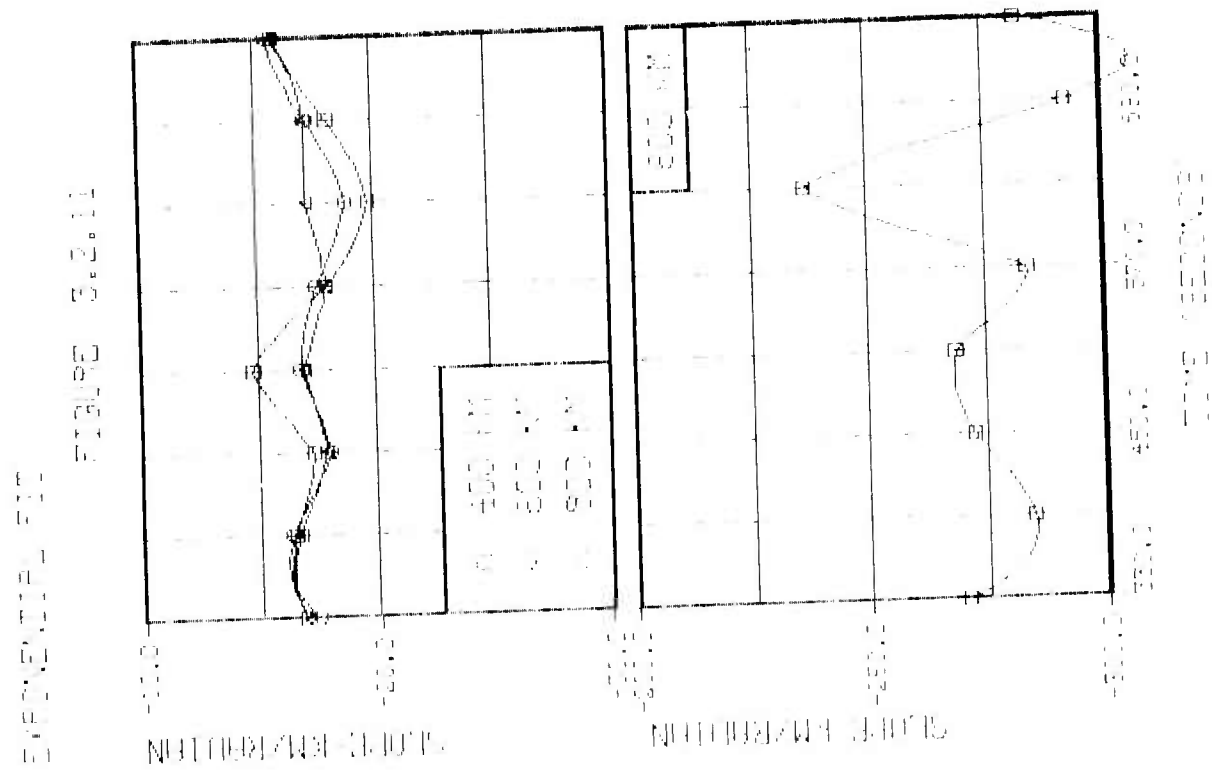
3.3 OTHER DATA ANALYSIS RESULTS

As previously reported[4] various other parameters are determined from the PSD by the Aurora computer program.

3.3.1 Radiation Profile Integral

For each scan line considered the optical power integral, $\simeq \Delta x \sum_{I=2}^{1168} 1/2[R(I-1)+R(I)]$, was determined from each relative radiance profile across the observed striations. The average value of this integral was determined for each of the five windows (illustrated on the enclosed photographs) by averaging over the total number of scan lines comprising each window. Table 3.3.1 summarized the results and illustrates the observed variation in optical power with altitude and time. The values were also averaged over altitude at each time, to remove the altitude fluctuations. The results of this averaging are presented in Figure 3.3.1. As expected, the time variation shows a decay of the radiant striation optical power with increasing time.

3.3.2 Power Spectral Integral

In all cases considered the integral $*\simeq \Delta \nu \sum_{I=2}^{2048} 1/2[P(I)+P(I-1)]$, over the sanitized power spectrum was determined at each altitude and time. The results of this integral as it varied with altitude and time are presented in Table 3.3.2. Also shown in this table are the average values after the altitude variation at each time were averaged out. Figure 3.3.1 illustrates the time variation of the average value of this integral. Its decay in time is similar to that of the optical power from which its value arises.

3.3.3 Frequency Where Filter Function Decreases By 10 db

In the data analysis, a filter function[4] was used in order to

* For plotted data Δx and $\Delta \nu$ are taken as one.

describe and correct for the spatial frequency response of the various components in the film measuring process. It can be assumed that no usable data exists in the power spectrum at frequencies larger than the frequency where the filter function operating on the "raw" power spectrum, suppresses its value be 10 db. The frequency at which this first occurred was determined as a function of time and altitude for all the PSDs. Some of the determined values of this frequency are presented in Table 3.2.3. The time variation of the value of this frequency after averaging over altitude at each time is graphically illustrated in Figure 3.3.1.

3.3.4   Number of Striations

It was indicated before that by following a procedure developed by SRI[5], the exponential fit parameters can be used to estimate the total number of striations in the imaged spatial volume. Using the expression given by Equation 2.3 and the required fit parameters, the number of striations were determined. The time/altitude values of striations which resulted in this analysis are presented in Table 3.3.3. As observed from a study of the data (and also Figure 3.3.2) it is clear that these values are not unique for they depend on the assumptions used and the frequency interval over which the semi-log linear fit is established. Figure 3.3.2 presents the time variation of the number of striations after the altitude variations of this value were averaged out. It is significant to note that over the time period considered the number of striations does not appear to change even though the relative radiant power has decreased by approximately a factor of three (see Figure 3.3.1).

3.3.5   Most Probable Striation Radius

As shown by Equation 2.4 a radius probability distribution can be determined from the exponential fit. The most probable radius values of this distribution which arises from the data at each altitude and time

are summarized in Table 3.3.4. The time dependence of the altitude-averaged value of this most probable radius is illustrated in Figure 3.3.2. This plotted data indicates that no significant change in this value is observed in the time span of this analysis.

3.3.6   Total Area Contained in Gaussian Striations

Another parameter that can be determined is the total area/π (or total unit volume, i.e., unit length along the striations) of all striations in the imaged spatial volume. This total area/π is defined as $\int N(r)r^2 dr$. $N(r)$ is the striation radius distribution (Equation 2.4) normalized such that $\int N(r)dr$ equals the total number of striations. The symbol r is the Gaussian striation radius (in cm). The time and altitude values of this parameter are presented in Table 3.4.5. Figure 3.3.2 presents the time dependence of the value of this parameter after the altitude averaging has been performed. A review of Figure 3.3.2 indicates that the striations occupy about 10% of the total volume used in these calculations for the imaged striation region. Likewise, except for the shift brought about by the ambiguity of the location of the striation volume, no time variation of this parameter is determined.

3.3.7   Relative Volume Emission

Having determined **the total** striation area A, (or unit volume along the striations) the volume emission of optical light can be determined from the expression $E = [4\pi \int R(x)dx]/\pi A$, where $R(x)$ is the measured, relative radiance profile across the striations. Thus, E is the relative volume emission in units of emitted power per cubic centimeter for each striation averaged over the emission along the camera line-of-sight. The value of this optical emission volume as determined for each altitude and time, using the measured relative power, is presented in Table 3.3.6. It is likewise graphically illustrated in Figure 3.3.1.

TABLE 3.3.1

AREA UNDER RADIANCE PROFILE 400 KM AT BURST POINT

TIME	ALTITUDE (KM)					AVG OVER
(SEC)	925.	915.	890.	851.	810.	ALTITUDE
330.	8.62E+03	8.57E+03	8.32E+03	9.20E+03	1.06E+04	9.02E+03
390.	7.60E+03	7.77E+03	8.25E+03	9.76E+03	1.17E+04	9.02E+03
450.	6.33E+03	6.68E+03	7.63E+03	9.40E+03	1.06E+04	8.13E+03
510.	4.90E+03	5.24E+03	6.54E+03	7.69E+03	8.38E+03	6.56E+03
570.	3.55E+03	4.31E+03	5.22E+03	5.90E+03	6.39E+03	5.07E+03
630.	2.93E+03	3.59E+03	4.34E+03	5.10E+03	5.36E+03	4.26E+03
690.	2.19E+03	2.65E+03	3.02E+03	3.53E+03	3.70E+03	3.02E+03
750.	2.03E+03	2.77E+03	3.19E+03	3.49E+03	3.71E+03	3.04E+03
TIME AVG	4.77E+03	5.17E+03	5.82E+03	6.75E+03	7.55E+03	

AREA UNDER RADIANCE PROFILE 600 KM AT BURST POINT

TIME	ALTITUDE (KM)					AVG OVER
(SEC)	1120.	1114.	1078.	1045.	1000.	ALTITUDE
330.	8.76E+03	8.53E+03	8.47E+03	9.20E+03	1.06E+04	9.11E+03
390.	7.60E+03	7.77E+03	8.24E+03	9.76E+03	1.17E+04	9.02E+03
450.	6.33E+03	6.68E+03	7.63E+03	9.40E+03	1.06E+04	8.13E+03
510.	4.56E+03	5.49E+03	6.42E+03	7.69E+03	8.37E+03	6.56E+03
570.	3.55E+03	4.31E+03	5.22E+03	5.90E+03	6.39E+03	5.07E+03
630.	2.93E+03	3.59E+03	4.34E+03	5.10E+03	5.36E+03	4.26E+03
690.	2.19E+03	2.65E+03	3.02E+03	3.53E+03	3.70E+03	3.02E+03
750.	2.03E+03	2.77E+03	3.19E+03	3.49E+03	3.71E+03	3.04E+03
TIME AVG	4.78E+03	5.22E+03	5.82E+03	6.76E+03	7.55E+03	

AREA UNDER RADIANCE PROFILE 800 KM AT BURST POINT

TIME	ALTITUDE (KM)					AVG OVER
(SEC)	1320.	1315.	1265.	1234.	1190.	ALTITUDE
330.	8.76E+03	8.53E+03	8.47E+03	9.20E+03	1.06E+04	9.12E+03
390.	7.60E+03	7.77E+03	8.25E+03	9.76E+03	1.17E+04	9.01E+03
450.	6.33E+03	6.68E+03	7.63E+03	9.40E+03	1.06E+04	8.13E+03
510.	4.56E+03	5.24E+03	6.54E+03	7.68E+03	8.47E+03	6.54E+03
570.	3.55E+03	4.31E+03	5.22E+03	5.90E+03	6.39E+03	5.07E+03
630.	2.97E+03	3.59E+03	4.54E+03	5.15E+03	5.36E+03	4.26E+03
690.	2.19E+03	2.65E+03	3.02E+03	4.54E+03	4.6 E+03	3.40E+03
750.	2.03E+03	2.77E+03	3.19E+03	3.49E+03	3.71E+03	3.04E+03
TIME AVG	4.67E+03	5.19E+03	5.84E+03	6.86E+03	7.67E+03	

85

TABLE 3.3.2

AREA UNDER POWER SPECTRA 400 KM AT BURST POINT
ALTITUDE (KM)

TIME (SEC)	920.	915.	840.	851.	810.	AVG OVER ALTITUDE
330.	1.39E+09	1.24E+09	1.24E+09	1.51E+09	2.03E+09	1.46E+09
390.	9.71E+08	1.03E+09	1.19E+09	1.75E+09	2.54E+09	1.50E+09
450.	7.17E+08	8.11E+08	1.13E+09	1.77E+09	2.20E+09	1.32E+09
510.	5.10E+08	6.0bE+08	4.66E+08	1.16E+09	1.36E+09	9.2 E+08
570.	2.16E+08	3.27E+08	5.05E+08	6.46E+08	7.52E+08	4.90E+08
630.	1.53E+08	2.41E+08	3.71E+08	5.18E+08	5.59E+08	3.66E+08
690.	7.92E+07	1.20E+08	1.6bE+08	2.16E+08	2.40E+08	1.63E+08
750.	6.87E+07	1.24E+08	1.77E+08	2.05E+08	2.30E+08	1.63E+08
TIME AVG	5.02E+08	5.63E+08	7.13E+08	9.72E+08	1.24E+09	

AREA UNDER POWER SPECTRA 600 KM AT BURST POINT
ALTITUDE (KM)

TIME (SEC)	1120.	1114.	1078.	1045.	1000.	AVG OVER ALTITUDE
330.	1.31E+09	1.24E+09	1.24E+09	1.51E+09	2.03E+09	1.47E+09
390.	9.71E+08	1.03E+09	1.19E+09	1.75E+09	2.54E+09	1.50E+09
450.	7.17E+08	8.11E+08	1.13E+09	1.77E+09	2.20E+09	1.32E+09
510.	4.19E+08	5.40E+08	7.40E+08	1.16E+09	1.36E+09	8.55E+08
570.	2.16E+08	3.27E+08	5.05E+08	6.46E+08	7.52E+08	4.90E+08
630.	1.53E+08	2.41E+08	3.71E+08	5.18E+08	5.59E+08	3.66E+08
690.	7.92E+07	1.20E+08	1.66E+08	2.18E+08	2.40E+08	1.63E+08
750.	6.87E+07	1.24E+08	1.73E+08	2.05E+08	2.30E+08	1.63E+08
TIME AVG	4.32E+08	5.54E+08	6.92E+08	9.72E+08	1.24E+09	

AREA UNDER POWER SPECTRA 800 KM AT BURST POINT
ALTITUDE (KM)

TIME (SEC)	1320.	1315.	1265.	1234.	1130.	AVG OVER ALTITUDE
330.	1.31E+09	1.24E+09	1.24E+09	1.51E+09	2.03E+09	1.47E+09
390.	9.71E+08	1.03E+09	1.19E+09	1.75E+09	2.54E+09	1.50E+09
450.	7.17E+08	8.11E+08	1.13E+09	1.77E+09	2.20E+09	1.00E+09
510.	3.10E+08	4.0bE+08	1.2bE+09	1.16E+09	7.52E+08	4.90E+08
570.	2.16E+08	3.27E+08	5.05E+08	6.46E+08	5.59E+08	3.69E+08
630.	1.53E+08	2.41E+08	3.71E+08	5.18E+08	4.73E+08	2.38E+08
690.	7.92E+07	1.20E+08	1.65E+08	3.99E+08	3.76E+08	1.63E+08
750.	6.87E+07	1.24E+08	1.73E+08	2.05E+08	2.76E+08	
TIME AVG	5.25E+08	5.52E+08	7.52E+08	8.99E+08	1.24E+09	

TABLE 3.3.3

NUMBER OF STRIATIONS IN SPATIAL VOLUME 4.0 KM AT BURST POINT

TIME (SEC)	ALTITUDE (KM) 920.	915.	890.	851.	810.	AVG OVER ALTITUDE
330.	5.42E+02	5.36E+02	5.94E+02	5.15E+02	5.78E+02	5.36E+02
390.	6.58E+02	6.01E+02	5.91E+02	7.27E+02	4.32E+02	6.01E+02
450.	6.58E+02	4.65E+02	7.82E+02	4.17E+02	5.74E+02	6.91E+02
510.	6.49E+02	7.94E+02	7.19E+02	4.47E+02	8.45E+02	5.60E+02
570.	6.73E+02	8.87E+02	5.94E+02	4.20E+02	4.23E+02	4.18E+02
630.	6.97E+02	5.92E+02	3.84E+02	3.06E+02	3.09E+02	5.44E+02
690.	6.27E+02	5.73E+02	5.75E+02	5.02E+02	4.42E+02	5.73E+02
750.	5.34E+02	5.89E+02	5.97E+02	4.93E+02	6.50E+02	
TIME AVG	6.30E+02	6.04E+02	5.64E+02	4.78E+02	5.07E+02	

NUMBER OF STRIATIONS IN SPATIAL VOLUME 600 KM AT BURST POINT

TIME (SEC)	ALTITUDE (KM) 1120.	1114.	1078.	1045.	1000.	AVG OVER ALTITUDE
330.	8.65E+02	7.53E+02	6.41E+02	7.26E+02	8.86E+02	7.70E+02
390.	9.86E+02	9.43E+02	1.10E+03	9.05E+02	6.94E+02	9.26E+02
450.	7.60E+02	7.40E+02	7.35E+02	6.83E+02	5.86E+02	7.02E+02
510.	8.76E+02	8.07E+02	7.07E+02	6.72E+02	7.76E+02	7.66E+02
570.	9.56E+02	1.17E+03	6.56E+02	7.27E+02	7.40E+02	8.50E+02
630.	8.71E+02	6.66E+02	7.06E+02	5.74E+02	6.09E+02	6.85E+02
690.	1.03E+03	9.51E+02	9.51E+02	7.35E+02	8.09E+02	8.95E+02
750.	9.12E+02	1.00E+03	1.05E+03	6.07E+02	8.04E+02	8.73E+02
TIME AVG	9.07E+02	8.76E+02	8.18E+02	7.04E+02	7.37E+02	

NUMBER OF STRIATIONS IN SPATIAL VOLUME 8.0 KM AT BURST POINT

TIME (SEC)	ALTITUDE (KM) 1320.	1315.	1285.	1235.	1190.	AVG OVER ALTITUDE
330.	1.17E+03	1.01E+03	1.04E+03	1.10E+03	1.21E+03	1.10E+03
390.	1.34E+03	1.21E+03	1.14E+03	1.00E+03	9.00E+02	1.14E+03
450.	1.04E+03	1.12E+03	1.04E+03	9.36E+02	7.46E+02	9.56E+02
510.	1.37E+03	1.09E+03	1.12E+03	4.31E+02	7.39E+02	1.04E+03
570.	1.19E+03	1.04E+03	9.21E+02	1.02E+03	9.04E+02	1.05E+03
630.	1.26E+03	1.05E+03	1.11E+03	6.55E+02	1.46E+03	1.16E+03
690.	1.34E+03	1.29E+03	1.24E+03	1.05E+03	1.04E+03	1.19E+03
750.	1.20E+03	1.27E+03	1.03E+03	6.21E+02	1.06E+03	1.04E+03
TIME AVG	1.26E+03	1.13E+03	1.09E+03	9.47E+02	1.03E+03	

88

TABLE 3.3.4

TIME	MOST PROBABLE STRIATION RADIUS 400 KM AT BURST POINT ALTITUDE (KM)					AVG OVER
(SEC)	920.	915.	890.	851.	810.	ALTITUDE
330.	1.00E+01	9.76E+00	9.84E+00	9.68E+00	9.44E+00	9.74E+00
390.	9.84E+00	7.12E+00	9.84E+00	8.00E+00	1.08E+01	9.52E+00
450.	8.96E+00	1.04E+01	8.48E+00	1.09E+01	1.10E+01	9.95E+00
510.	8.96E+00	8.48E+00	9.20E+00	9.84E+00	6.16E+00	8.53E+00
570.	8.32E+00	8.72E+00	1.17E+01	1.14E+01	1.15E+01	1.03E+01
630.	8.88E+00	1.14E+01	1.19E+01	1.25E+01	1.22E+01	1.14E+01
690.	9.60E+00	1.06E+01	1.04E+01	9.92E+00	1.14E+01	1.04E+01
750.	9.28E+00	9.68E+00	8.88E+00	9.04E+00	8.80E+00	9.14E+00
TIME AVG	9.23E+00	9.78E+00	1.00E+01	1.02E+01	1.02E+01	

TIME	MOST PROBABLE STRIATION RADIUS 600 KM AT BURST POINT ALTITUDE (KM)					AVG OVER
(SEC)	1120.	1114.	1078.	1045.	1000.	ALTITUDE
330.	9.84E+00	1.03E+01	1.02E+01	1.02E+01	9.52E+00	1.00E+01
390.	9.76E+00	8.64E+00	8.96E+00	8.96E+00	1.08E+01	9.42E+00
450.	9.76E+00	1.01E+01	1.00E+01	1.08E+01	1.13E+01	1.04E+01
510.	9.12E+00	1.00E+01	1.07E+01	1.02E+01	8.40E+00	9.68E+00
570.	8.08E+00	8.96E+00	1.14E+01	1.09E+01	1.11E+01	1.01E+01
630.	9.44E+00	1.09E+01	1.09E+01	1.17E+01	1.12E+01	1.08E+01
690.	8.80E+00	1.01E+01	9.84E+00	1.02E+01	1.06E+01	9.90E+00
750.	8.56E+00	8.96E+00	8.32E+00	9.68E+00	9.44E+00	8.99E+00
TIME AVG	9.17E+00	9.74E+00	1.00E+01	1.03E+01	1.03E+01	

TIME	MOST PROBABLE STRIATION RADIUS 800 KM AT BURST POINT ALTITUDE (KM)					AVG OVER
(SEC)	1320.	1315.	1265.	1239.	1190.	ALTITUDE
330.	9.75E+00	1.02E+01	9.68E+00	9.84E+00	9.36E+00	9.76E+00
390.	9.44E+00	8.64E+00	9.60E+00	9.84E+00	1.06E+01	9.63E+00
450.	9.68E+00	9.60E+00	9.76E+00	1.12E+01	1.13E+01	1.03E+01
510.	8.88E+00	9.76E+00	1.02E+01	1.02E+01	9.76E+00	9.78E+00
570.	8.08E+00	1.04E+01	1.13E+01	1.10E+01	1.10E+01	1.03E+01
630.	8.88E+00	1.01E+01	1.02E+01	1.10E+01	9.20E+00	9.87E+00
690.	8.48E+00	1.00E+01	1.00E+01	1.00E+01	1.07E+01	9.84E+00
750.	8.16E+00	8.98E+00	9.20E+00	9.92E+00	9.36E+00	9.10E+00
TIME AVG	8.92E+00	9.69E+00	9.99E+00	1.04E+01	1.02E+01	

TABLE 3.3.5

TOTAL AREA (KM**2) IN GAUSSIAN STRIATIONS AT 400 KM AT BURST LATITUDE

TIME (SEC)	ALTITUDE (KM) 920.	915.	890.	851.	810.	AVG OVER ALTITUDE
330.	9.53E+04	9.20E+04	8.78E+04	8.64E+04	9.22E+04	9.09E+04
390.	1.14E+05	8.90E+04	1.02E+05	8.27E+04	9.01E+04	9.55E+04
450.	9.47E+04	8.96E+04	1.01E+05	8.82E+04	8.16E+04	9.11E+04
510.	9.34E+04	1.03E+05	1.09E+05	7.76E+04	5.79E+04	8.82E+04
570.	8.42E+04	1.22E+05	9.66E+04	9.71E+04	1.00E+05	9.99E+04
630.	9.92E+04	9.17E+04	9.71E+04	8.58E+04	8.26E+04	9.13E+04
690.	1.04E+05	1.16E+05	1.12E+05	8.86E+04	1.02E+05	1.05E+05
750.	8.26E+04	9.82E+04	8.46E+04	7.15E+04	9.07E+04	8.55E+04
TIME AVG	9.60E+04	1.00E+05	9.88E+04	8.47E+04	8.72E+04	

TOTAL AREA (KM**2) IN GAUSSIAN STRIATIONS AT 600 KM AT BURST LATITUDE

TIME (SEC)	ALTITUDE (KM) 1120.	1114.	1078.	1045.	1000.	AVG OVER ALTITUDE
330.	1.50E+05	1.41E+05	1.21E+05	1.34E+05	1.43E+05	1.38E+05
390.	1.70E+05	1.27E+05	1.57E+05	1.31E+05	1.45E+05	1.46E+05
450.	1.31E+05	1.33E+05	1.32E+05	1.43E+05	1.33E+05	1.34E+05
510.	1.31E+05	1.43E+05	1.46E+05	1.24E+05	9.82E+04	1.28E+05
570.	1.12E+05	1.70E+05	1.52E+05	1.55E+05	1.63E+05	1.50E+05
630.	1.38E+05	1.42E+05	1.50E+05	1.41E+05	1.36E+05	1.41E+05
690.	1.42E+05	1.74E+05	1.65E+05	1.38E+05	1.62E+05	1.56E+05
750.	1.19E+05	1.45E+05	1.29E+05	1.03E+05	1.29E+05	1.25E+05
TIME AVG	1.37E+05	1.47E+05	1.44E+05	1.33E+05	1.39E+05	

TOTAL AREA (KM**2) IN GAUSSIAN STRIATIONS AT 800 KM AT BURST LATITUDE

TIME (SEC)	ALTITUDE (KM) 1320.	1315.	1265.	1239.	1190.	AVG OVER ALTITUDE
330.	1.98E+05	1.86E+05	1.72E+05	1.88E+05	1.88E+05	1.86E+05
390.	2.19E+05	1.60E+05	1.91E+05	1.83E+05	1.82E+05	1.87E+05
450.	1.73E+05	1.83E+05	1.86E+05	2.11E+05	1.69E+05	1.84E+05
510.	1.91E+05	1.85E+05	2.09E+05	1.76E+05	1.36E+05	1.79E+05
570.	1.39E+05	2.01E+05	2.11E+05	2.19E+05	2.07E+05	1.95E+05
630.	1.76E+05	1.88E+05	2.05E+05	2.05E+05	2.20E+05	1.99E+05
690.	1.75E+05	2.31E+05	2.24E+05	1.91E+05	1.99E+05	2.04E+05
750.	1.43E+05	1.79E+05	1.57E+05	1.44E+05	1.69E+05	1.58E+05
TIME AVG	1.77E+05	1.89E+05	1.94E+05	1.90E+05	1.84E+05	

TABLE 3.3.6

RELATIVE VOLUME EMISSION (VE) 400 KM AT BURST POINT

TIME (SEC)	920.	915.	ALTITUDE (KM) 890.	851.	810.	AVG OVER ALTITUDE
330.	1.32E-06	1.33E-06	1.35E-06	1.45E-06	1.49E-06	1.39E-06
390.	9.80E-07	1.28E-06	1.16E-06	1.61E-06	1.68E-06	1.34E-06
450.	9.83E-07	1.09E-06	1.08E-06	1.45E-06	1.68E-06	1.26E-06
510.	8.15E-07	8.20E-07	9.15E-07	1.35E-06	1.87E-06	1.15E-06
570.	6.20E-07	5.20E-07	7.70E-07	8.28E-07	8.25E-07	7.13E-07
630.	4.35E-07	5.73E-07	6.38E-07	3.10E-07	8.40E-07	6.59E-07
690.	3.10E-07	3.33E-07	3.88E-07	5.43E-07	4.68E-07	4.08E-07
750.	3.63E-07	4.13E-07	5.40E-07	5.65E-07	5.30E-07	5.02E-07
TIME AVG	7.28E-07	7.95E-07	8.54E-07	1.09E-06	1.17E-06	

RELATIVE VOLUME EMISSION (VE) 600 KM AT BURST POINT

TIME (SEC)	1120.	1114.	ALTITUDE (KM) 1078.	1045.	1000.	AVG OVER ALTITUDE
330.	1.05E-06	1.08E-06	1.21E-06	1.15E-06	1.19E-06	1.14E-06
390.	8.05E-07	1.09E-06	9.05E-07	1.25E-06	1.29E-06	1.07E-06
450.	8.65E-07	8.93E-07	9.98E-07	1.10E-06	1.28E-06	1.03E-06
510.	6.68E-07	6.85E-07	7.58E-07	1.04E-06	1.36E-06	9.02E-07
570.	5.68E-07	4.55E-07	5.95E-07	6.38E-07	6.28E-07	5.77E-07
630.	3.80E-07	4.50E-07	5.00E-07	6.05E-07	6.33E-07	5.14E-07
690.	2.78E-07	2.73E-07	3.18E-07	4.30E-07	3.68E-07	3.33E-07
750.	3.05E-07	3.40E-07	4.25E-07	5.70E-07	4.60E-07	4.20E-07
TIME AVG	6.15E-07	6.59E-07	7.13E-07	8.47E-07	9.00E-07	

RELATIVE VOLUME EMISSION (VE) 800 KM AT BURST POINT

TIME (SEC)	1320.	1315.	ALTITUDE (KM) 1265.	1239.	1190.	AVG OVER ALTITUDE
330.	9.35E-07	9.65E-07	9.99E-07	9.67E-07	1.08E-06	9.89E-07
390.	7.33E-07	1.02E-06	8.74E-07	1.06E-06	1.23E-06	9.82E-07
450.	7.70E-07	7.65E-07	8.28E-07	8.85E-07	1.20E-06	8.89E-07
510.	2.21E-06	2.54E-07	2.51E-07	8.67E-07	1.17E-06	9.50E-07
570.	5.41E-07	4.50E-07	5.00E-07	5.34E-07	5.88E-07	5.23E-07
630.	3.50E-07	4.01E-07	4.29E-07	4.94E-07	4.65E-07	4.28E-07
690.	2.53E-07	2.41E-07	2.74E-07	1.60E-06	1.53E-06	7.81F-07
750.	3.00E-07	3.25E-07	4.12E-07	4.80E-07	4.20E-07	3.87E-07
TIME AVG	7.62E-07	5.52E-07	5.71E-07	8.61E-07	9.59E-07	

NUMBER OF STRIATIONS IN SPATIAL VOLUME

MOST PROBABLE STRIATION RADIUS

PROB OF GAUSSIAN STRIATIONS

3.3.2
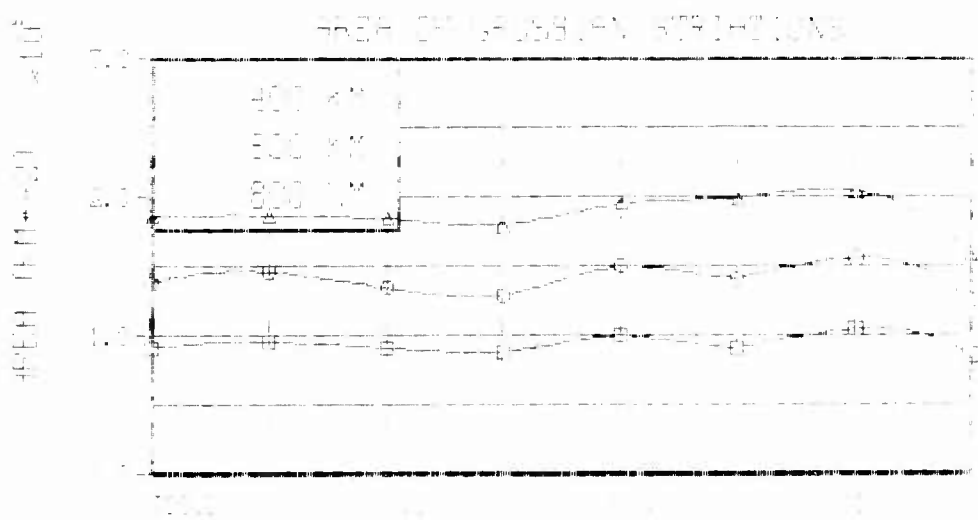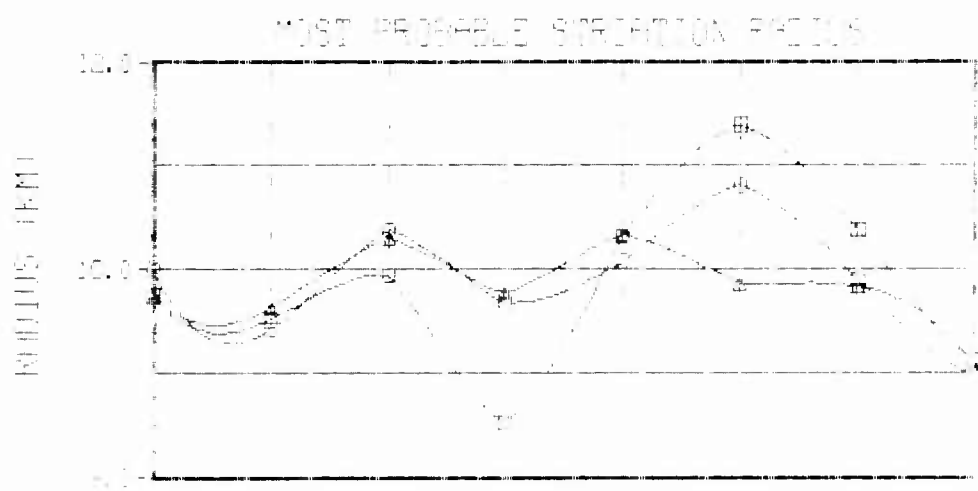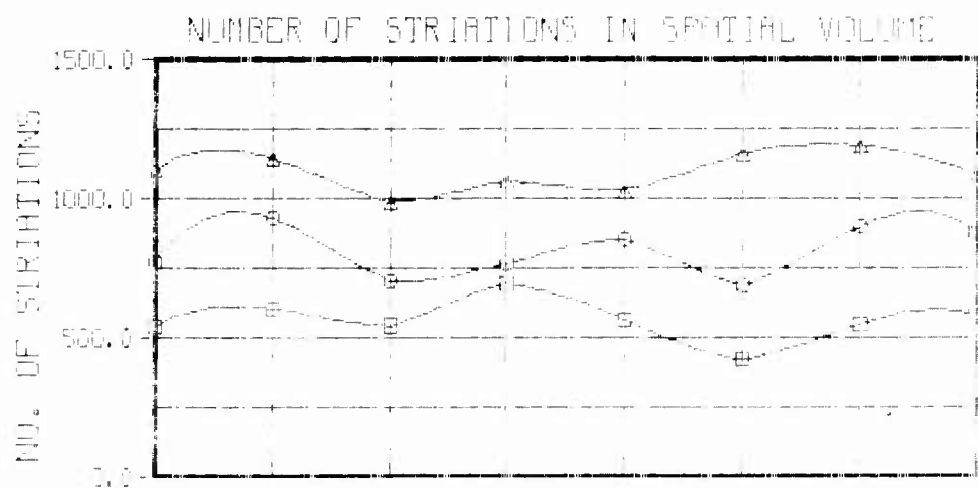
SECTION 4

CONCLUSIONS

In this report we have summarized results of derived parameters
of simple analytic representations of spatial frequency power spectra that
arose from relative radiance measurements of STARFISH striations as recorded
on film at Canton Island. We have tried to establish a time and altitude
dependence of the power spectra. Because of the allowable time element for
this study, and complexity of the data, we were not successful in this en-
deavor. Study of the presented data reveals that it is not obvious if one
exists in the time period and location of our analysis. It could very well
be, that at these late times, the striation region, which is far removed
from the burst location, is substantially the same and regions within this
striation volume of different character, which ought to be described by
different PSDs, do not exist. In any event the data is presented in suffi-
cient detail to allow review by others, as to the existence of possible
time/altitude effects on the determined PSDs.

Although ambiguity exists as to the actual altitude of the stria-
tion volume, the results of the fit parameters describing the two considered
analytic fits to the PSDs (log-log linear, semi-log linear) are quite insen-
sitive to this ambiguity. This is not true regarding derived parameters that
are model dependent (such as number of striations, striation area, volume
emission, etc.). As shown by the presented data these parameters are sensi-
tive to the selected location of the striation volume. The time dependence
of these model dependent parameters likewise indicates that the sampled
striation region, is substantially the same over the time/altitude interval
studied.

The prime purpose of these measurements was to establish the power spectral density from the striation properties and determine if these striation properties would restrict the PSD to a relatively simple analytic form. It is clear from the presented results how well this can be achieved by a power law or a single exponential fit. It is also shown in Figures 3.2.1 through 3.2.10 that a much better fit to the data is achieved by a two-term exponential fit. Although time did not allow to review the data in terms of a similar two-term power law fit, it is certain that because of the sharp PSD drop a $k = 0.01$ rads/km, a better representation of the PSDs would be achieved by such a consideration. This is easily seen by a review of Figure 4.1 and 4.2 where one of the PSDs from Figure 3.1.1 is reproduced.

In Figure 4.1 analytic fits of Equation 2.2 are overlayed for a fixed slope ($\nu = 0.014$, i.e., $\gamma = 2.03$) and six different values of the outer scale size, L. Likewise in Figure 4.2 analytic fits of Equation 2.2 are overlayed over the experimentally determined PSD for an outer scale, $L = 390$ and five different values of ν represented by the slope, γ. It will be noted that for wave numbers greater than 0.03 rads/km, a very good fit to the data is achieved by a power law fit having a slope of about 2 (i.e., $\nu = 0$) and an outer scale size of $20 \lesssim L < 100$ km/rad. If this were selected then the power region at lower wave number (km/rad) values could be expressed by an added second function. Our endeavor to fit all the data by one simple expression forces the selection of a large value (~ 400) for the outer scale size. Since this is about the distance of the entire scan length across the striations, it seems clear that this very large outer scale size is not a result of stochastic large scale fluctuations, but is instead related to the deterministic gross structure of the radiance profile. On several of the PSD plots shown in Section 3 there appears to be a short flat shelf at $k \simeq 0.03$ rads/km. This suggests that the true outer scale for the stochastic fluctuations may be in the range of 20 to 40 km/rad, and that the increase in the PSD for $k < 0.03$ km/rad is due to the deterministic structure of the radiance profile.
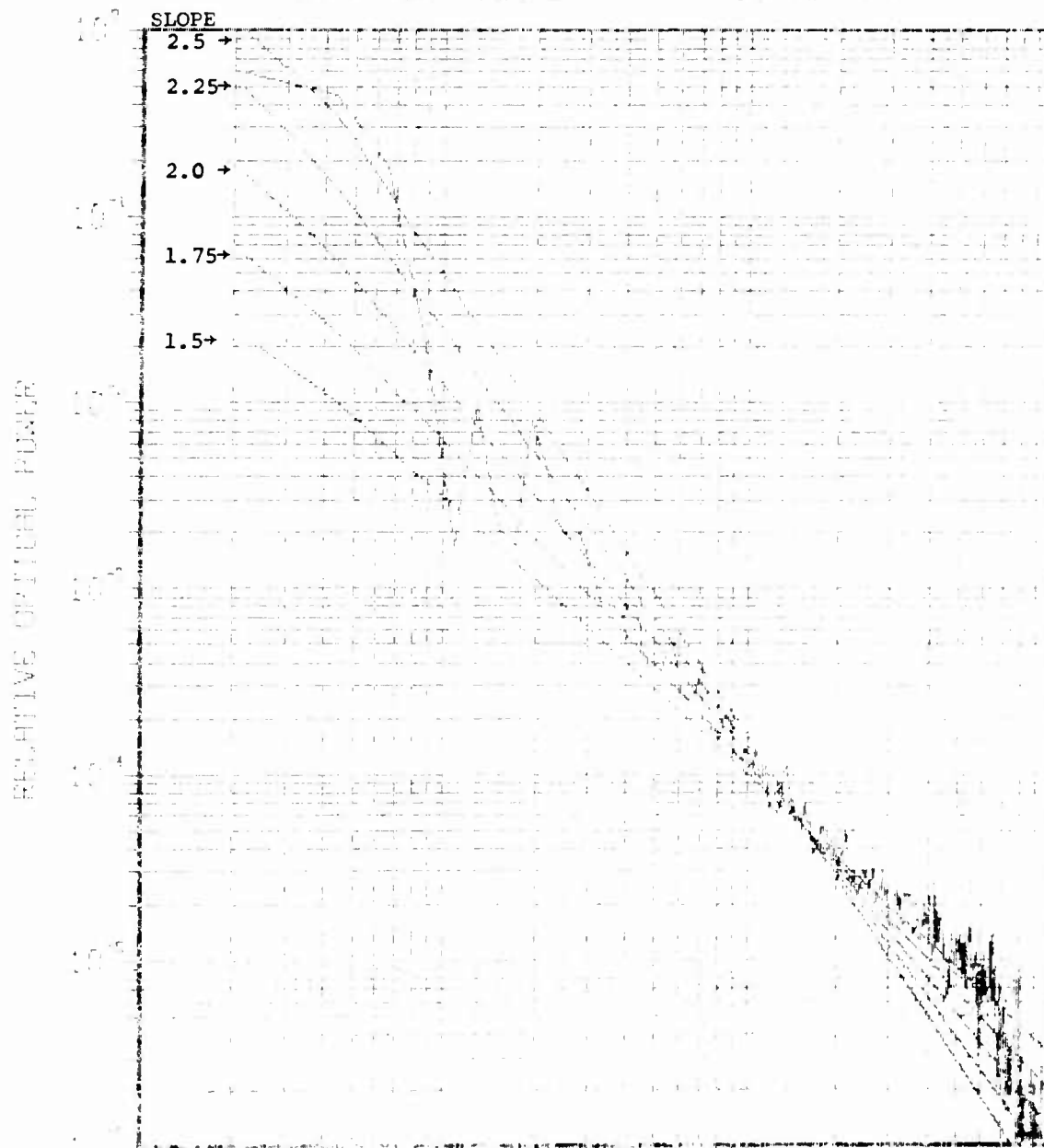
POWER LAW FIT

DIFFERENT L VALUES   FIGURE 4.1

ABCISSA x $\frac{\pi}{2}$ = k (radians/kilometer)

95
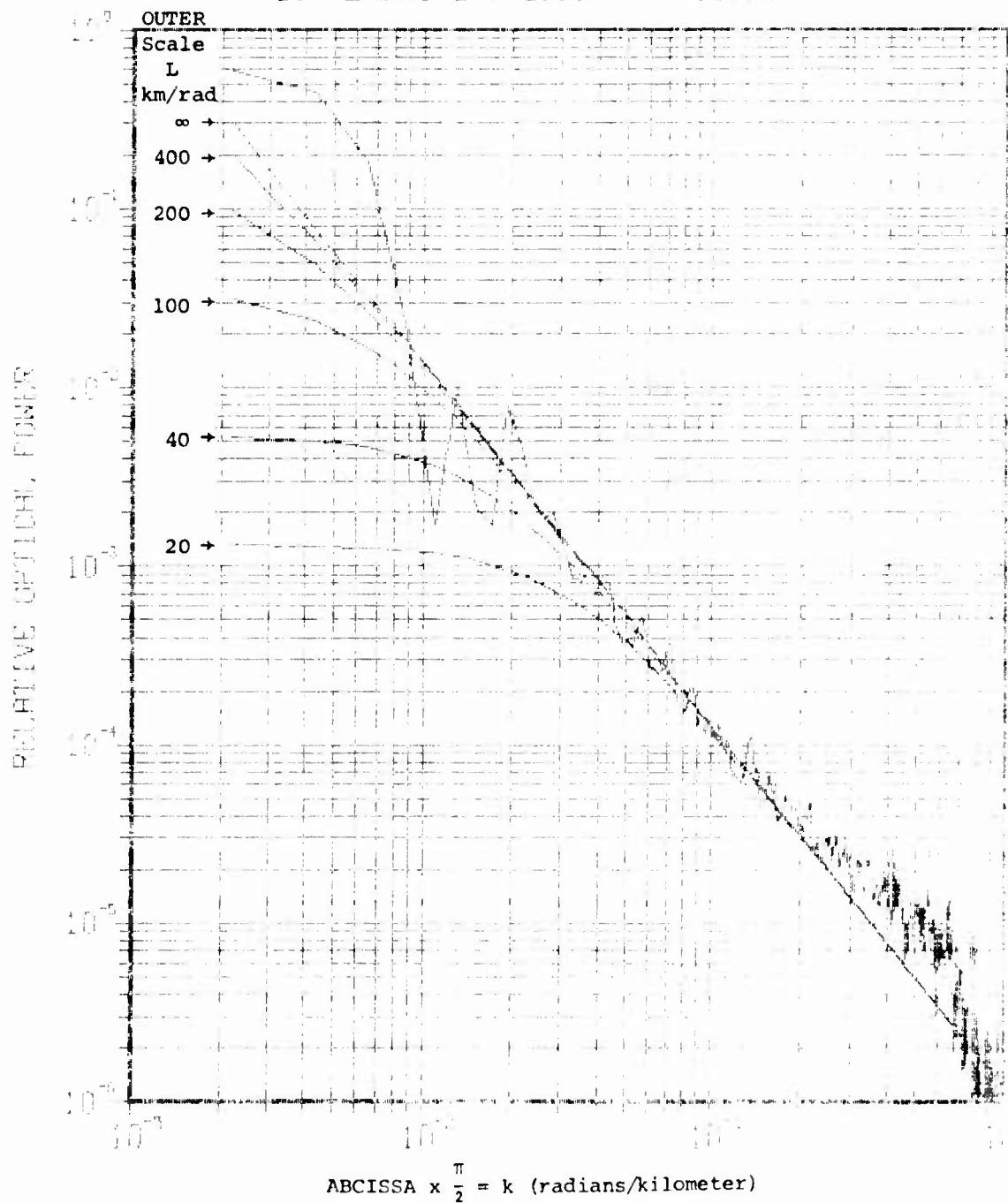
POWER LAW FIT

DIFFERENT SOURCES   FIGURE   4.2

ABCISSA x $\frac{\pi}{2}$ = k (radians/kilometer)

REFERENCES

1. Wortman, W.R., R.W. Kilb, "The Relation Between PSDs and Striation Properties", Mission Research Corp., unpublished.

2. Herman Hoerlin, "United States High-Altitude Test Experiences", LA-6405, Los Alamos Scientific Laboratory, 1976.

3. Hodges, J.C., W.G. Chesnut, "Starfish Photography from the Equator", DASA 2361, SRI International, 1969.

4. Dudziak, W.F., D.I. Devan, "Characterization of Checkmate Striations, Information Science, Inc., unpublished.

5. Chesnut, W.G., "Spatial Frequency Analysis of Striated Nuclear Phenomena", SRI International, unpublished.

6. Leonard, L.H., R.E. McDevitt, "Starfish Late Time Streaks and Aurora", EG&G Inc., unpublished.

7. Dudziak, W.F., Unpublished Starfish film records from Maui.

8. Strassinopoulos, E.G., G.D. Mead, "Computer Programs for Geomagnetic Field Line Calculations", NASA, NSSDC 72-12, 1972.

9. Wittwer, L.A., "Propagation of Satellite Signals through Turbulent Media", AFWL TR-77-183, Air Force Weapons Laboratory, 1978.

10. Schurin, B.D., et. al., "Long-Wave Infrared Background", unpublished.

11. Overbye, DNA3213F, "Operation Dominic - Nuclear Induced Striation Characteristics Of Fishbowl Magnetic Conjugate Aurora", Technology International, Nov. 1973.

DISTRIBUTION LIST

DEPARTMENT OF DEFENSE

Defense Nuclear Agency
      ATTN: NAFD
      ATTN: NATD
      ATTN: STNA
      ATTN: RAEE
3 cy ATTN: RAAE
4 cy ATTN: TITL

Defense Technical Information Center
12 cy ATTN: DD

Field Command
Defense Nuclear Agency
      ATTN: FCPR

Field Command
Defense Nuclear Agency
Livermore Branch
      ATTN: FCPRL

DEPARTMENT OF THE ARMY

BMD Advanced Technology Center
Department of the Army
      ATTN: ATC-T, M. Capps

DEPARTMENT OF THE NAVY

Naval Research Laboratory
      ATTN: Code 7500, B. Wald
      ATTN: Code 4700, T. Coffey
      ATTN: Code 7550, J. Davis
      ATTN: Code 4780, S. Ossakow
      ATTN: Code 7950, J. Goodman
      ATTN: Code 4187

DEPARTMENT OF THE AIR FORCE

Air Force Geophysics Laboratory
      ATTN: OPR, H. Gardiner
      ATTN: OPR-1
      ATTN: LKB, K. Champion
      ATTN: OPR, A. Stair
      ATTN: S. Basu
      ATTN: PHP
      ATTN: PHI, J. Buchau
      ATTN: R. Thompson

Air Force Weapons Laboratory
      ATTN: SUL
      ATTN: NTYC
      ATTN: NTN

Electronic Systems Division
Department of the Air Force
      ATTN: DCKC, J. Clark

DEPARTMENT OF ENERGY CONTRACTORS

Los Alamos National Scientific Lab
      ATTN: D. Simons
      ATTN: E. Jones
      ATTN: MS 664, T. Zinn

DEPARTMENT OF DEFENSE CONTRACTORS

Berkeley Research Associates, Inc
      ATTN: J. Workman
      ATTN: C. Prettie

ESL, Inc
      ATTN: J. Marshall

General Research Corp
      ATTN: J. Ise, Jr.

University of Illinois
      ATTN: Security Supervisor for r. sen

Information Science, Inc
      ATTN: W. Dudziak
      ATTN: P. Lad

JAYCOR
      ATTN: J. Sperling

Kaman TEMPO
      ATTN: W. Knapp
      ATTN: DASIAC

M.I.T. Lincoln Lab
      ATTN: D. Towle

Mission Research Corp
      ATTN: R. Hendrick
      ATTN: F. Fajen
      ATTN: D. Sappenfield
      ATTN: Tech Library
      ATTN: R. Kilb
      ATTN: R. Bogusch

Pacific-Sierra Research Corp
      ATTN: H. Borde

Physical Dynamics, Inc
      ATTN: E. Fremouw

R & D Associates
      ATTN:
      ATTN:
      ATTN:
      ATTN:
      ATTN:

R & D Associates
      ATTN:

Rand Corp
      ATTN: E. Bedrozian

Science Applications, Inc
      ATTN: D. Hamlin
      ATTN: L. Linson

SRI International
      ATTN: A. Burns
      ATTN: W. Chesnut
      ATTN: C. Rino
      ATTN: M. Baron